ACCURATE ULTRA-LOW ENERGY SIMS DEPTH PROFILING OF SILICON SEMICONDUCTORS

Terence J Ormsby B.Sc.(Hons) M.Sc.

Thesis for the degree of Doctor of Philosophy

submitted to

The University of Warwick

Department of Physics

September 2000

Table of Contents.

List of Figures

List of Tables

Glossary of Terms

Z_o - is the original location of a suitable feature i.e. the peak centroid of a boron delta layer. This can be determined by extrapolating the apparent depth of a feature at a number of different beam energies back to zero energy.

Apparent depth – is the depth of a feature in a SIMS profile, after carrying out any inaccurate quantification procedure, which converts ion dose/frame number/analysis time to depth.

Apparent transient width – is taken as the position where a matrix signal intensity reaches 95% of the equilibrium level, calculated using the bulk erosion rate.
True transient width – is taken as the position where a matrix signal intensity reaches 95% of the equilibrium level, calculated using the true faster average pre-equilibrium erosion rate. This should correspond to the actual number of matrix atoms sputtered in the transient region.

Actual transient shift – is the difference between the apparent and true transient widths.
Terminal shift – is the correction needed to the last ordinate to account for the actual number of matrix atoms removed during SIMS profiling. This is can be due to beam oxidation induced swelling of the crater base and also any directional relocation of dopant atoms. This may also include an underestimate of the actual number of matrix atoms sputtered due to a surface profilometer stylus tip riding over the crests of any roughening on the bottom of a crater.

Acknowledgements

I would like to acknowledge the following people for their help and guidance during the period of this research project.

First and foremost I would like to thank Professor Mark Dowsett for his invaluable direction and help, without which this project would not have been possible, and also for having faith in the ability of an old chemist.

All the members of the Advanced SIMS Projects group (ASP) at Warwick for the many discussions we have had, in particular Dr. Graham Cooke, Dr. Dapping Chu and Roger Gibbons for sharing their extensive knowledge in this field of research.

I would also like to thank Gerry Smith and Steve Yorke in electron microscopy, Adrian Lovejoy in the electronics workshop, and fellow student Salim Al-Harti for his work on the MEIS / SIMS collaborative projects.

Dr. Allan Pidduck from the electronic and optical materials centre, DERA deserves a special mention for obtaining the high resolution atomic force microscopy data, clearly showing ion bombardment induced ripple formation.

I would like to acknowledge EPSRC and Atomika Instruments GmbH for funding myself and this project.

Finally, I would like to thank my family and friends for all their moral support, encouragement and nagging, especially my son Sean for making the last 3½ years extra difficult but much more enjoyable.

Declaration.

This thesis is submitted to the University of Warwick in support of my application for the degree of Doctor of Philosophy. It contains an account of my work in the Department of Physics at the University of Warwick during the period October 1996 to September 1999, under the supervision of Prof. M. G. Dowsett.

No part of this thesis has been used previously in a degree thesis submitted to this or any other university. The work described is the result of my own research except where specifically acknowledged in the text.

T. J. Ormsby

September 2000

List of Publications

Ultra Low Energy Ion Mass Spectrometry and Transient Yields at the Silicon Surface.

M. G. Dowsett, T. J. Ormsby, G. A. Cooke and D. P. Chu,

Proceedings of the 4th International Workshop on the Characterization of Ultra Shallow Doping Profiles in Semiconductors, MCNC, North Carolina, March 1997,

and published in, *J. Vac. Sci. Technol.*, **B16,** 302, (1998).

Establishment of Equilibrium in the Top Nanometers, using Sub-keV Beams.

M. G. Dowsett, T. J. Ormsby, D. I. Elliner and G. A. Cooke

Secondary Ion Mass Spectrometry, SIMSXI, edited by G. Gillen, R. Lareau, J. Bennett and F. Stevie, p. 371 Wiley, Chichester (1998).

Experimental Techniques for Ultra-shallow Profiling using Sub-keV Primary Ion Beams.

M. G. Dowsett, G. A. Cooke, D. I. Elliner, T. J. Ormsby and A. Murrell,

Secondary Ion Mass Spectrometry, SIMSXI, edited by G. Gillen, R. Lareau, J. Bennett and F. Stevie, p. 285 Wiley, Chichester (1998).

Is Ultra Shallow analysis possible using SIMS?

D. P. Chu, M. G. Dowsett, T. J. Ormsby, and G. A. Cooke

Proc. Int. Conf. on Characterisation and Metrology for ULSI Technology, March 1998, AIP Conference Proceedings 449, New York p771.

The Advantages of Normal Incidence Ultra-Low Energy SIMS Depth Profiling.

T. J. Ormsby, D. P. Chu, M. G. Dowsett, G. A. Cooke and S. B. Patel,

Oral presentation at QSA10 IVC Birmingham 1/9/98

and published in *Applied Surface Science*, **144-145**, 292, (1999)

The Establishment of Accuracy in Ultra Shallow SIMS Depth Profiles.

G. A. Cooke, M. G. Dowsett, T. J. Ormsby, D. P. Chu and A. J. Pidduck,

Proceedings of the 5th International Workshop on the Characterization of Ultra Shallow Doping Profiles in Semiconductors, MCNC, North Carolina, March 1999

The use of Two Beam Energies in SIMS Analysis of Shallow Implants: Resolution Matched Profiling.

G. A. Cooke, T. J. Ormsby, M. G. Dowsett, C. Parry, A. Murrell and E. J. H. Collart

Proceedings of the 5th International Workshop on the Characterization of Ultra Shallow Doping Profiles in Semiconductors, MCNC, North Carolina, March 1999,

and published in, *J. Vac. Sci. Technol.*, **B18**, 493, (2000).

ABSTRACT

Since the invention of the bipolar transistor in 1947, lateral dimensions of semiconductor devices have reduced by a factor of 4 and in-depth dimensions by some two orders of magnitude. This size reduction is continually making the accurate measurement of the latest generation of semiconductor devices more difficult. Secondary ion mass spectrometry (SIMS) is a highly effective analytical technique, traditionally used to measure concentration depth profiles, due to its high sensitivity and good depth resolution. The development of the floating ion gun (FLIG) at Warwick, allows the routine use of sub-keV beam energies for rapid SIMS depth profiling.

The aim of this research project was to find and investigate ultra-low energy SIMS depth profiling conditions, suitable for the accurate analysis of modern silicon semiconductor devices.

This work has shown that ultra-low energy ion beams at normal incidence, not only produce the most accurate SIMS depth profiles, at 250 eV the entire depth scale is accurate to within 1.5 nm (2.5 nm at 500 eV), but also for boron with the highest depth resolution.

Two significant errors introduced into the depth scale of calibrated boron depth profiles, the surface transient shift and a largely overlooked parameter - the terminal shift, were quantified. Utilising these two shifts a simple universal depth correction procedure has been described, applicable when profiling boron samples using O_2^+ at normal incidence.

The development of surface topography has two detrimental effects, a loss in depth resolution and a variation in the sputter yield, both of which have been quantified. A wide range of analysis conditions were investigated, at O_2^+ beam energies up to 1 keV, the only angles where ripples do not develop within the top 200 nm of a profile are those using near-normal incidence ($\theta_p \leq 30°$) ion bombardment.

1.0 Introduction

1.1 Introduction to the Problem

Since the invention of the bipolar transistor in 1947, lateral dimensions of semiconductor devices have reduced by a factor of 4 and in-depth dimensions by some two orders of magnitude. While this cannot continue indefinitely, there are no obvious signs that the rate of change is slowing, or will do so in the next few years. The manufacture of semiconductor devices with reduced dimensions, along with developments in thin film technology across a broad base of materials, continually places more stringent demands on the supporting analytical techniques. One of the most important tools used in the design and manufacture of integrated circuit technology, are the device modelling tools. If these are to work correctly, they require an accurate database, describing implant shape and the effects of thermal and chemical processes (such as annealing and preamorphization). Unfortunately, whilst there is a large database for relatively deep implants (e.g. >5 keV for boron), this data cannot be scaled reliably, as the shape of ultra-shallow implants (e.g. <1 keV for boron) are especially susceptible to modification through sputtering, dopant reflection during implantation, increased channelling, and by gettering due to the close proximity of the surface during annealing. Accurate and reproducible measurements of ultra-shallow implants, both before and post-anneal is critical to process development.

Traditionally, SIMS has been shown to be a highly effective technique, possessing both high sensitivity and good depth resolution. However, accurate data for ultra-low energy implants, as low as 200 eV for boron, requires the use of ultra-low

energy SIMS. This is because the analysis of these structures at conventional energies results in undetected material, because of the relatively large transient region, as well as distortion of the profile shape by the high degree of atomic mixing. Optimisation of the shallow doping of silicon requires the use of analytical techniques which can profile dopants in the outermost several nanometers and are capable of quantitative analysis right from the surface, with sub-nm depth resolution, concentration accuracy of 1%, and a depth scale accurate to within 1 nm.

The move from very large scale integrated (VLSI) technology to ultra-large scale integrated circuits (ULSI) technology over the last 15 years, has seen the typical energy of the primary beam used in SIMS profiling of these devices reduced from 10 keV to 500 eV. Nevertheless, accurate analysis of ultra-shallow junctions remains a major challenge (Wittmaack K and Corcoran S F, 1998; Jiang Z X and Alkemade P F A, 1998). This is because there are two significant differences between ULSI and VLSI technology. Firstly, a significant part of the implanted dose is in the top few nm of the wafer, which are also of unknown composition and morphology. There may be a native or thin gate oxide present, and the surface may be crystalline or amorphized. Secondly, the near surface region of the wafer may be less than 70 % silicon, due to high dopant concentrations, impurities (i.e. fluorine from BF_2 implantation), or from the use of a preamorphizing implant, such as germanium. These factors will all influence ion yields and erosion rates.

As SIMS is based on ion beam sputtering, the transient region before equilibrium is reached poses a serious problem (Vandervorst W *et al.*, 1985). During this surface transient, the secondary ion intensities can vary over several orders of magnitude, and the erosion rate may reduce by a factor of more than 10, for a perfectly clean silicon surface at sub-keV energies (Wittmaack K, 1996a), introducing errors in

both the concentration and depth scales. Surface transients are intrinsically associated with the removal of the native oxide and the build-up of the primary ions at and below the surface. Depending on the experimental conditions (primary ion energy and species, angle of incidence, and substrate material) a significant amount of material (and profile information) is removed during this transient region. It is therefore of prime importance to limit the thickness of the transient region when profiling very shallow structures, in order to minimise any errors in the quantification process.

Accurate analysis of the latest semiconductor devices requires sub-nm depth resolution, which is fundamentally limited by primary ion beam mixing. Cascade and recoil mixing effects are reduced by lowering the primary ion beam energy. Reducing the energy of the primary ion beam results in lower secondary ion yields, and hence poorer detection limits and a reduced dynamic range. Alternatively, increasing the angle of incidence relative to the sample normal, reduces the normal energy component thus improving depth resolution, whilst enabling a faster sputter rate.

In summary, if accurate analysis of ultra-shallow junctions is to be achieved, it is important that the following requirements are complied with:

I. All important parts of the profile should be beyond the transient region, otherwise some of the profile will be entirely the wrong shape and cannot be accurately quantified by any known means, however reproducible it maybe.

II. The erosion rate, beyond the transient region must be constant.

III. The SIMS depth resolution must be sufficient to reveal implant structure.

IV. If the total impurity level is above the dilute limit (>1%), steps must be taken to establish the size of any resulting matrix effects.

1.2 Thesis Overview

It has been the aim of this project to find and investigate ultra-low energy SIMS depth profiling conditions, suitable for the accurate determination of modern silicon semiconductor devices.

Chapter 1 provides an introduction to the problem, along with a brief overview of this thesis. Chapter 2 contains a review of the main depth profiling techniques available, while chapter 3 focuses on SIMS and the present state of the technique. Most of the experiments carried out, are described in chapter 4.

Chapter 5 contains results and discussion on the determination of an accurate depth scale, and focuses on three main areas. Surface transient studies, the apparent and the true transient widths (which are significantly different) have been determined for a wide range of analysis conditions. Quantification of a largely overlooked parameter - the terminal shift which for boron is due to two main factors: the incorrect assumption that the measured crater depth corresponds to the depth of matrix eroded and a upward migration of boron into the altered layer. An investigation into matching the primary beam ion energy to the requirements of the analysis was undertaken, focusing on the quantification issues of changing the beam energy within a single depth profile.

Chapter 6 focuses on surface topography issues, identifying the conditions using O_2^+ at $\leq$1 keV beam ion energies, which do <u>not</u> develop ripples within the top 200 nm of a profile. The formation of ripples has two detrimental effects, they induce a variation in the sputter yield and a loss of depth resolution, both of which have been quantified.

Finally in chapter 7 some conclusions have been drawn from the presented results, followed by suggestions for future investigations.

2.0 A Review of Depth Profiling Techniques

2.1 Introduction

The importance of understanding surfaces and interfaces, particularly in the fields of catalysis and corrosion, was first recognised in the early 1900's. However, it was not until the 1960s with the development of ultra-high vacuum techniques, that major advances were made. There was an explosion of new developments and methods for the characterisation of surfaces, however, only a few of these have established themselves as suitable for determining the chemical concentration and its distribution in the surface and sub-surface regions of solids. Auger electron analysis (AES), medium energy ion scattering (MEIS), Rutherford back-scattering spectrometry (RBS), secondary ion mass spectrometry (SIMS) and X-ray photoelectron spectroscopy (XPS) are techniques often employed when information on device structure is being sought.

The relationship between the properties of a surface and the process history of the material must be understood, since control of the properties of the surface region is critical in many technological processes e.g. crystal growth. Hence surface analysis is a necessary tool to determine whether a surface has the desired properties (electrical, chemical, optical and mechanical). The ability to analyse the surface composition and geometry is playing an ever increasing important role in a wide range of industries particularly, since the composition of the surface may differ considerably from that of the bulk as minority elements often segregate at free surfaces, interfaces or at grain boundaries. When deciding on which method(s) to use, it is important to know what the limitations of the various techniques are, with regard to the analytical problem, as unfortunately the ideal technique still does not exist.

The necessary surface sensitivity can be achieved, either by using a surface-sensitive method of exciting the analytical signal, or by employing a signal of high surface-sensitivity. The most popular methods today are based on the use of surface sensitive signals consisting of charged particles having suitable kinetic energies. Hence, either electron spectroscopic methods (XPS, AES) or analysis of secondary ions (SIMS) are presently the most common routine methods for chemical surface characterisation. From the viewpoint of surface sensitivity only, SIMS is clearly the best technique. Although the sensitivity of SIMS varies greatly with the species and the chemical state of the sample, it is typically at least 2-3 orders of magnitude better than AES, MEIS, RBS or XPS. SIMS is also capable of analysing every single element from H to U, no matter what the bulk composition of the sample. Methods using electromagnetic signals are not generally used for routine surface characterisation, but numerous variations with excellent surface sensitivity have been developed for special applications *e.g.* multiple total reflectance IR. spectroscopy.

Although the information depth is different for all the techniques mentioned, sputter erosion of the sample surface by a primary ion or atom beam is normally required for AES, SIMS and XPS to reveal buried features. Erosion-induced surface-roughening can be a major problem for those techniques where a probe is used to successively erode the surface. This can even occur on 'ideal' flat surfaces, because of differing erosion rates for different crystal faces, or chemical phases of differing composition. However, angle resolved XPS can generate shallow (<10 nm) depth profiles without sample erosion (Tielsch B J and Fulghum J E, 1994), MEIS has a slightly deeper range of around 25 nm, whereas depth profiles of up to 2 μm can be acquired by RBS, without any sputter erosion of the sample surface.

2.2 Carrier Profiling

The chemical, physical and electrical properties of a semiconductor device are usually closely related. When a dopant is incorporated into a sample, it can be either electrically active or non-active depending on the lattice site. The resistivity of a semiconductor is proportional to the activated dopant concentration. This can only be determined using electrical measurement techniques, such as the four-point probe, capacitance-voltage (CV) and spreading resistance.

The four-point probe, while being one of the fastest measurement techniques for determining dopant concentration, has limited applicability to epi-layers that are grown on a lightly doped substrate of the opposite conductivity type. The resistivity ρ of a epi-layer is calculated using

$$\rho = R_s T F \qquad (2.1)$$

where R_s is the sheet resistivity, T is the epi-layer thickness, and F is the geometric correction factor. Low currents must be used to avoid ohmic heating or reaching a punch-through voltage, and extra-care must also be taken when measuring thin layers to prevent the probe tips penetrating the layer.

The C-V technique is rapid and non-destructive, and utilises a mercury contact to form a Schottky barrier diode. By applying a reverse bias, the capacitance as a function of voltage is measured, and the doping profile is calculated from the following equation

$$N(x) = - C^3[q\, \varepsilon A^2\, (dC/dV)] \qquad (2.2)$$

and

$$x = \varepsilon A / C\,(V) \qquad (2.3)$$

where C is the capacitance, q is the electric charge, ε is the permittivity of silicon, A is the junction area, x is the distance from the junction, and V is the bias voltage. The

C-V technique works best in the doping range of 10^{14} to 10^{17} atoms/cm^3.

When doping concentrations need to be measured across a wider range (10^{14} to 10^{20} atoms/cm^3), the spreading resistance technique is preferred. A two-point probe is used to measure the resistivity of a cleaved and bevelled sample at several points, starting at the surface to the layer/substrate interface. The doping concentration and its profile are calculated using complex data reduction, by correlating the measured change in resistivity between each point with carrier concentration. The technique tends to suffer from poor accuracy, often due to the effects of wear on the probe tip.

However, if the total dopant concentration or profile is required, surface spectroscopic techniques, such as AES, MEIS, RBS, SIMS, and XPS must be used.

2.3 Methods for Dopant Depth Profiling

2.3.1 Auger Electron Spectroscopy (AES)

AES uses an energetic electron beam (typically 2-10 keV) which can ionise atoms by ejecting an inner core electron, to probe the surface,. When an outer-core electron falls back to the inner-core to replace the ejected electron, the atom can give up its excess energy by emitting either an x-ray or a second "Auger" electron. The energy of an Auger electron is dependent on the atom from which it comes, allowing the elemental composition of the surface to be determined. While the electron beam penetrates ten's of nm's into the surface, only Auger electrons generated in the top 3 nm of the sample, can be collected. By scanning the electron beam, maps of surface element distribution can be obtained. AES is in itself non-destructive, but it is normally

combined with an ion beam to erode the sample, to enable it to generate profiles of composition against depth.

Auger electrons were first discovered by Pierre Auger in 1923, when he was studying x-ray induced photoelectrons in a Wilson cloud chamber. He noticed that certain electrons had discrete energies, which depended only on the gas species present in the cloud chamber. His discovery of the link between atom species and energy of the Auger electron is the fundamental principle behind AES.

The energy of an Auger electron is small in comparison with the incident beam, typically ranging from several tens of eV to one or two thousand. Auger electrons are readily absorbed in all solids, and can only escape for detection from the outermost monolayers (typically <10) of the sample. Self absorption is the key to the extreme surface sensitivity of Auger electron spectroscopy. This combined with a high cross-section for emission from light elements, makes the technique particularly useful for carbon-based contamination, identification and control in semiconductor applications.

Auger electrons only make up a very small fraction of the total available signal generated in a sample by an incident electron beam. In a scanning electron microscope, there is typically one Auger electron produced for every 1,000 secondary electrons, which are the predominant source of signal used in image formation. The small discrete Auger peaks are superimposed on a large background caused by the secondary electrons of random energy in the acquired data. However the Auger features can be more easily resolved by taking the derivative of the energy spectrum, which removes the high secondary electron background.

For every element in the periodic table, there is a unique pattern of discrete energies. The energy of the KLL Auger electrons increases non-linearly with atomic number from about 60 eV for Li to 1620 eV for Si. The lighter elements tend to have

intense KLL lines that are easily measured in Auger spectra, in contrast to their x-ray lines. This complementary behaviour originates from the fact that Auger and x-ray emission are competitive processes within a single atom.

2.3.2 X-Ray Photoelectron Spectroscopy (XPS)

XPS is also known as electron spectroscopy for chemical analysis (ESCA), uses a beam of monochromatic low-energy x-rays to bombard a sample. The x-ray photon energy is sufficient to remove an outer-shell electron from an atom. The kinetic energy of the emitted electron is equal to the difference between its bonding energy and the x-ray photon energy. The energy of the electron is analysed not only to determine from which atom it was emitted from, but also to obtain useful chemical bonding information, this is the major advantage of XPS. Like AES only electrons from the top few layers are collected enabling quantitative analysis.

2.3.3 Ion Scattering Techniques

Ion scattering was first used for materials analysis in the mid-1960's (Smith D P, 1967; Turkevich A L *et al.*, 1968). By the late 1970's, several different ion-scattering techniques including Rutherford back-scattering spectrometry (RBS - incident energies in the MeV range), medium energy ion scattering (MEIS - incidence energies in the 100 keV range) and low energy ion scattering (LEIS), which is also known as ion scattering spectrometry (ISS - incidence energies from 1 to 10 keV) were been used to determine the atomic structure of solid surfaces (Poelsema B 1977; Stensgaard I *et al.*, 1978; Turkenburg W C,1978). Ion scattering has become an increasingly important

technique for the study of surface and interfaces during the last twenty years. This is mainly due to the fact that results from an ion scattering experiment can be interpreted quantitatively, in contrast to many other techniques.

The amount of energy transferred in an elastic collision depends upon the mass of the target atom, analysing the energy of the scattered particles provides a means of identifying the atoms responsible for scattering the ions. A major advantage of ion scattering over other surface crystallographic techniques, such as low-energy electron diffraction (LEED), or X-ray diffraction, is that the structural information is available in co-ordinate space, rather than reciprocal space. For incidence energies greater than 1 keV, the de Broglie wavelength is $< 10^{-4}$ nm, which is smaller than the lattice constant of any solid. Generally, with the exception of rainbow scattering, quantum-mechanical effects can be ignored because there are neither interference effects nor diffraction from the lattice. The anisotropy in the ion yield for keV-MeV ions scattered from a crystalline surface is due to a series of classical collisions, and therefore Newtonian mechanics can be used to calculate (model) the intensity of the back-scattered yield. Hence the observed peaks and valleys in the angular dependence of the scattering yield data can often be directly related to the relative positions of atoms with respect to each other in the surface region. As ion scattering techniques are primarily probes of local structure near a particular scattering site, they do not require long-range order to provide structural information.

As the nature of ion scattering is strongly energy-dependent, each of the different energy ranges used for ion scattering and recoiling has particular advantages and disadvantages. Traditionally, ion scattering techniques have been divided into the three regimes defined above namely RBS, MEIS and LEIS. At energies less than 1000 eV the physics of the scattering events is more complex and significantly different from that at

higher energies, so a fourth category, the hyperthermal energy regime must also be defined (Hulpke E and Mann K, 1983; Horn T C M *et al.* 1988). In the RBS regime, due to the high kinetic energy of the incident ions at the distance of closest approach, the nucleus of the projectile is entirely within the electron cloud of the target, as can be seen from equation (2.4).

$$E_{inc} \approx \frac{Z_1 Z_2 e^2}{r_{ca}} \qquad (2.4)$$

E_{inc} is the incident kinetic energy of a light projectile scattering from a heavy target with the repulsive Coulomb potential of the bare nuclei. The distance of closest approach is r_{ca}, Z_1 is the atomic number of the projectile, Z_2 is the atomic number of the target atom, and e is the unit electrical charge. For a 1 MeV He^+ ion scattering from a Ag atom, r_{ca} is 1.3 x 10^{-4} nm. The electron screening of the nuclei from each other is negligible, the scattering trajectories involve nearly head-on collisions, and can be calculated from the bare Coulomb potential of the interacting nuclei.

The effective cross-sectional area of the target atom is πr_{ca}^2, which varies as the inverse square of the projectile energy. If this area is compared to that of the unit cell of elemental Ag, it yields a probability of an incident 1 MeV He^+ scattering off a monolayer of Ag atom of only 5E-7, so the probability of multiple scattering is insignificant. This makes RBS an extremely quantitative technique for determining the areal density of species, and by performing triangulation measurements a great deal of surface-structure information can be obtained. The main disadvantage of RBS is the poor depth resolution, which at best is 50 Å.

On lowering the energy of the incident ions into the MEIS regime, depth resolution is improved by at least a factor of 10, allowing detailed analyses of surface structures. r_{ca} has increased to ~10^{-3} nm, so a bare Coulomb potential is no longer

sufficiently accurate for calculating projectile trajectories. The probability of backscattering off a surface monolayer has increased to ~ 5E-5, meaning multiple scattering can be no longer neglected, and now becomes a major part of the analysis of scattering data (van der Veen J F, 1985). The sensitivity of the cross sections to electron screening of the nuclei is tiny, making a reasonable approximation of the scattering potential easy, thus enabling accurate results to be obtained. This enables MEIS to determine absolute amounts of species present on a surface quantitatively.

On further lowering the energy of the incident ions into the LEIS regime, the technique becomes more surface sensitive. Electron screening becomes extremely important as r_{ca} can approach 0.1 nm, and the calculated cross sections depends strongly on the potential model used. The probability of backscattering off a surface monolayer is highly energy dependent ranging from approximately 0.005 to 0.5 for ion incident energies of 10 to 1 keV, and multiple scattering events become significant. The major advantage of LEIS is that the scattering cross sections are so large, that it is possible to determine which atomic species terminates a surface (Buck T M *et al.*, 1980). However, it is extremely difficult to use LEIS to determine absolute amounts of species present on a surface quantitatively.

In the hyperthermal energy regime ($E_{inc} < 1000$ eV), the cross sections are now so large that incident ions do not interact with a solid via a series of binary collisions, but with several target atoms simultaneously along their entire trajectory (Hulpke E and Mann K, 1983; Horn T C M *et al.*, 1988). In this energy regime, attractive forces between the incident ion and target atoms are no longer negligible, so that scattering calculations are extremely sensitive to the potentials used. Scattering of particles in this regime is not extremely useful for determining unknown surface structures, due to the complexity of the interactions. However, when analysing known structures, they

provide useful information on the scattering processes in this technologically important energy regime.

RBS employs high energy ≥ 1 MeV high-energy He^{2+} ions to obtain the depth profile of the sample. The technique is non-destructive and utilizes the elastic collision theory to obtain the chemical information. Ion scattering techniques use an ion with mass m_1 which moves with a velocity v_0 governed by its kinetic energy $\frac{1}{2}m_1v_0^2$, to collide with an atom at rest which has a mass m_2. As it is an elastic collision, conservation of total energy and momentum describe the collision completely. When m_1 is deflected over a scattering angle θ (see Figure 2.1) its kinetic energy after the collision is

$$E_1 = k^2 E_0 \tag{2.5}$$

where the kinematic scattering factor k^2 is given by

$$k^2 = \left[\frac{\left(m_2^2 - m_1^2 \sin^2\theta\right)^{1/2} + m_1 \cos\theta}{m_2 + m_1} \right]^2 \tag{2.6}$$

When the He^{2+} ions penetrate the surface, they collide with atoms, and some are backscattered with an energy loss that is characteristic of both the atom struck and the distance below the surface where the collision occurred. Both the elemental composition and a depth profile of the sample are obtained simultaneously. Whilst RBS can obtain quantitative chemical information without the use of standards, it has only relatively poor depth resolution.

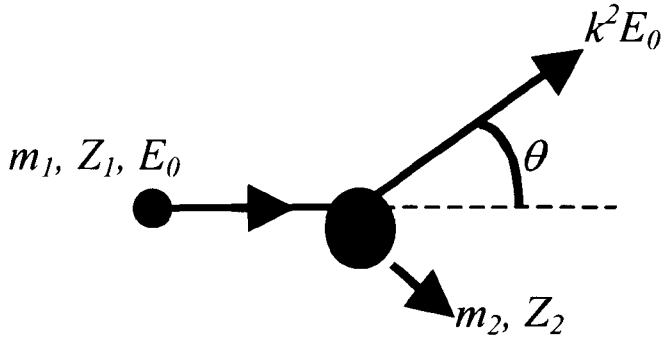

Figure 2.1: An ion with mass m_1, atomic number Z_1 and energy E_0 is scattered by a target atom with mass m_2 and atomic number Z_2 over a scattering angle θ. After scattering the ion has an energy k^2E_0.

As the energy of the incident ions increases scattering cross sections become small and shadow cones narrow, and neutralisation ceases to be important. The strong neutralisation and broad shadow cones are the key factors producing the excellent surface specificity of LEIS, so RBS is essentially a bulk technique, used in studies of the subsurface rather than surface regions.

The RBS scattered ion energy spectrum contains broad peaks whose high energy edges are governed by equation (2.5) and result from scattering off surface atoms. The lower energy component is due to ions scattered from the same atomic species but deeper in the sample, which have lost additional energy to electronic excitations. The rate of electronic energy loss is virtually constant per unit path length, as energy losses due to multiple atom scattering are infrequent, and the fact that the electronic interactions do not deflect the ion path. For any particular scattering species the size of the scattered signal at the binary collision energy is related to the surface composition, and the size of the scattered signal at lower energies to the composition at a depth below the surface proportional to the additional energy loss.

A major distinction between the two techniques of MEIS and RBS is the type of detector used. MEIS instruments tend to use electrostatic analysers, which have excellent energy and therefore depth resolution, almost capable of single atomic layer separation. The toroidal electrostatic analyzer with position-sensitive detection, typically has an energy resolution ΔE of 10^{-3} or better, and is also capable of detecting ions over a range of 25° with an angular resolution better than 0.3° (Smeenk R G *et al.*, 1982). This enables detection of both the energy and the scattering angle of the scattered ions to be determined, enabling significantly faster measurement times than previously used cylindrical detectors. This has the additional advantage of limiting ion-induced radiation damage, and reducing surface contamination of any samples. A major disadvantage of the MEIS technique in the area of semiconductor analysis is its limited depth profiling capabilities, as ions scattered from only the top 20-25 nm of the target are detected.

However, electrostatic analysers have a high energy limit of around 300 keV. By contrast, RBS instruments tend to use solid state (surface barrier) detectors, which possess much poorer energy resolution (typically by as much as 2 orders of magnitude) and hence their depth resolution is only 100-300 Å. RBS is capable of analyzing significantly greater sample depths of up to 2 μm than MEIS, this is a major reason for the much wider use of RBS in the area of semiconductor analysis.

Both methods possess the disadvantage that they only work well (with a few exceptions) for the analysis of heavy (high atomic number, Z) elements in light (low Z) matrices. This is because the scattering cross-sections are proportional to Z^2, so for light elements the low energy scattered ions are often superimposed on a background of scattering from heavier atoms. The lack of ion neutralisation and weak screening of both methods can be used to give absolute surface and subsurface compositions.

At high ion energies, the narrow shadow cones generally lead to poor surface specificity, but for low index single crystal samples subsurface scattering can be excluded, by choosing certain angles of ion incidence relative to the crystallographic structure. At these narrow angles the incident ions only interact with the top one or two atomic layers and the shadow cones, which are aligned along principal crystal axes exclude all deeper layer scattering. At these angles the resultant spectrum contains only the surface (no electronic loss) scattering and as for LEIS is dominated by peaks at the binary collision energy given by equation (2.5).

An important application area of the MEIS technique, which utilizes its atomic scale depth resolution, is the study of not only the structure of adsorbed layers on the surface, but also that of layers slightly below the surface. This ability to investigate the structure of shallow buried interfaces in a non-destructive manner is almost unique, therefore MEIS can be an invaluable tool to the semiconductor industry. The role of MEIS will become more important, as device size continue to shrink, as the technique will be able to analyse the whole junction region.

MEIS experiments are typically performed in the energy range 50 to 500 keV, because at these energies the scattered ions can be analyzed with an electrostatic analyzer. The electrostatic analyzer typically has an energy resolution of at least 500 eV at 100 keV, substantially better than approximately 15 keV with solid-state detectors used in RBS experiments. This results in a superior depth resolution of 3-10 Å, compared with at best 100 Å for RBS.

MEIS is also more surface sensitive than RBS, due to the lower ion energies used. The angular dependence of the scattering signal is used to determine the atomic structure of crystalline samples and buried interfaces in great detail. While many of the physical principles for MEIS and RBS are the same, the possibilities and limitations of

the two methods can be different. This is mainly due to the different experimental requirements of the two techniques, MEIS requires higher energy resolution and the measurement of scattering intensities as a function of the scattering angle.

As the cross-section is proportional to the square of Z_1 and Z_2, changing the ion species from H^+ to He^+ the scattering intensity increases fourfold. Also the cross-section is highly dependant on the scattering angle θ, proportional to $1/\sin^4(\theta/2)$, meaning the scattering cross-section for θ=90° is 4 times larger than at θ=180°. Typically MEIS experiments, are performed at scattering angles ≤90°, to take advantage of the larger scattering cross-sections. Whereas RBS experiments are normally performed at scattering angles in the region of 170°, because the mass separation in the energy spectrum is better at larger scattering angles.

The sensitivity of the experiment is dependent on the species studied, due to the scattering cross-section dependence on Z_2^2. Oxygen on silicon can only be detected at the 0.1 monolayer level, whereas for nickel the sensitivity improves to 0.01 of a monolayer (Tromp R M, 1992).

As an ion moves through a sample it loses energy due to inelastic interaction with the sample's electrons. The rate of energy loss, is dependent on the ion species, the composition of the sample and the energy of the ion, and is often refered to as the stopping power. As the ion moves through a sample its energy decreases continuously, therefore the inelastic energy loss per unit length is not constant, and the energy scale does not have a linear relationship with depth. However as MEIS is typically used to analyse thin layers, whose inelastic energy losses are sufficiently small to consider the stopping power to have two constant values, before and after the back-scattering event.

In the surface approximation, the inelastic energy loss (incoming path plus outgoing path) per unit length measured along the surface normal is then given by-

$$\frac{dE}{dz} = \left[\frac{k^2}{\cos\theta_1} \left(\frac{dE}{dx} \right)_{E_0} + \frac{1}{\cos\theta_2} \left(\frac{dE}{dx} \right)_{k^2 E_0} \right] \quad (2.6)$$

and an ion scattered from a depth t suffers an inelastic energy loss of

$$E_{loss} = \frac{dE}{dz} t \quad (2.7)$$

The energy loss in an elastic collision is dependent on m_1 and m_2, so the energy scale is also a mass scale. At a given scattering angle θ the ion loses more energy in a collision with a light target atom than a heavy target atom.

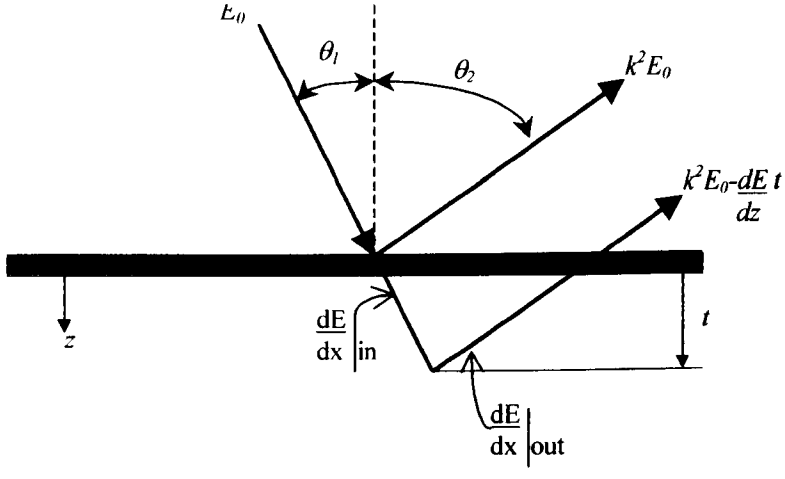

Figure 2.2: Inelastic energy loss for an ion beam impinging at an angle θ_1 and leaving at an angle θ_2, relative to the sample normal.

If the incident ion beam is aligned with a major crystallographic direction only atoms close to the surface are visible to the ion beam. This is induced by a shadowing effect: the first atom in each atomic row casts a shadow cone on the deeper atoms. Channelling occurs when incident ions undergo a small angle collision with near-surface atoms, and are steered away from the atomic rows into channels between the atomic rows, and travel deep into the solid before coming to rest, or undergoing a hard

collision. Channelling gives rise to high surface sensitivity in ion scattering experiments, because only atoms close to the surface contribute to the backscattered signal. Blocking is a similar related phenomenon: ions scattered below the surface of the target cannot escape into the vacuum along a major crystallographic direction, as atoms closer to the surface block their path. The effects of channelling and blocking are put to good advantage when studying the detailed atomic structure of surfaces and interfaces.

2.3.4 Secondary Ion Mass Spectrometry (SIMS)

SIMS uses ions that are accelerated by a high voltage (typically 500 to 5000 eV), as the probe beam to sputter secondary ions, from the surface of interest. The secondary ions are extracted and analysed with a mass spectrometer to determine the elemental composition of the surface. Oxygen and cesium ion beams are typically used for SIMS measurements due to their beneficial ionisation effects. Oxygen is more effective for electropositive elements like B, Al, and Cr, whereas cesium for more electronegative elements like C, O, and As. As SIMS involves sputtering of the surface, layers of 1 μm thickness can be routinely depth profiled with a depth resolution of 1 to 5 nm. These properties ensure SIMS is a powerful technique for measuring total doping profiles in silicon and other materials, with doping levels as low as 10^{15} atoms/cm^3.

A unique feature of SIMS relative to most other surface characterisation techniques is the ability to distinguish different isotopes of an atomic species. This is useful in the study of surface chemical reactions using 'labelled' reactants (Benninghoven A, 1975), formation of the altered layer (Kilner J A *et al.*, 1985) and

also in the identification and quantification of contaminants and their sources in semiconductor manufacture.

2.4 Two Dimensional Dopant Characterisation

Two dimensional (2D) dopant profiling has always been a highly ranked need in both the integration and TCAD (simulation) sections of the National Technology Roadmap for Semiconductors (NTRS). Although much progress has been made towards addressing these needs in recent years, a lot more remains to be done to meet the continually shrinking target requirements.

The 1997 Roadmap lists the dopant spatial resolution requirements as 5 nm for existing 250 nm technology and 2 nm for the 150 nm generation. [The National Technology Roadmap for Semiconductors, Semiconductor Industry Association, Table 61, p. 181, 1997]. However, the dopant concentration near a junction is typically 10^{18} atoms cm^{-3} = 10^{-3} atoms nm^{-3}, whereas a cube having 10 nm sides only contains one dopant atom at this concentration, *c.f.* 5,000 silicon atoms. This means the average dopant spacing at 10^{18} atoms cm^{-3} is 10 nm, increasing to 22 nm at 10^{17} atoms cm^{-3}, and the desired spatial resolution near the junction is significantly lower than the actual dopant spacing. A smooth and continuous profile is obtained, as the profiling methods utilised tend to average over a large area, yet a device (*i.e.* a transistor) operates at a very local level.

Most 2D dopant characterisation techniques analyse near surface carrier concentration or use surface potential measurements on a cross-section of the device. Thus a time consuming and demanding sample preparation step is required. This must

result in a well-characterised and reproducible condition, which is vital for accurate measurement.

In a recent round-robin study (Ukraintsev V A *et al.*, 1998) of several techniques (quantitative scanning capacitance microscopy (SCM), scanning spreading resistance microscopy (SSRM) and transmission electron microscopy (TEM)), used in groups claiming the ability of quantitative 2D dopant characterisation, very large differences in results were reported. The determined values of the source, drain and gate overlap in PMOS and NMOS devices varied by at least a factor of 3. None of the methods provided the necessary accuracy and resolution required at this time for process simulators. The most likely cause of these large differences was poor sample preparation, due possibly to contamination, or displacement of dopant atoms. It is impossible at this time to unambiguously judge the accuracy of any experimental or theoretical effort to characterise 2D silicon doping, as there is no 2D dopant standard.

3.0 Introduction to Secondary Ion Mass Spectrometry

In SIMS a monoenergetic, mass filtered, ion/atom beam is directed towards the sample of interest. This primary beam is usually scanned over an area a few hundred microns square in order to establish a uniform primary beam dose across the analysis area. Each primary particle initiates a collision cascade, breaking bonds and displacing atoms from their original sites within the sample (Sigmund P, 1969). If the collision cascade intersects the sample surface, target atoms leave the material and are said to be 'sputtered'. Whilst neutral atoms are usually the main constituent of the sputtered material, secondary electrons and ions make up a significant fraction of the ejected particles. Some of the positive or negative ions are extracted from the sample surface, analysed by a mass spectrometer and counted. As the material is being eroded, it is possible to build up information on the sputtered species concentrations as a function of depth.

The sensitivity of SIMS is species dependent, but in favourable situations the detection limit can be $<10^{14}$ atoms cm^{-3}. SIMS has been shown to be able to measure changes of impurity concentrations (dynamic range) over as many as seven orders of magnitude (von Criegen R *et al.*, 1990). Most depth profiling SIMS instruments are capable of analysing for all the elements in the periodic table, with some (especially time -of -flight mass spectrometers) having a mass range that extends to over 10^4 Daltons. Both mass range and mass resolution are dependent on the type of mass spectrometer used.

Depth resolution is predominantly dependent on the extent of the atomic mixing, resulting from energy deposition of the primary beam. The depth of mixing is governed by the energy of the primary ion beam, the mass ratio of the beam to target atoms, the

sputter yield, the incident angle of the primary beam and chemical segregation. Provided the sample surface is eroded uniformly across the region of interest and there is no degradation of the surface topography, depth resolution should be constant to depths of over 1 μm. Above 1 keV primary beam energies, the best achievable depth resolution is several nm, unless very glancing angles are employed (Wittmaack K, 1996a). Unfortunately as the primary beam energy is reduced to maximise depth resolution, the primary beam current is also reduced. Typically, primary ion guns are only capable of generating primary beam currents of <<50 nA at energies of ≤1 keV, making high resolution depth profiling time consuming and difficult for deep structures. For this reason analyses are typically performed at energies between 2 - 15 keV. However, the floating low energy ion gun (FLIG) developed by our group (Dowsett M G *et al.*, 1997; Smith N S, 1996), and fitted to all the SIMS instruments used for this work, overcomes the problem by transporting the ions close to the sample at high energy (typically 3-10 keV), before retarding them at the final lens. This makes possible currents of >1 μA at 1 keV and >200 nA at 250 eV.

The production of sputtered secondary ions was first recognised in 1910, during an experiment studying the wave-particle duality of the electron (Thomson J J, 1910). The first reported construction of a secondary ion mass spectrometer was in 1949 (Herzog R F K and Viehböck F, 1949). The first commercial SIMS analytical instrument was built by Herzog and co-workers in 1963, under a NASA contract to study the spatial and isotropic distributions of all elements from H to U in samples brought back to Earth (Liebl H J and Herzog R F K, 1963). By 1970, SIMS had emerged as a distinct technique which subsequently fragmented into many new variants *e.g.* sputtered neutral mass spectrometry (SNMS) that post-ionises sputtered neutrals before mass analysis, fast atom bombardment (FAB) SIMS that uses a neutral primary

atom beam for sample sputtering and laser ablation mass analysis (LAMA) that uses a laser as a means for sample ablation.

SIMS divides into two main areas, namely static SIMS and dynamic SIMS. Static SIMS (Benninghoven A, 1970) employs a low primary beam dose ($<10^{13}$ ions cm^{-2}) in order to explore the top monolayer of a sample, whilst the high primary beam current densities of dynamic SIMS (Wittmaack K, 1980) provide the means to analyse the top few microns of a material in depth.

The high sensitivity and dynamic range of SIMS is due to four fundamental attributes, which also establish its limitations (Dowsett M G and Clark E A, 1992):

1) Mass spectrometry is inherently background free, as the mass spectrum is discrete and not superimposed on a continuum. Giving a typical rejection ratio $I_M/I_{M\pm1}$ of $>10^8$, where I_M is the intensity recorded at mass M, etc.

2) Secondary ion yields are high in comparison with other analytical techniques, typically 10^{-1} -10^{-4}, giving useful quantitative precision for a small dose of primary ions. However, they are also very matrix dependent and vary by a factor of 10^4 or more across the matrix-species combinations of interest in microelectronic applications.

3) The analytical precision of SIMS is determined by the volume of material consumed to make the measurement, as is the detection limit (in the absence of a background signal). The fractional atomic concentration C_x of an atomic species X in a measurement which consumes N sample atoms is determined by

$$C_x = \frac{n_x}{NT_x\alpha_x} \qquad (3.1)$$

where n_x is the number of secondary ions of X detected; T_x is the product of the collection, transmission and detection efficiencies of the mass spectrometer for species X; and α_x is the emission probability for the charge state detected. T_x and α_x are

difficult to measure independently, however their product τ_x ($=T_x\alpha_x$) known as the useful yield of X, is easily obtained and is an indication of instrumental quality.

4) The interactions between the primary ion beam and sample lead to complex mass transport effects (see later) in the near surface region, because of energy deposition by the beam and the incorporation of the beam ions. These processes distort the sample's three-dimensional chemical distribution prior to measurement, and can lead to the development of surface topography. Whilst these effects can be minimised by the correct choice of experimental conditions, they can not be totally eliminated.

3.1 Applications of SIMS.

SIMS is recognised as one of the most useful techniques for the characterisation of industrial materials due to its high sensitivity, surface selectivity, good spatial resolution and depth profiling capabilities. It has been used to analyse a very diverse range of samples such as metals, semiconductors, polymers, ceramics and organic superlattice films. However, the main application area of dynamic SIMS remains the chemical analysis of semiconductors.

Several good comprehensive books have been written on the subject of dynamic SIMS, these include the 'Biblical tome' (Benninghoven *et al.*, 1987) and a comprehensive review (Briggs D and Seah M P, 1992). Up to date research and method development is published in the proceedings of the biannual Secondary ion mass spectrometry conference.

3.2 SIMS Instrumentation.

All SIMS instruments consist of the following main components (Jede R *et al.*, 1992):

Vacuum system

The vacuum chamber and its pumping system have to be designed and manufactured according to Ultra-High Vacuum (UHV) rules, in order to achieve good reproducibility and reasonable detection limits for species present in the residual gas. This is especially so for the analysis chamber as residual gas coverage of the sample affects the secondary ion yields in both static and dynamic SIMS.

In areas like the primary ion source or analysis chamber where gas loads occur, turbo-molecular pumps are preferred over diffusion pumps, due to their small size and also because the residual gas remains free of hydrocarbons, even in the absence of cold traps. If a SIMS instrument is operated using a noble gas ion gun, differential pumping by turbo-molecular pumps is advisable, especially if the pump attached to the analysis chamber is an ion pump.

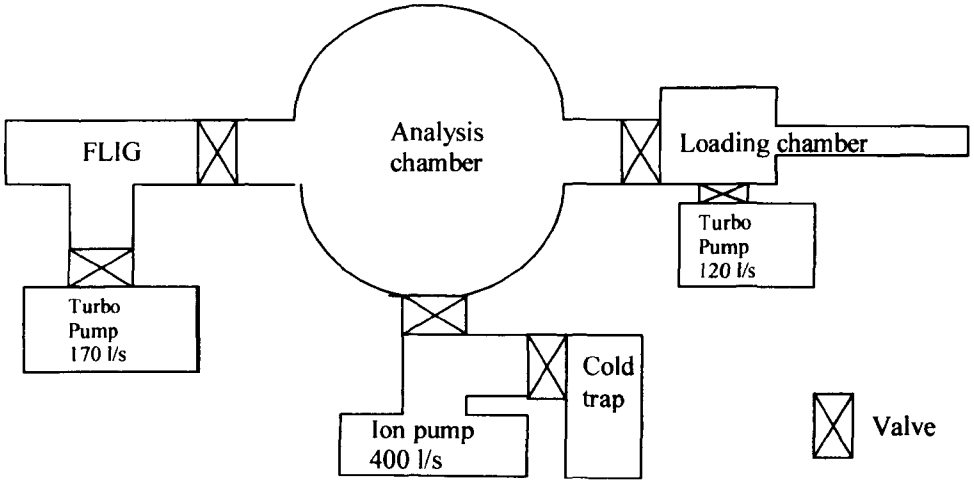

Figure 3.1: EVA3000 vacuum chamber.

Sample insertion system.

To enable relatively fast sample exchange without seriously affecting the vacuum in the main chamber, SIMS instruments are fitted with valveless or valved sample insertion locks. Modern instruments may have automatic sample loading capabilities to enhance system reproducibility, and some may allow sample sizes up to several inches in diameter for whole wafer analysis.

Sample manipulation stage.

This manual or automatic device is used to select the sample area for analysis, and sometimes to vary bombardment conditions i.e. by tilting the sample with respect to the ion beam (to optimise the ion yield).

Ion sources.

Three basic types of ion sources are used: gas phase sources (electron impact and plasma types), surface ionisation sources which are widely used for the generation of alkali metal ions, such as caesium (Alton G D, 1988) and liquid metal field emission ion sources (Prewett P D and Jefferies D K, 1980). This range of primary ion sources is needed to enable the many modes of SIMS, from static surface studies to quantitative depth profiling, and submicrometer elemental mapping. Plasma ion sources have become the workhorses for dynamic SIMS applications, with the duoplasmatron being the most popular.

All the work carried out in this thesis was carried out on instruments fitted with a duoplasmatron ion source (von Ardenne M, 1963; Cheniakin S P *et al.*, 1985) due to its many advantages. This type of ion source is capable of operating with reactive and inert gases without a hot filament, and generates an intense plasma in the vicinity of the

anode aperture thus it acts as a bright source of ions, with a narrow energy spread of only 10 eV (Drummond I W, 1984), and it also has the ability to produce negative ions with relatively few modifications. The duoplasmatron design used in this study (Dowsett M G, 1998), also has a relatively long lifetime of several months when operating on pure oxygen.

Primary ion optics.

The primary ion optics are needed to extract ions from the source, accelerate them, filter out impurities, eliminate neutrals formed by gas phase interactions down the beam line, and form a focused ion beam, which can be raster scanned across the sample surface. An example of which is shown in figure 3.2.

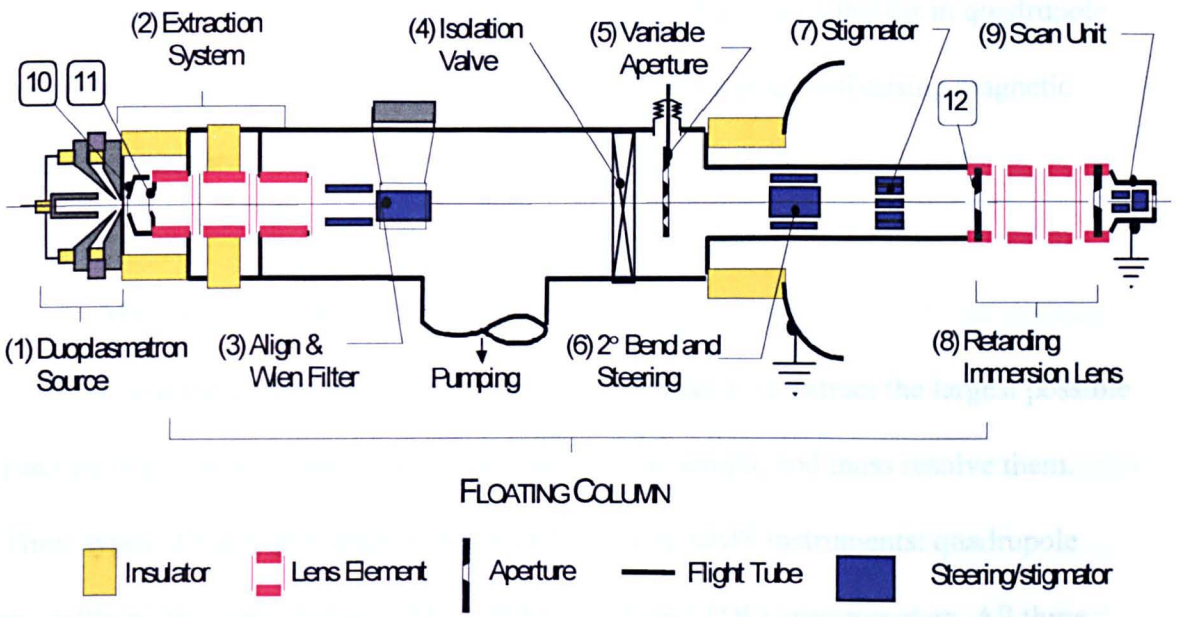

Figure 3.2: FLIG Schematic (Dowsett M G et al., 1997).

Secondary ion extraction and transfer optics.

The purpose of the secondary ion extraction and transfer optics serve is to collect as many ions as possible from the sputter region and to transfer them to the mass filter. They match the ion emittance from the sample to the acceptance of the mass filter. In a quadrupole based instrument the transfer optics are designed in order to inject the mass filter with a source of ions having a small energy spread of 10 - 20 eV and a mean beam energy of $\approx$ 10 eV. The mass resolving power of the quadrupole is highly dependent on the ion transit time, so only a small energy window is permissible.

Energy filter.

The energy filter selects an energy window from the broad energy distribution of the secondary ions for optimum mass filter operation and eliminates scattered primary ions. The energy filter may be a separate device from the mass filter (as in quadrupole based systems), or part of it (the electrostatic sector) in a double-focusing magnetic sector instrument.

Mass spectrometer.

The general requirement of a mass spectrometer is to extract the largest possible fraction of all the secondary ions sputtered from the sample and mass resolve them. Three types of mass spectrometer are widely used in SIMS instruments: quadrupole mass filters, magnetic sector field, and time-of-flight (TOF) spectrometers. All three types can be operated with a number of different ion species over a wide range of primary beam energies. The main limits of instrumental performance and application depend on the selection of the mass spectrometer type. It also has a strong influence on the design of the sample environment, secondary ion extraction system and detectors. It

also has performance implications, especially so when using ultra-low primary ion beam energies, to undertake accurate high depth resolution analysis of ultra-shallow implants.

Detector.

The detector in most cases operates in a pulse counting mode to detect single ions, and is typically either a channeltron or a secondary electron multiplier. Two-dimensional ion detection is possible using channel plate arrangements with either a fluorescent screen and camera arrangement or a resistive anode encoder.

Data acquisition and evaluation system.

Depending on the application, a wide range of computer systems is used, mainly based on personal computer systems or work stations. Two-dimensional imaging requires fast dedicated data systems with large memories. Many instruments are fully controlled by computers.

Charge compensation.

Many SIMS applications are performed on insulating samples, whose surfaces build up electrical charge during analysis. This charge can have dramatic effects on the SIMS analysis, altering the energy distribution of the secondary ions and their collection efficiency. The most common method for charge compensation is to employ simultaneous electron bombardment from a separate gun to flood the analysed surface with low energy electrons. The low energies enable the electrons to 'react' on local charge build up and lead to a self-adjusting compensation system.

Dynamic SIMS is one of the most powerful and highly regarded techniques for depth profile analysis, because of its combination of high depth resolution with low

detection limits (often at or below the PPM level). Drawbacks like its sample destructiveness, generally poor lateral resolution, and its large number of artefacts are tolerated because of these two unique assets.

Currently available SIMS instruments used for dopant depth profiling can generally be sub divided into three categories (i.e. Dual-beam TOF, quadrupole and magnetic sector based instruments). Double focusing mass spectrometers exploit the complementary energy dispersive properties of electrostatic and magnetic sector fields. Their main advantages are high secondary ion transmission, T_m, of the order of 10^{-2} or better, and very high mass resolution ($M/\Delta M$) of around 10^4 which enable them easily to analyse ^{31}P in Silicon. However, the two are inversely related. Most magnetic sector instrument designs use normal incidence secondary ion transfer optics, with consequently non-normal (>30°) primary ion beam incidence (Drummond I W, 1968). While this improves the extraction efficiency of the secondary ions, it introduces the disadvantage of primary beam deflection (Merris M *et al.*, 1989), especially at low primary ion beam energies. The primary ions must typically transverse through a 500 V/mm secondary ion extraction field. The main disadvantages with working at non-normal primary ion beam incidence at ultra-low energies are the deflection of the beam and the resulting non-uniform current density across the analysed area, the development of surface topography and the subsequent variations in erosion rates and ion yields at shallow depths <50 nm when using an oxygen primary beam to analyse silicon samples (see chapter 6). Other disadvantages are their relatively high cost and large size.

The main advantages of the quadrupole mass filter are their relative low cost and small size, the rapid switching of mass, and their low secondary ion extraction fields of only 2 V/mm. The low extraction field above the sample means the instruments

acceptance and transmission is less dependent on surface microtopography, or sample position. This operational flexibility is a major advantage, especially in a research environment.

The main disadvantages of quadrupole mass filters are their low mass range of typically 200, their lower transmission (*c.f.* magnetic sector and TOF instruments) and a mass resolution limit of a few thousand (enabling only unit mass separation).

The main advantages of the TOF mass spectrometer are their almost perfect extraction and transmission efficiencies, which along with parallel mass detection and their virtually unlimited mass range (>10^6 Daltons), means nearly 100% of the total secondary ion yield can be detected, together with high mass resolution of 10^4 or better and all at a relatively low cost. This is what makes TOF-SIMS a very powerful and attractive surface analysis technique, and has lead to its dominance in the field of static SIMS analysis.

The main disadvantages of TOF spectrometers for ultra-low energy (<1 keV) depth profiling are the secondary ion extraction potentials in the low kV regime, which are typically normal to the sample surface, leading to primary beam deflection and non-uniform current densities as in magnetic sector instruments, and the very low erosion rates resulting from using a pulsed primary ion beam, which is typically on for only 1-100 ns in every 50-200 μs cycle. At present, the low erosion rate of the dynamic profiling TOF-SIMS technique are negated by the use of a second low energy reactive probe (*e.*g. O_2^+ or SF_5^+) to erode the sample for the majority of the duty cycle (Benninghoven A *et al.*, 1997). The Cameca TOF-SIMS IV instrument can be simultaneously equipped with up to 4 ion sources, with the additional option of O_2 flooding to enhance the secondary ion yield and to slow the development and reduce the magnitude of surface topography, which can be a major problem at the typical angles

of incidence (52.5 ± 10°) used. This can lead to complicated altered layer been formed at two different beam energies and containing up to 3 new species e.g. Ar, SF_5 and O. This can have severe implications on the transient region in terms of stabilisation of ion yields and erosion rates, and the development of surface topography. As the size of microelectronic devices continually shrink the low erosion rate will cease to be as important. This along with further instrumental developments, TOF-SIMS has the potential to be a very useful tool for analysing ULSI technology.

As the quadrupole mass spectrometer only filters low-energy ions, all quadrupole based instruments apply a fairly small (2 V/mm) acceleration field to collect the secondary ions. This makes the region around the sample nearly field free. In contrast, magnetic sector based SIMS instruments, need to use a high acceleration field to provide adequate beam transport through the magnetic spectrometer. This large field between the sample and immersion plate of the secondary ion column encloses the entire sample area, this deflects the primary ion beam away from its nominal incidence axis of typically 30° when positive secondary ions are analysed, with a positive beam. This means that for each primary energy there is a different incidence angle and the two are strongly coupled. This is not true for all magnetic sector instruments for example the modified Vacuum Generators IX70S SIMS microprobe (Jiang Z X and Alkemade P F A,1997) can operate at angles between 56-77° at 1 keV net impact energy, by varying the voltage applied to the deceleration/extraction electrode, also recently there has been similar modifications made to the Cameca range of SIMS instruments (Schuhmacher M *et al.*, 2000). However, most magnetic sector based instruments still cannot operate with normal incidence primary ion bombardment. A few magnetic sector instruments have been designed to perform SIMS analysis using a primary ion beam at normal incidence, these include the ion microprobe mass analyser (Liebl H, 1967) and the

universal microprobe analyser (Liebl H, 1971) both designed by Liebl, and more recently the Cameca Nanosims 50 (Hillion F *et al.*, 1994). In fact the lower the primary beam energy, the higher the angle of incidence when the instrument is used in its normal mode of positive secondary ion detection, with positive primary ions, as in the case of oxygen bombardment. While the sputter yield decreases slowly with decreasing energy for a fixed angle of incidence, it is highly angle dependent ($\sim \cos^{-2}\theta$ for $\theta \leq 70°$) for a fixed energy (Wittmaack K, 1996a). Hence the sputter yield will be very high for the lowest primary beam energies, but the steady-state oxygen concentration is inversely proportional to the sputter yield. As the ionisation yield is extremely sensitive to the oxygen concentration ($\sim C(O)^n$, where $3 \leq n \leq 4$), this leads to low ionisation yields, and reduced steady-state matrix signals (Wittmaack K, 1981). Vandervorst and Shepherd (1987), showed an approximate 10 fold decrease in the steady-state matrix signal ($^{30}Si^+$) on decreasing the oxygen primary beam energy from 8 keV ($\theta = 37°$) to 1.5 keV ($\theta = 70°$), on a Cameca-3f ion microscope. Depending on the species of interest this effect maybe larger or smaller than that reported above. The non-normal incidence of the primary beam also results in a much larger transient region, resulting in greater uncertainty on the depth scales of shallow profiles.

The use of low primary beam energies in magnetic sector instruments is not as simple as in a quadrupole instruments. The deceleration of the beam by the high positive sample potential, results in poor beam focusing, while the large angle of incidence combined with the extraction field can make the beam spot very elongated in one direction. This can result in asymmetrical crater bottoms due to non-uniform current beam density and the development of surface topography, with only a small flat area, making reliable crater depth measurement difficult. However by reducing the

acceptance area of the secondary ion column, serious crater edge effects can still be avoided and profiles with good dynamic range can be obtained.

Erosion inhomogeneity results in a linear symmetrical decrease in resolution with depth ($\Delta z \propto z$). At shallow depths it is usually masked by other resolution-limiting or degrading contributions, like atomic mixing and chemical segregation, but eventually it will become a dominant factor. Erosion inhomogeneity can be caused by ion-induced sample roughening, but also by problems with focus variations over the rastered area, impact angle changes, and the effects of crater wall shadowing and redeposition, all of which are potentially greater problems at non-normal angles of incidence.

Oxygen flooding is often used with the objective of minimizing transient effects, and enhancing secondary ion yields. When the oxygen absorption rate on the sample is sufficiently high, a surface oxide layer will be formed continuously, leading to a more rapid ionisation yield enhancement. However it has several major disadvantages; the high pressure in the analysis chamber results in poorer focusing of the primary beam (through increased scattering with the residual gas atoms); the reduced sputter yield leads to longer measurement times but still faster than at normal incidence, larger decay lengths and higher background signals leading to a reduction in the observed dynamic range, along with poorer detection limits.

Decay lengths larger by a factor of 2-3 have been reported for As, when using either oxygen, caesium or argon as the primary ion species, in conjunction with oxygen flooding (Vandervorst W and Shepherd F R ,1987; Yu M L, 1981). The increase in decay length is due to the As atoms segregating at the SiO_2-Si interface, and being continuously pushed deeper into the sample. Direct evidence for this has been obtained by RBS analysis of an oxygen-bombarded As implant (Vandervorst W and Shepherd F R ,1986), the data showed a large pileup of As at the SiO_2-Si interface. A large number

of elements are known to segregate, therefore it is expected that the use of oxygen flooding, during their SIMS analysis would similarly lead to larger decay lengths.

The higher background signals observed when using oxygen flooding are particularly noticeable during boron analysis and are due to the increased scattering of secondary ions at higher pressures, leading to increased sputtering of the surrounding areas. Boron exhibits higher sticking coefficients on oxidised surfaces, and the resputtered material has a higher ionisation yields due to the high oxygen pressure (Wittmaack K, 1983). Differences in the memory effects of various elements (for instance As shows no deterioration in its dynamic range), are attributed to differences in their sticking coefficients and resputtering yields.

While these effects can be minimised by operating at lower oxygen pressures, the development of surface topography is known to be an even larger problem at intermediate oxygen pressures, especially at ultra-low beam energies (Jiang Z X and Alkemade P F A, 1998a; Jiang Z X and Alkemade P F A, 1998b; Vajo J J *et al.*, 1996). This means the optimum profiling conditions for silicon using oxygen primary ions at ultra-low beam energies is near-normal incidence. Although this may lead to longer analysis times, profiling rates of >20 nm/min have been reported (Maul J L and Patel S B, 1997) at 1 keV, this value is too rapid for accurate analysis of ultra-low energy implants, due to the requirement of obtaining sufficient data density in the top 2 nm of such microelectronic devices.

3.3 Sputtering.

In dynamic SIMS erosion of the sample surface is achieved by bombardment from an energetic primary ion/atom source (<1 keV to 15 keV). Only a small fraction

of the ion energy is returned into the vacuum by the backscattered species (the actual amount is dependent on the actual bombardment conditions, and is largest at oblique and grazing angles of incidence), most of the energy is dissipated via elastic and inelastic interactions. Electronic excitation and ionization processes are not significant at typical SIMS primary ion energies. The ensuing target erosion is a complex phenomenon, depending on primary ion type, energy and direction of incidence, in addition to a number of target material parameters.

The most widely accepted and successful theoretical explanation for neutral sputtering was developed by Sigmund (1969). From the Sigmund theory of sputtering, an energetic primary ion hitting the surface of a solid loses its energy in a series of elastic (nuclear energy loss) and inelastic (electronic) collisions with target atoms and electrons. Due to the large cross-section for elastic energy transfer, an incident ion will set many target atoms in motion, either directly or via collisions with primary knock-on atoms with other target atoms. Above a certain energy limit, the struck target atom may be displaced permanently from its original site. At 4 keV, the majority of displaced atoms travel distances of the order of 1 nm before coming to rest, but transport over a distance as large as 7 nm may take place occasionally. High energy recoils that are directed back out of the surface account for the majority of the sputtered energy, but lower energy recoils that surround the fast moving atoms account for the majority of the sputter yield. According to the theory, the peak of the energy distribution for the sputtered particles is made up from atoms that have originated from the first couple of atomic layers. Evidence for this is provided by the fact that the peak of the energy spectrum of the sputter material is peaked at low energies ~10 eV meaning that these atoms are likely to have been set in motion in the immediate locality of the surface. The overall interaction event is termed the 'collision cascade'. Generally, if the primary ion

kinetic energy is in the low keV regime, the target surface will intersect the cascade, so that the energy and momentum are transferred to the surface atoms. Sputtering takes place if recoiling atoms end up at the solid-interface with an outward directed momentum and an energy exceeding the surface potential barrier.

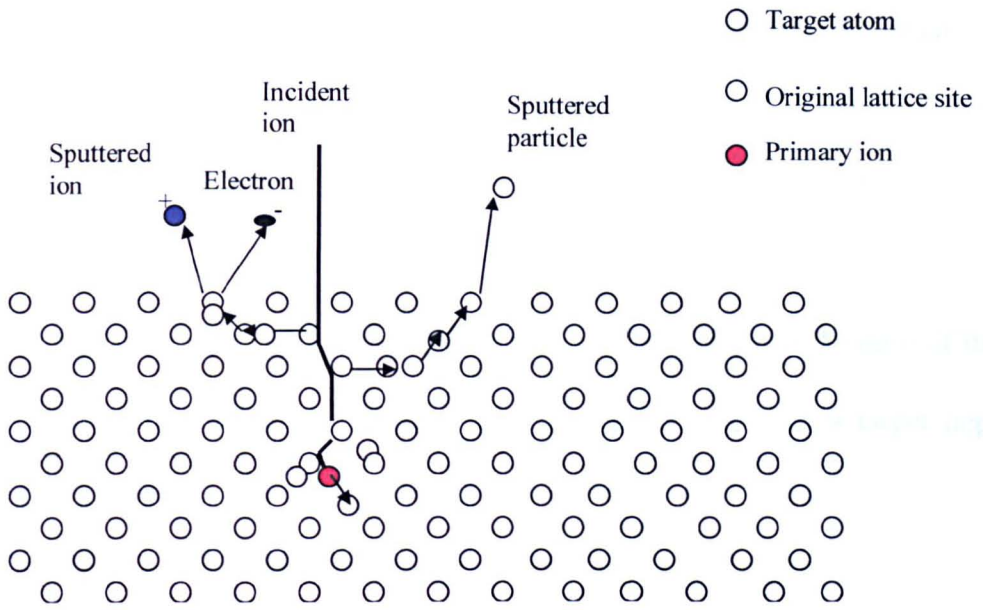

Figure 3.3: Two dimensional representation of a low energy collision cascade.

With 250 eV O_2^+ bombardment at normal incidence the thickness of the altered layer is still significantly thicker by a factor of 3-4 than the depth from which the majority of sputtered particles come from (Dowsett M G *et al.*, 2000). Each collision cascade can be thought as non-interactive events (Werner H W, 1974), when using typical primary beam current densities of a few 10's of mA/cm^2, has each event as a lifetime of approximately 10^{-12} s (Sigmund P, 1989) and a lateral range of around 10 nm.

From Sigmund's theory, the sputter yield Y_S (number of sputtered target atoms/primary ion) can be described as a function of primary beam energy:

$$Y_S(E) = \Lambda F(z, E) \tag{3.2}$$

where $F(z,E)$ is the deposited energy function at distance z below the surface. Sputtering therefore depends on the amount of energy deposited at the surface (where $z = 0$). In the limit of $z = 0$, the deposited energy function, $F(0,E)$ can be written

$$F(0, E) = \alpha N S_n(E) \tag{3.3}$$

where S_n the nuclear stopping cross-section and α is dependent on the ratio of the mass of the incident ion M_1, to the mass of the target atom, M_2. Λ is a target dependent parameter, given by

$$\Lambda = \left(\frac{0.042}{N U_O} \right) \tag{3.4}$$

Here, N is the atomic number density of the target ($Å^{-3}$) and U_O is the surface binding energy.

At low energies (<1 keV) and normal beam incidence, Sigmund has parameterised $S_n(E)$, to give a simplified expression for low energy sputtering (eqn. 3.5).

$$S(E) = \frac{3\alpha}{4\pi^2} \left(\frac{T_{\max}}{U_O} \right) \tag{3.5}$$

where T_{max} is the maximum recoil energy of the target atoms.

Equation (3.5) implies a linear energy dependence of sputter yield at low energies (at energies above 1 keV, the dependence is much weaker).

3.4 Secondary Ion Emission.

A small percentage of the sputtered particles ejected from a sample surface during ion bombardment is itself ionized, and it is this phenomenon of secondary ion emission that SIMS exploits. Useful ion yields (number of detected secondary ions per primary particle), vary over many orders of magnitude for different elements and are dependent on the detailed chemistry at the sputtered surface. The diversity of experimental data has led to many different theoretical models which describe ion emission with varying degrees of success. There are, however, some qualitatively reproducible phenomena that need to be explained by any accepted model.

The kinetic energy distribution of atomic secondary ions, has an intense peak at between 5 eV and 20 eV, with a high energy tail extending to over 100 eV. However, molecular ion distributions show a much reduced intensity at energies above 50 eV. Generally speaking, the more atoms in the molecular ion, the narrower the energy distribution.

An important requirement for any secondary ion emission model is that it can account for the selective enhancement of ion yields through the use of reactive primary ion beams, such as O_2^+ and Cs^+. The use of these primary ion types can result in secondary ion yield enhancements of more than 5 orders of magnitude.

3.5 The Interaction Of The Primary Beam With The Sample.

The near-surface composition of multi-component samples changes as a result of ion bombardment, several physical and chemical processes have been identified. These processes are preferential sputtering, collisional mixing (or displacement mixing), radiation-enhanced diffusion, radiation-induced Gibbsian surface segregation (or Gibbsian adsorption) as well as radiation- and implantation-induced (bulk) segregation.

One of the most important aspects of ion implantation phenomena is that the sputtering yield varies dramatically whilst equilibrium is been established. Accurate depth calibration of the recorded data in the pre-equilibrium region is extremely difficult. Apart from the problems encountered in passing through the pre-equilibrium region, it introduces an apparent shift in the rest of the profile. For boron in silicon, analysis at normal incidence the shift towards the surface has been reported to be approximately 2 nm/keV/atom for oxygen (Wittmaack K and Wach W, 1981; Clegg J B, 1987). The size of the pre-equilibrium region at oblique angles of incidence using oxygen ion bombardment has been found to be larger than at normal incidence (Vandervorst W and Shepherd F R, 1985), although the induced shifts maybe smaller.

Oxygen, caesium, gallium and argon are the most commonly used species in primary ion beams. The reactive species are used to enhance ion yields, with oxygen being used to enhance positive ion yields. When a solid is bombarded by a beam of ions, the accompanying sputtering, beam-induced mixing and probe incorporation lead to the formation of an altered layer in the surface of the sample (Littmark U and Hofer W O, 1980; Sigmund P and Grasmarti A, 1981). The extent, structure and properties of the resulting altered layer, is responsible for the measurement induced distortions in a SIMS depth profile experiment. All the processes that give rise to distortions in SIMS

data take place in this altered layer or at its boundaries. In addition the observed ion yields are determined by the chemistry of the top 2-3 monolayers of the altered layer.

If (doped) silicon samples are analysed by SIMS using either oxygen or nitrogen beam induced oxide or nitride formation occurs (Sigmund P, 1983). Due to the implantation and incorporation of oxygen (or nitrogen) the sputtering yield of the matrix is typically reduced by a factor of two relative to the yield predicted from data obtained using noble gas bombardment. This is due to the fact that in the equilibrium region the deposited energy is used not only to remove matrix and dopant atoms, but also previously implanted and reacted oxygen or nitrogen atoms.

In the case of silicon bombarded with oxygen at angles of incidence <20° (the exact angle increases as the primary beam energy decreases) the sample surface is known to be converted to SiO_2 over a depth related to the range of the primary ions (Wittmaack K, 1992). At larger angles of incidence the amount of oxygen retained in the sample decreases rapidly, so only a suboxide is formed. This leads to large variations in the sputtering yield for small increase in the angle of incidence.

There have been many studies of the SiO_2 altered layer formed when a silicon matrix is bombarded with an oxygen beam under varying conditions, for which techniques such as RBS (Gill S S and Wilson J H, 1978), XPS (Schulze D *et al.*, 1983) and transmission electron microscopy (TEM) have been employed (Dowsett M G and Clark E A, 1992). Under near-normal incidence bombardment and beam energies ≥ 1 keV, a thick stoichiometric SiO_2 layer is formed, with a thickness of ~ 4-4.5 nm/keV (Dowsett M G and Clark E A, 1992; Dowsett M G *et al.* 2000; Fox H S *et al.*, 1991), beneath which a thin SiO_x sub-oxide layer resides, providing a sharp transition to the unperturbed silicon matrix. At beam energies < 1 keV, the width of the stoichiometric

SiO_2 layer formed departs from the above formula becoming thicker (e.g 2.6 nm at 250 eV O_2^+).

An ion dose of the order of 10^{17} ions cm^{-2} is required to bring the altered layer to steady state, and in the pre-equilibrium period, sputtered depth and ion yields do not scale proportionately with primary ion dose or analyte concentration respectively. Consequently sample features within the depth sputtered by this ion dose are regarded as being unquantifiable (Wittmaack K and Wach W, 1981). Once equilibrium has been attained, the width and chemical nature of the altered layer imposes a limitation on depth resolution, mainly due to cascade mixing or chemical segregation (Boudewijn P R *et al.*, 1984).

The formation and presence of the altered layer also introduces problems with depth calibration of sample features. Typically, the sputtered crater depth is measured ex-situ with a surface profilometer. The depth calibration of the profile data is then done under the assumption that the erosion rate is constant and that the crater depth measured represents the depth of material removed. However, the erosion rate in the pre-equilibrium region is faster than that in the post-equilibrium region. In addition, the depth of the measured crater will be a little less than the depth of material removed during the SIMS experiment, since the incorporation of oxygen in the eroded surface results in a slightly swollen crater base. 4.4 Å of silicon swell up to 10 Å of silicon dioxide when grown by thermal oxidation (Sze S M, 1985). As a consequence, the measured depth of sample features are displaced from their actual depth, by an amount dependent on the altered layer thickness. This contributes towards the effect known as the differential shift and consequently is reduced by the use of low beam energies.

The formation of the SiO_2 altered layer is intimately linked to the observation of chemical segregation for dopants such as copper (Boudewijn P R *et al.*, 1984) and the

anomalous redistribution of arsenic and germanium (Dowsett M G *et al.*, 1990; Vandervorst W and Remmeire J, 1986) during analysis.

Unfortunately for accurate quantitative analyses, features of interest must be buried to at least the depth eroded during equilibration plus the altered layer thickness. Until recently, primary ion energies used in routine depth profiling were in the range 2-15 keV at angles from 45° to normal incidence. Under these conditions, tens of nm of sample are sputtered before equilibrium is achieved, with accompanying large variations in secondary ion signals (known as surface transients), hence special precautions must be taken if accurate quantifiable data is to be obtained from the top 50 nm of a sample. At present, few people attempt to accurately quantify data from the pre-equilibrium region, choosing either to ignore the data or to quantify the entire profile with a single calibration factor and sputter rate.

However, the size of microelectronic devices continue to shrink, with shallow dopants and very thin gate dielectric layers. The junction depths of CMOS transistors will soon require SIMS instrumentation to reliably measure junction profiles of less than 15 nm, with a depth resolution of < 1 nm (Corcoran S F, 1997). Many analytical problems require dopant profiles through interfacial regions e.g. thin silicon dioxide or oxynitride layers for gate dielectrics in MOS devices. The quantification of dopant distributions across interfacial regions is extremely difficult, due to variations in sputter yield and sputter rate across the interface, and whilst a new altered layer is established. It has been shown that different analytical conditions can result in profiles of completely difference appearance (Morgan A E and Maillot P, 1987).

Inevitably, when depth profiling with an O_2^+ primary ion beam after the start of the profile there will be a finite depth eroded whilst the surface chemistry equilibrates. During this initial transient time period, when the altered layer is forming, the generated

ion yield is unquantifiable. As a consequence, information regarding near surface features can be lost (see section 5.1.3). As mentioned previously, the reduction in primary beam energy results in a reduced altered layer thickness, enabling accurate quantification at shallower depths as well as improving depth resolution.

4.0 Experimental

4.1 Introduction

The experiments described in this thesis can be divided into two distinct areas; those concerned with the determination of an accurate depth scale, and those investigating the development of surface topography.

4.2 Depth Profile Quantification

Depth profile data was collected as ion counts/frame (ion counts/second on the Atomika 4500 SIMS instrument) using an electronically defined gate (Von Criegern R and Weitzel I, 1984). On the Atomika 4500 instrument the size of this gate can be adjusted post-analysis to maximise sensitivity, whilst ensuring crater-edge effects remain minimal. In the case of a single matrix sample containing analyte(s) whose concentration remain below the dilute limit (≈1%), quantification normally involves the linear mapping of the frame number and count rate, to the depth and concentration respectively. This process assumes there is no variation in either the ion yield or erosion rate in the pre-equilibrium region, the latter gives rise to the differential shift (Wittmaack K and Wach W, 1981).

Generally with any SIMS experiment the depth scale is calibrated post-analysis by measuring the crater depth, using a surface profilometer of some description. In all the experiments carried out at Warwick, a DekTak 3030 has been used for crater depth measurements. This method can measure crater depths with an accuracy of at best of

2% (Wittmaack W, 1996a). However the accuracy of the DekTak measurement tends to be poorer on shallower craters, and when the sample is not perfectly flat. As this measurement can only be carried out post-analysis it requires the erosion rate to be constant during analysis for a single matrix sample, or a prior knowledge of relative erosion rates for multi-layer structures. Figure 4.1 shows a typical trace acquired with the DekTak 3030 (in this case eroded with a 500 eV O_2^+ beam at normal incidence).

A range of reference materials was used to provide absolute sensitivity factors for the conversion of counts to concentration.

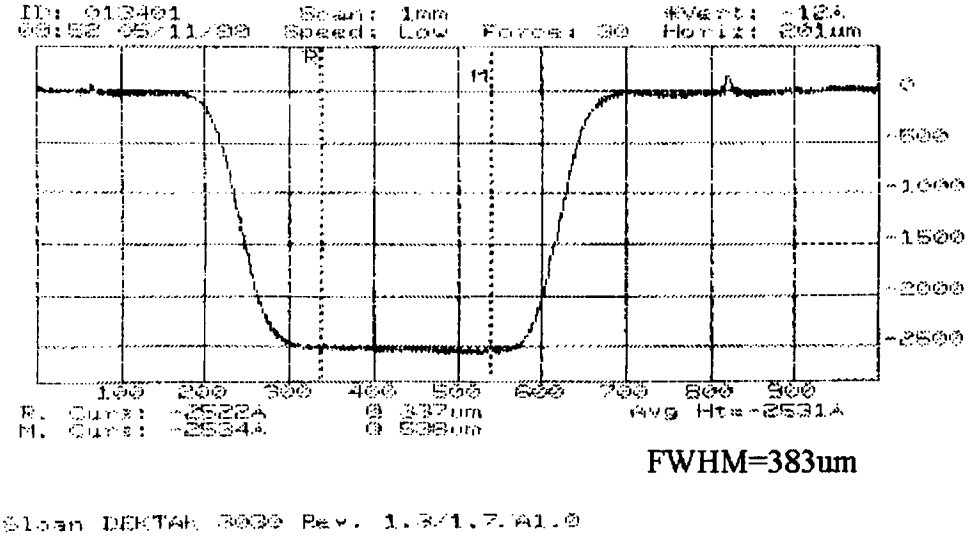

Figure 4.1: Example of a crater depth measurement, obtained with a DekTak 3030 surface profilometer.

4.3 SIMS Depth Profiling Experiments at Ultra-Low Energies

Outlined below is the general procedure used for all the experiments described in this thesis, unless otherwise stated.

The samples along with a suitable standard were mounted in a sample holder and placed into the load lock of one of the SIMS instruments, which was evacuated with a

turbomolecular pump until the pressure decreased to 1 - 5 x 10^{-6} torr, when the sample was transferred into the main sample analysis chamber. After selecting the required beam energy the voltages in the FLIG™ were adjusted to tune first for maximum current and then for spot shape in both the x- and y- scan directions. This is achieved by scanning the ion beam across a 500 x 500 μm square hole (a 300 or 600 μm circle on the Atomika 4500), and monitoring the ion current on an oscilloscope using the scan voltage as the second input. Both the shape and the size of the spot can be estimated using this procedure, by assuming it is Gaussian in shape, the 83 - 16% (2σ) drop in the current can be used to describe the probe diameter. Particular attention must be paid to the rate of decay in the last 16% of the probe current, to ensure the core of the beam does not have an extended tail or halo as the resultant SIMS depth profile would then exhibit a poor dynamic range.

The secondary ion column and quadrupole mass spectrometer settings for the mass channels of interest were adjusted for maximum sensitivity. Occasionally a different sample bias would be applied to a silicon matrix channel, to protect the channeltron from an excessive count rate. Typically a spot with a diameter of 30-50 μm and a current of 50-200 nA was rastered over a 500 X 500 μm area of the sample, the generated data collected for the desired time period and stored on a computer.

4.3.1 Surface Transient Studies

For the initial studies pieces of a phosphorous doped (35 - 65 Ω cm) float zone (100) silicon wafer was dipped in 5% HF solution in de-ionised water for 150 seconds, until the surface dewetted perfectly. The surface was not subsequently rinsed to avoid any reaction with de-ionised water. For one experiment the wafer surface was allowed to

age in laboratory air for varying periods prior to analysis, otherwise the samples were transferred into the load lock of EVA3000 within 1.5 hours. The undipped wafer (≥ 7 years old) is expected to have approximately 1 nm of native oxide on the surface and was used as a reference.

Analyses were obtained using an O_2^+ beam at seven primary energies 300 eV ≤ *Ep* ≤ 2.5 keV (i.e. between 150 eV and 1.25 keV per oxygen atom) all at normal incidence on EVA3000. The transient behaviour of Si^+, SiO^+, SiO_2^+, Si_2O^+ and O^+ were recorded, together with B^+ and F^+ as indicators of surface contamination, and HF residue. Note that at normal incidence, and in this energy range we find that all the Si and O related transients come to equilibrium at the same dose, which is not the case for all other angles of incidence (Wittmaack K and Corcoran S F, 1998; Jaing Z X and Alkemade P F A, 1999). A visual estimate of the dose at which the gradient of the SiO^+ signal had dropped to zero was found to provide a consistent definition of the dose to equilibrium ϕ_{tr}.

The dose scale was converted to apparent depth using uniform erosion rates for low energy ions (Smith N S, 1996; Gibbons R).

Later studies used sample 25.47 which was grown by silicon MBE at a nominal temperature of 500 °C and contained 10 boron delta doped layers with an approximate spacing of 18 nm. The peak maximum and centroid position for all ten of the boron delta layers had previously been determined. The sample after HF dipping was analysed using a normally incident O_2^+ beam at six primary beam energies 230 eV ≤ E_p ≤ 10 keV on EVA3000. The apparent transition width was taken as the position where the $^{30}Si^+$ intensities reached 95% of the equilibrium level. The true transient width was calculated using the known depth of the next two delta layers beyond the equilibrium point, from which the post-equilibrium steady state erosion rate can be calculated.

This latter procedure was also used, when dipped pieces of sample 25.47 was analysed on EVA2000FL using a 490 eV O_2^+ beam at five different angles of incidence in the range 0 - 60°, in order to determine apparent and true transient widths under these analysis conditions.

4.3.2 Determination of the Terminal Shift

Two samples containing multiple boron delta doped layers were used during this investigation. In all cases immediately prior to analysis, the analyte surface was dipped in a 5 % HF solution in de-ionised water until the surface was fully hydrophobic. Therefore, all profiles started on a surface with similar properties. The first sample (25.47) was grown by silicon MBE at a nominal temperature of 500 °C and contained 10 boron delta doped layers with an approximate spacing of 18 nm. The HF dipped sample was analysed using a normally incidence O_2^+ beam at six primary beam energies 230 eV $\leq E_p \leq$ 10 keV on EVA3000.

At each of the six primary beam energies used, the apparent centroid and apparent peak maximum positions of each of the 10 delta layers in the sample were determined. For each delta layer, the centroid and peak maximum positions were plotted against primary beam energy, and the relevant z_o values determined by fitting the data with a polynomial. To minimise any possible errors in the data, theoretical values of the peak centroid position were calculated (using the equations from the polynomial fit). The difference between the z_o values and the theoretical values was then calculated for each delta layer, and plotted against the apparent depth at each E_p. The data at each energy was fitted with an exponential linear curve fit function of the general form.

$$Y = a_1 e^{-X/a2} + a_3 + a_4 X \qquad (4.1)$$

The linear region at each energy was extrapolated to the measured crater depth, to calculate the terminal shift.

To confirm the size of the terminal shift obtained using sample 25.47, which for boron, the magnitude was found to be almost identical to the total thickness of beam synthesised oxide, a second sample 59.25 was also analysed. Sample 59.25 nominally contained 16 boron delta layers all at a concentration of 5E13 atoms cm^{-2} whose spacing was as follows; 5 delta layers spaced 5 nm apart , followed by 9 delta layers spaced 15 nm apart, 1 delta layer spaced 10 nm apart, and 1 delta layer spaced 5 nm apart. The HF dipped sample was analysed using a normally incidence O_2^+ beam at seven primary beam energies 230 eV $\leq E_p \leq$ 4 keV on EVA2000FL. The same data processing steps were repeated for this data set, and a similar result obtained.

To provide further data on the terminal shift a simpler set of experiments was carried out on the second sample 59.25. An undipped piece of this sample was profiled to different depths using a normally incidence O_2^+ beam at 3 keV on the Atomika 4500 SIMS instrument.

4.3.3 Dual Beam Energy Profiling

This section investigates the use of matching the primary beam ion energy to the requirements of the analysis, in particularly the quantification issues of changing the beam energy within a single depth profile.

The technique of dual energy profiling is ideally suited to shallow implant analysis, as both high resolution and high sensitivity are available in the desired parts of the profile, whilst the analysis time can be significantly decreased. As the trend of using lower implantation energies during the manufacture of modern semiconductors

continues, it will require the use of lower primary beam energies for accurate quantification and implant shape determination. However this leads to decreases in available current, ion yields and sputter yields, leading to extended analysis times and decreased sensitivity, but these disadvantages can be avoided by switching the beam energy to a higher value.

During the measurement of ultra-shallow implants using dual beam energy profiling, we naturally start with a very low energy to minimise the unquantifable pre-equilibrium region. The beam energy is increased once the measured decay length is smaller than the limiting decay length at the second higher energy. The opposite case, of lowering the beam energy was also investigated, for the application of detailed analysis of deep structures and interfaces.

Sample 59.25 containing sixteen boron delta layers all at a concentration of 5E13 atoms cm^{-2} whose spacing was as follows; 5 delta layers spaced 5 nm apart , followed by 9 delta layers spaced 15 nm apart, 1 delta layer spaced 10 nm apart, and 1 delta layer spaced 5 nm apart, was used to characterise any shifts in the profile. This sample has been carefully characterised, and the z_0 position of each delta layer is known, thus providing at least two of these layers are included the sample is self calibrating in depth. Three O_2^+ primary beam energies at normal incidence were investigated, 250 eV - for very high depth resolution and near surface quantification, 500 eV - for a higher erosion rate and good depth resolution, 1 keV - for a fast erosion rate and best sensitivity. Increasing the beam energy above 1 keV, brings little improvement in sensitivity or erosion rate, while the depth resolution continues to degrade.

Prior to performing the measurements on EVA2000FL the three sets of analysis conditions were optimised, and the individual settings saved. In order that the profile can be carried out in the same crater at two different beam energies it is necessary to

have accurate registration of the beam position. This was accomplished by ion imaging a feature at each energy and using the scan offset control to centre the feature in the scanned area. With this information also recorded the beam energy can easily be switched, the settling time of the primary column is approximately 2 seconds, during which time the beam is blanked. A further precaution of reducing the size of the raster from an initially large 900 μm to 500 μm at the second energy was also taken, as any contribution to the signal from the crater walls, or from the surface, to the recorded profile could have a significant detrimental affect on the dynamic range.

On quantifying the depth profiles obtained by switching the beam energy from 250 to 1000 eV, 500 to 1000 eV and 1000 to 250 eV, it was found that the only correction needed to the depth scale was the transient shift associated with the first energy used i.e. there is no depth correction required at the second energy (< 0.1 nm). Each dual-energy profile did contain a secondary transient region on switching the beam energy, there is a region (typically 0.8 - 1.0 nm) where there is a change in ion yield, but provided that this does not obscure a feature it can be neglected from the final result.

4.3.4 Depth Resolution at Ultra-Low Primary Beam Energies

The depth resolution pertaining to a particular set of experimental conditions was investigated using two samples containing multiple boron delta layers, over a wide range of energies at normal incidence, and also at various angles of incidence at two primary beam energies of 500 and 1000 eV. A limited amount of data at 500 eV was also obtained utilising the technique of oxygen flooding at various angles of incidence.

The first sample (25.47) was grown by silicon MBE at a nominal temperature of 500 °C and contained 10 boron delta doped layers with an approximate spacing of

18 nm. Sample 25.47 was analysed at normal incidence on EVA2000FL at five primary beam energies in the range 230 eV $\leq E_p \leq$ 5.01 keV and also at five angles of incidence at E_p = 490 eV in the range $0 \leq \theta \leq 60°$. After depth calibration, the FWHM for each of the 10 delta layers was determined by two separate methods; the first using our in house software Prowin and secondly by plotting the data in Origin (version 4.1) and physically measuring the parameter. Both methods gave almost identical results for all the data ($\pm$ 0.1 nm).

The second sample (59.25) nominally contained 16 boron delta layers all at a concentration of 5E13 atoms cm^{-2} whose spacing was as follows; 5 delta layers spaced 5 nm apart , followed by 9 delta layers spaced 15 nm apart, 1 delta layer spaced 10 nm apart, and 1 delta layer spaced 5 nm apart. The sample was analysed using an O_2^+ beam at two primary beam energies of 500 and 1000 eV at various angles of incidence in the range $0 \leq \theta \leq 65°$ on the Atomika 4500 instrument. This time the data was only processed using Prowin software.

4.3.5 Sputter Yield as a Function of Energy and Angle of Incidence

The sputter yields for silicon under O_2^+ bombardment are fairly well characterised for primary beam energies above 1 keV (Wittmaack K,1992), especially at normal incidence. However, the variation of sputter yield at ion beam energies at and below 1 keV have not been extensively published prior to starting this work, especially at non normal incidence. It was important to assess the stability and variation of sputter yield as a function of both depth and angle of ion bombardment, as much faster erosion rates are possible at non-normal angles of incidence and also possibly better depth resolution.

The sputter yield Y, can be easily calculated provided the volume of crater is known, V, for a given primary ion beam current, I_p, eroding the sample over a given period of time, t.

$$Y = \frac{V \rho q}{I_p t} \qquad (4.2)$$

Where ρ is the atomic density of the material and q is the charge of an electron. V is determined from the DekTak profiles, acquired in both x- and y-scan directions. The accuracy of this latter measurement is limited by the formation of the altered layer and surface topography effects, especially so for shallow craters (< 50 nm deep) and also those eroded at high beam energies (> 5 keV).

Sample 59.25 was analysed at two beam energies of 500 eV and 1 keV over the range of angles of incidence 0 - 65°, on the Atomika 4500 SIMS instrument. Post SIMS profiling, the depth and the FWHM width of the craters in both the x- and y- scan directions, were carefully determined using a DekTak 3030. The average sputter yield for each crater, and hence analysis condition was determined using equation 4.2.

The relative erosion rates were calculated by dividing the apparent distance between two adjacent peak centroid positions in the quantified depth profiles by the true distance between the same data points, using the previously determined z_0 values.

5.0 Determination of an Accurate Depth Scale

Since the invention of the bipolar transistor in 1947, there has been considerable competition and investment in increasing the switching speed of semiconductor devices. This has been achieved by reducing the lateral dimensions of semiconductor devices by a factor of 4 and in-depth dimensions by some two orders of magnitude. This not only results in faster devices, but also has the added economic advantage that a greater number of chips per wafer can be produced. While this cannot continue indefinitely, there are no obvious signs that the rate of change is slowing. A consequence of this, is the need for increasing control of the processes involved in the manufacture of integrated circuit technology, which in turn places more stringent demands on the supporting analytical techniques (Zalm P C, 1995). Accurate device and process modelling requires quantified electrical and dopant profiles from the outermost few nanometers. SIMS is a well developed analytical technique capable of measuring dopant concentration depth profiles, and is commonly used in the semiconductor industry. Accurate information is only now becoming available for ultra-shallow implants, through the utilisation of ultra-low energy SIMS. This is because the analysis of these structures at conventional energies results in undetected material because of the relatively large transient region, as well as distortion of the profile shape by the high degree of atomic mixing. Nevertheless, accurate analysis of ultra-shallow junctions remains a major challenge (Wittmaack K and Corcoran S F, 1998; Jiang Z X and Alkemade P F A, 1998b).

As SIMS is based on ion beam sputtering, the transient region before equilibrium is reached poses a serious problem (Vandervorst W *et al.*, 1985). During this surface transient, the secondary ion intensities can vary over several orders of

magnitude, and the erosion rate may reduce by a factor of more than 10, for a perfectly clean silicon surface at sub-keV energies (Wittmaack K, 1996a). Surface transients are intrinsically associated with the removal of the native oxide and the build-up of the primary ions at and below the surface. Generally it is assumed that the achievement of constant matrix secondary ion intensities are indicative of equilibrium in sputtering and hence erosion rate. Recently Jiang and Alkemade (1999) have proposed that this is not the case, and that "the dose needed at normal incidence to form a full and stable oxide layer and hence to achieve stable ionisation probabilities might deviate substantially from the dose needed to obtain equilibrium in sputtering because chemistry, and not the balance between implantation and sputtering, determines the stable oxygen/silicon ratio at near-normal incidence." At oblique incidence (no oxygen flood) the equilibrium oxygen content is much lower and therefore, chemical effects related to the formation of an oxide do not interfere with the establishment of equilibrium in sputtering. However, at non-normal incidence several workers (Wittmaack K and Corcoran S F, 1998; Chu D P *et al.*, 1998; Jiang Z X and Alkemade P F A, 1999) have found that not all the matrix signals reach equilibrium at the same depth (dose). Jiang and Alkemade (1999) have shown during the analysis of $Si_{30}Ge_{70}$ using 1.0 keV O_2^+ at 60°, that whilst the Si^+, SiO^+, Ge^+ and GeO^+ all reach equilibrium at a depth of 5.2 ± 0.2 nm, the O^+ signal achieves this at a depth of 4.6 nm, more than a 10% difference. The lowest value for the transition width reported in their work was 3.2 nm for 560 eV O_2^+ at 70°.

There are two key differences between ULSI and VLSI technology:

Firstly, a significant part of the implanted dose is in the top few nm of the wafer, which are also of unknown composition and morphology. There may be a native or thin gate oxide present, and the surface may be crystalline or amorphized, these can all be factors affecting the rate of oxidation on exposure to air (Dowsett M G *et al.*, 1998a).

These factors will all influence ion yields and erosion rates, therefore if the sample is to be quantified accurately, a great deal must be known about its composition.

Secondly, the near surface region may be less than 70% silicon, due to dopant concentrations as high as 10% (Bennent J, 1998), and in the case of an ultra-low energy BF_2 implant, the total impurity (boron and fluorine) level may rise to 30% for a 10^{14} cm^{-2} dose. In addition the use of preamorphizing implants, such as germanium, can lead to a further variation in the matrix composition. Little is known about SIMS in this non-dilute regime, except that significant yield and/or erosion rate variations are to be expected (Canteri R *et al.*, 1992).

This leads to six key requirements for accurate ultra-shallow profiling (Dowsett M G, 1998).

I. All important parts of the profile should be beyond the transient region, otherwise some of the profile will be entirely the wrong shape and cannot be accurately quantified by any known means, however reproducible it maybe.

II. The erosion rate, beyond the transient region must be constant.

III. The erosion rate must be commensurate with the required resolution and accuracy. Low erosion rates of the order of 0.1 nm s^{-1} are mandatory for ultra-shallow profiling. In order to sample the minimum number of data points (at least 10 per nm), with the required precision of at least 1%.

IV. The SIMS depth resolution must be sufficient to reveal the implant structure.

V. If the total impurity level is above the dilute limit (>1%), steps must be taken to establish the size of any resulting matrix effects, and minimize any errors through the use of appropriate measurement conditions, or an accurate quantification procedure used.

VI. Factors such as the change of erosion rate across the transient region, and the presence of oxide on the surface will affect the accuracy of the depth scale by up to several nm (Wittmaack K, 1996b; Wittmaack K and Corcoran S F, 1998).

5.1 Experiments on the Surface Transient Region.

Depending on the experimental conditions (primary ion energy and species, angle of incidence, and substrate material) a significant amount of material (and profile information) is removed during this transient region. It is therefore of prime importance to limit the thickness of the transient region when profiling very shallow structures, in order to minimise any errors in the quantification process.

5.1.1 Dependence of the Ion Dose and Transient Width on Primary Beam Energy in the keV and Sub-keV Regime.

The transient behaviour of silicon and oxygen related signals were recorded for a normally incident O_2^+ beam at seven primary energies 300 eV $\leq Ep \leq$ 2.5 keV (i.e. between 150 eV and 1.25 keV per oxygen atom). The samples were a phosphorous doped (35-65 Ω cm) float zone (100) silicon wafer ≥ 7 years old, and the same wafer dipped in 5% HF solution in de-ionized water until the surface dewetted perfectly. The latter surface was not subsequently rinsed to avoid any reaction with de-ionized water. These are referred to as undipped and dipped respectively. The undipped sample is expected to have approximately 1 nm of native oxide on the surface, whilst the dipped sample should maintain negligible levels of native oxide for several weeks after HF dipping (Gräf D *et al.*, 1990). SIMS depth profiling was carried out in the EVA 3000

SIMS instrument using the floating low energy gun (FLIG) designed by Dowsett (Smith N S *et al.*, 1997; Dowsett M G *et al.*, 1997). The transient behaviour of Si^+, SiO^+, SiO_2^+, Si_2O^+ and O^+ were recorded, together with B^+ and F^+ as indicators of surface contamination, and HF residue. Note that at normal incidence, and in this energy range we find that all the Si and O related transients come to equilibrium at the same dose, which is not the case for all other angles of incidence (Wittmaack K and Corcoran S F, 1998; Jaing Z X and Alkemade P F A, 1999). A visual estimate of the dose at which the gradient of the SiO^+ signal had dropped to zero was found to provide a consistent definition of the dose to equilibrium ϕ_{tr}.

No significant fluorine signal was detected in any of the wafer profiles. The undipped wafer exhibited a low level of boron at the surface which is very common in wafers with native oxide. This decreased by a factor of 100 in 2 nm apparent depth at 300 eV (decay length $\approx$0.4 nm).

Figure 5.1 shows the general appearance of the data for the undipped surface. The species displayed are Si^+ and SiO^+, at 2.5 keV (Figure 5.1(a)) and 300 eV (Figure 5.1(b)). The abscissae are ion dose. The 2.5 keV data are typical of previously published normal incidence surface transients - a surface spike, followed by a minimum and a rise to a plateau. However, the 300 eV data are quite different - there is no surface spike, and the signals rise monotonically from a very low level.

Figures 5.2 (a) and (b) show the same combination of data for a dipped sample, pumped down within 1.5 h after dipping. The surface spike is again only visible for the high energy data, but the minimum is lower and occurs for a lower dose than that for the reference wafer (see also Figure 2(b) in Ref. [Wittmaack K, 1996a]). The 300 eV data shows significantly lower near surface intensities than for the undipped wafer. Both high and low energy data are consistent with a significantly thinner native oxide on the

dipped sample, but one should not conclude at this stage that either gives any indication of its thickness.

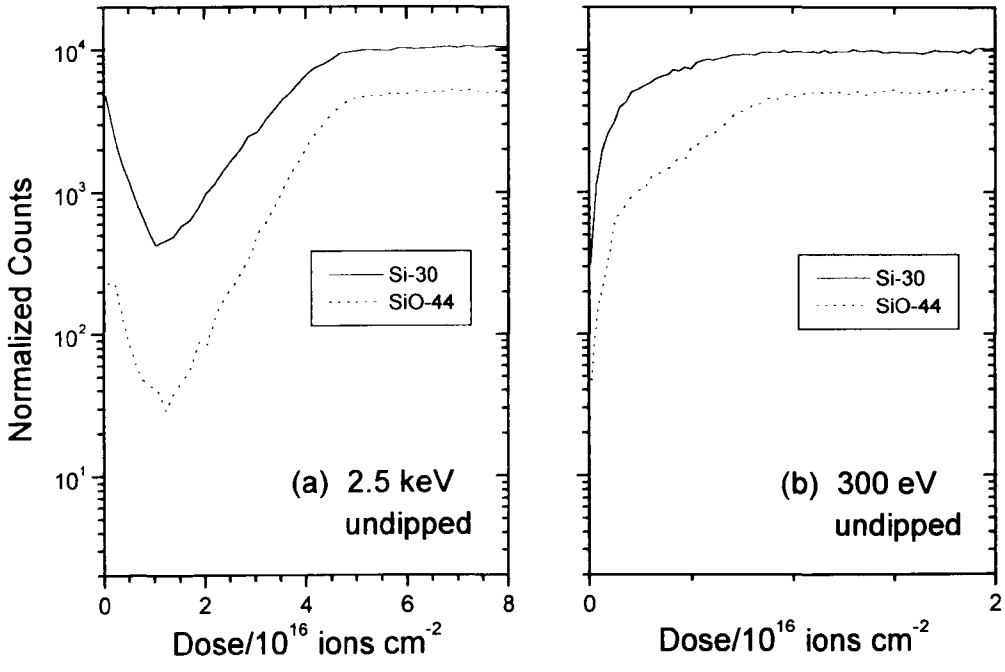

Figure 5.1: Si^+ and SiO^+ 2.5 keV and 300 eV surface transients for a 7 year old float zone wafer stored under clean conditions.

Whilst the rapid establishment of equilibrium at 300 eV (c.f. 2500 eV) can be explained by the following facts (as shown in figures 5.3 to 5.7), they do not explain why a surface spike for a sample containing a native oxide layer is not observed in the profile obtained at 300 eV.

I. 300 eV O_2^+ at normal incidence have a narrow implant distribution (Rp ~ 0.5 nm) along with a relatively low Y_0 and Y_∞ ~0.04. This enables the altered layer at this low beam energy to be fully formed whilst the native oxide is being sputtered.

II. 2500 eV O_2^+ at normal incidence have a relatively wide implant distribution (Rp ~ 10 nm) and significantly larger Y_0 and Y_∞ ~0.4 values, so that several nanometers of silicon are eroded whilst the near-surface oxygen concentration approaches that of SiO_2.

III. As the beam energy is reduced, and the Y_∞ become smaller the value of Y_{ave}/Y_∞ increases, as a greater proportion of the beam energy is distributed in the near surface region, increasing the probability that a collision cascade will intercept the surface and a sputtering event will occur .

Apart from the very rapid achievement of equilibrium, the 300 eV data are rather similar to Si^+ and SiO^+ transients observed for Ar^+ and O_2^+ bombardment of SiO_2 (Wittmaack K, 1977; Dowsett M G *et al.*, 1983). In addition, it was reported in Ref. [Wittmaack K, 1977] that the Si_2O^+ yield saturated faster than other signals. We find in general Si_2O^+ comes to equilibrium for the same dose as other channels at a given energy. However the onset of a surface spike is at 750 eV and the height of the spike relative to the steady state level grows more rapidly than for other species. For the undipped sample at 500 and 750 eV the Si_2O^+ appears to stabilise rapidly because there is either a spike or a sub-surface yield enhancement which blends into the steady state region.

A partial explanation of the overall transient behaviour is that native oxide (and perhaps other contaminants) at the surface caused the surface spike by promoting a high ion yield, and that the minimum occurred where the native oxide was sputtered off, but the steady state level of oxygen in the sample from the beam was not yet established. This cannot be wholly correct, otherwise the surface spike would be present in the low energy data as well. Examination of all data available shows the onset of the surface spike to

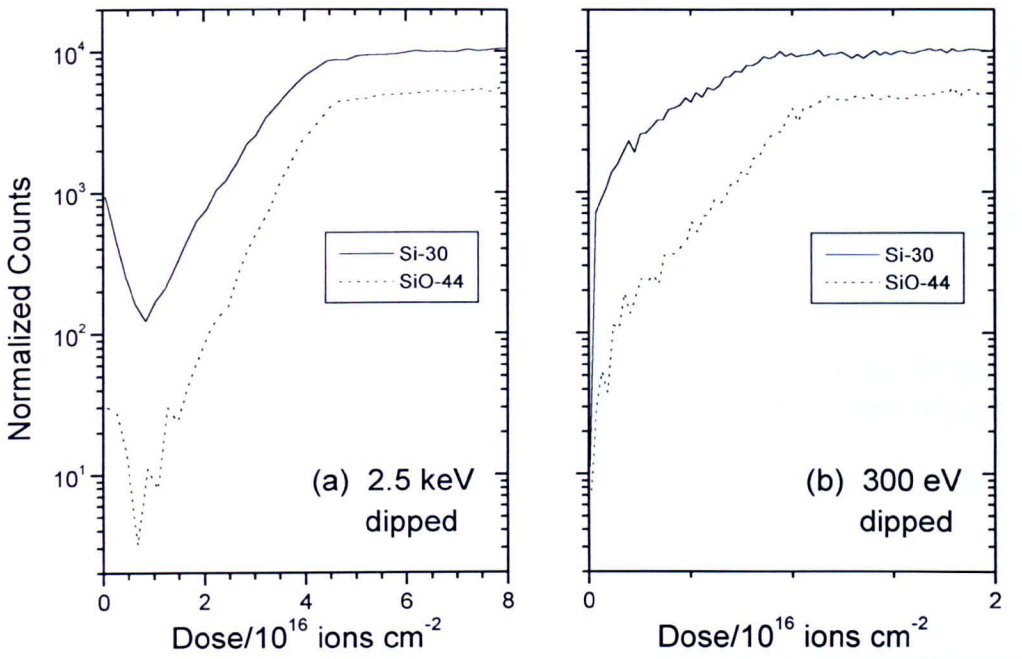

Figure 5.2: Si^+ and SiO^+ 2.5 keV and 300 eV surface transients for an HF dipped float zone wafer with minimal air exposure (~1.5 hours).

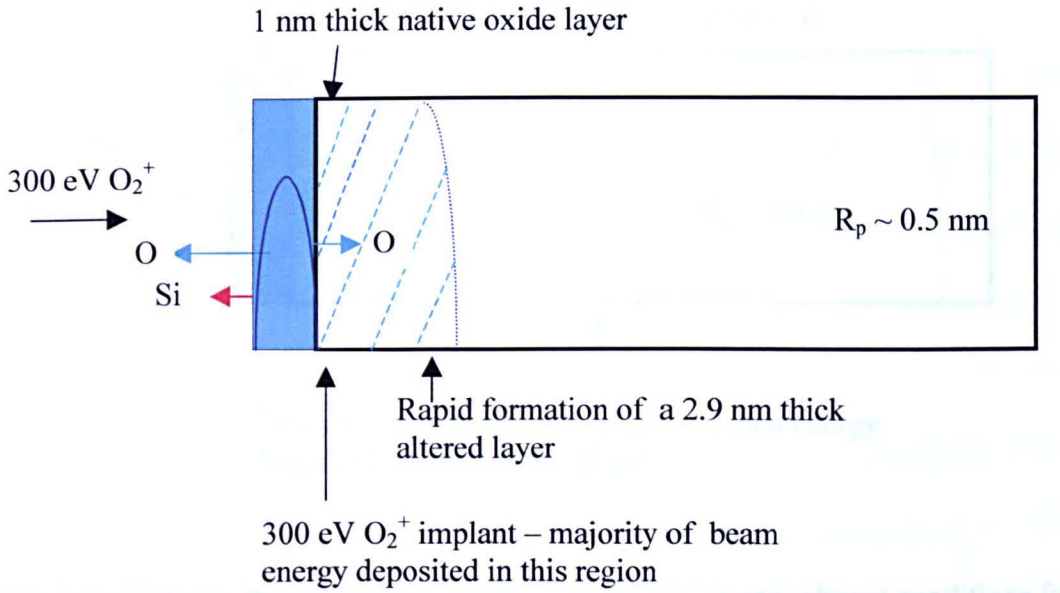

Figure 5.3: Diagram representing the initial 300 eV O_2^+ bombardment conditions for a silicon sample containing a 1 nm thick native oxide layer.

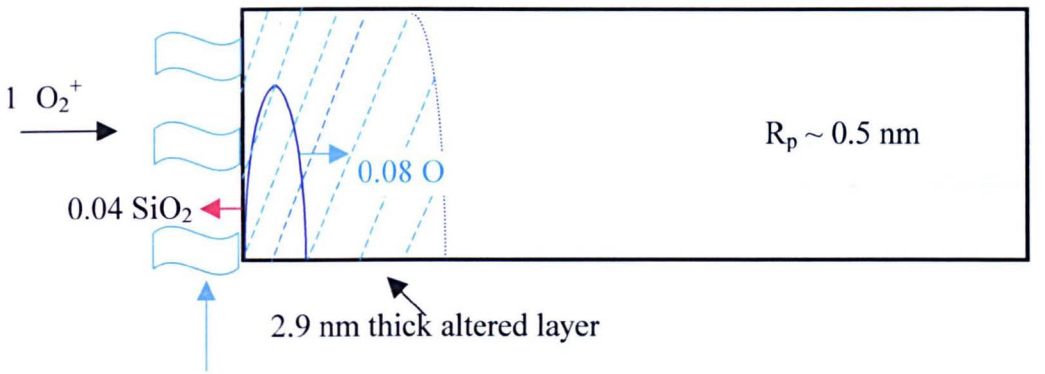

Excess 1.92 O atoms must either be sputtered, diffuse out of the sample or be back-scattered. Producing a local region above the surface of high oxygen concentration.
The remaining 0.08 O atoms must remain in the altered layer and form Si_xO_y to maintain equilibrium.

Figure 5.4: Diagram representing the steady state condition for a silicon sample under 300 eV O_2^+ bombardment at normal incidence.

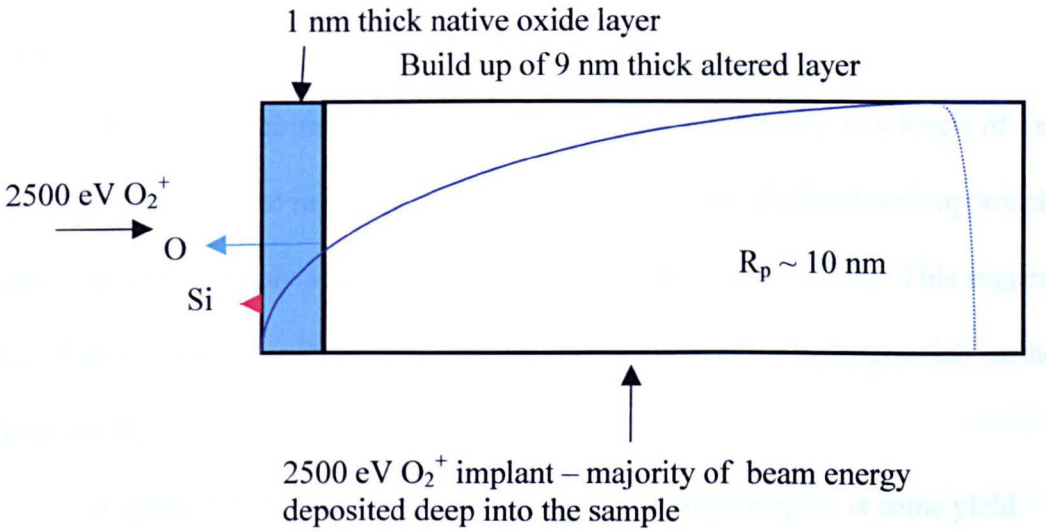

Figure 5.5: Diagram representing the initial 2500 eV O_2^+ bombardment conditions for a silicon sample containing a 1 nm thick native oxide layer.

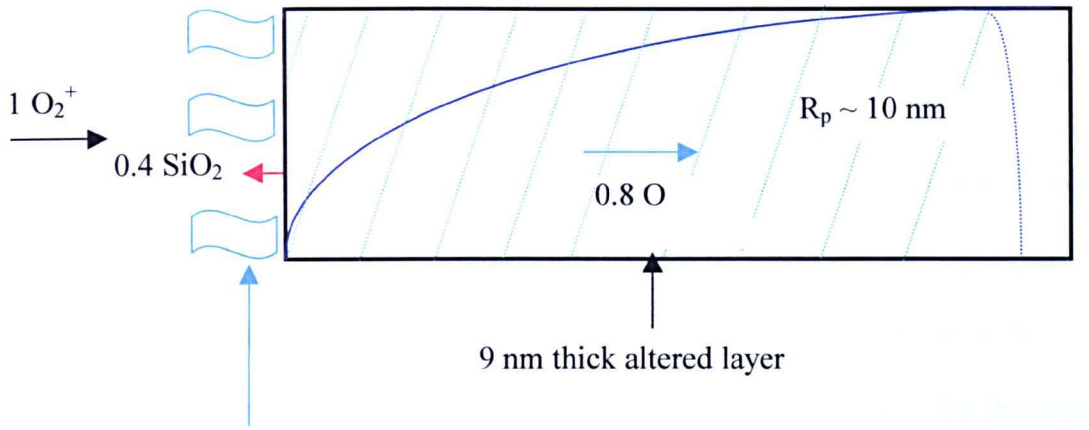

Excess 1.2 O atoms must either be sputtered, diffuse out of the sample or be back-scattered. Producing a local region above the surface of high oxygen concentration.
The remaining 0.8 O atoms must remain in the altered layer and form Si_xO_y to maintain equilibrium.

Figure 5.6: Diagram representing the steady state condition for a silicon sample under 2500 eV O_2^+ bombardment at normal incidence.

be at ~900 eV, and also that the spike is present in all silicon and oxygen related channels recorded. The surface to valley intensity ratio of the spike increases progressively across the energy range and is greatest for the undipped sample (by a factor of 5 at 2.5 keV).

Dipped and unrinsed wafers are known to have extremely low levels of oxygen on the surface, and the rate of growth of oxide is very low. In fact levels approaching one monolayer are only achieved after one year (Gräf D *et al.*, 1990). This suggests that the silicon surface is passivated by something else, possibly a hydrogen rich surface from the HF.

It appears that the general explanation of the surface spike is some yield enhancement due to the top surface chemistry, but that this yield enhancement mechanism is not available to silicon related emission below 900 eV.

There are several possible explanations of this behaviour:

(i) Masking of Si-related species by contamination.

This is a possible explanation, particularly if the contaminants contain no oxygen (since there is no O^+ spike either at low energy) and if they are light e.g. Hydrogen bonded to Si or Oxygen right at the surface. In that case one could argue that the masking was progressively less effective as beam energy increased, and that the spike was due to just "subsurface" oxygen enhanced yield. This would require that both the dipped and undipped surface had a light contaminant $\leq$ 1 monolayer in thickness, and is insufficient on its own because one would still expect to see a sub-surface spike in the low energy data.

(ii) The erosion rate is much higher at the surface.

According to Wittmaack (1996a) the ratio between the surface erosion rate Y_0 and that at steady state Y_∞ goes on increasing as the energy is reduced. Although our latest measurements support this view, if the effect was causing the spike it would lead to the opposite behaviour to that observed here- i.e. the surface spike would increase as the energy reduced. Taking these observations together implies that at low beam energies the ionisation probability for silicon and silicon/oxygen -related species are extremely low in the first monolayer.

(iii) The energy density at the surface due to sub-keV O_2^+ ions is initially insufficient to sputter ions from either Si or SiO_2 and some damage must accumulate in the material before ions are observed.

(iv) The ion yield at the surface contains a component due to electronic stopping which is negligible for sub-keV ions. (In the keV region around 10% of neutral sputtering is

believed to be due to electronic energy deposition rather than screened nuclear interaction (Biersack J P, 1987)).

Figures 5.7 (a) and (b) show the behaviour of the Si^+ and SiO^+ transients as a tentative function of depth assuming uniform erosion rates for low energy ions due to Smith (1996) and Gibbons (defined as "apparent" depth by Wittmaack (1996a). For depths significantly less than 1 nm, this should be taken as an approximate indication of the numbers of silicon atoms sputtered per unit area and in any case it should be taken as indicative of the relative, rather than the absolute differences between high and low energy bombardment. Of course, the erosion rate in the pre-equilibrium region will not be constant, and its initial value, for a perfectly clean silicon surface at sub-keV energies, may even be a factor of 10 higher than its equilibrium value (Wittmaack K, 1996a). Estimating the effect of the presence of some native oxide, we could assume that the average erosion rate in the transient region is about 3 times higher than the stationary value, so the true "depths" to equilibrium may be greater by a factor of 3, than those shown in figures 5.7(a) and (b). Nevertheless, a very different picture emerges from that presented by the intensity vs. dose data. At 300 eV both the undipped and dipped samples apparently achieve equilibrium in $<<1$ nm, irrespective of the level of surface oxide, suggesting that energies ≤ 300 eV are capable of profiling the very shallow regions of low energy implants with freedom from surface transients. The SiO^+ signal exhibits a near surface change of slope in each case (at a lower level in the dipped sample) which may be due to exposure of native oxide, beneath a hydrogen monolayer. The 500 eV data also equilibrates in <1.2 nm, this is about twice the depth of the 300 eV data. Both the Si^+ and SiO^+ exhibit shoulders in this case. The 2.5 keV transient persists for at least 3 nm - well past the range of many low energy implants.

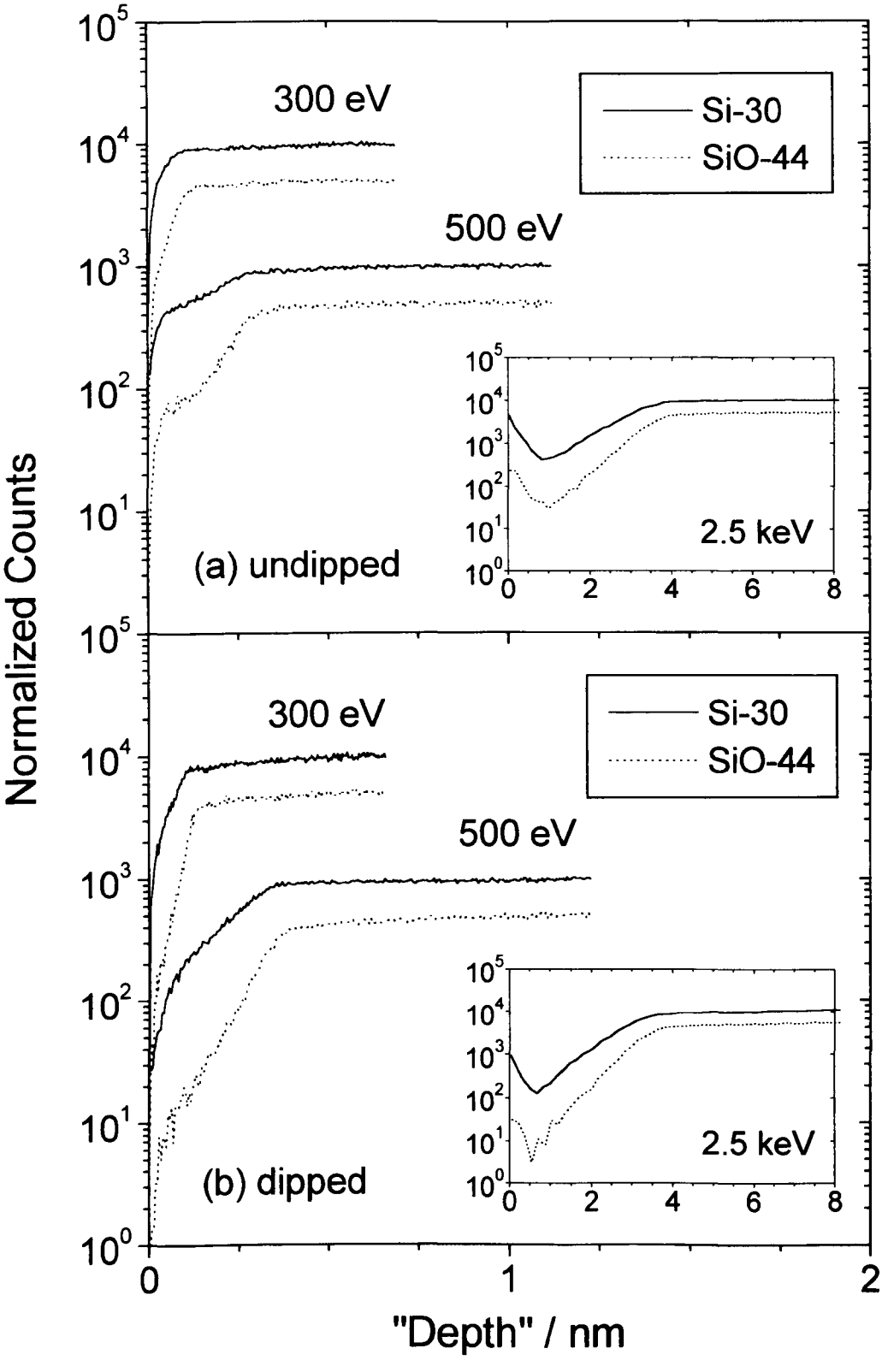

Figure 5.7: Si^+ and SiO^+ 300 eV, 500 eV and 2.5 keV surface transients as a tentative function of depth for (a) a 7 year old float zone wafer stored under clean conditions and (b) after HF dip with minimal air exposure.

The low energy data exhibit clear differences in the dipped and undipped samples. However, with a seven year old wafer with an otherwise uncontaminated surface, one would expect 1-1.5 nm of oxide (Gräf D *et al.*, 1990). However, there is no real indication of an oxide/silicon interface in the undipped data. Other recent data from thin gate oxides on silicon show a similar effect. At energies above ~1 keV (the same threshold which determines whether a surface spike is observed) species such as Si^+, SiO^+ etc. show a transiently decreasing behaviour going from oxide to silicon, which enables the interface position to be identified. Below 1 keV, neither Si/SiO related channels, nor impurity channels such as B^+ or As^+ display transient behaviour - the signals maintain continuity across the interface. (This is consistent with the argument that there is an electronically stimulated component to the degree of ionization for the oxygen bombardment of oxide which is absent at low energy, but it is not clear why both impurities having about the same concentration either side of the interface, and silicon which has a lower concentration in the oxide are both continuous). The erosion rate still decreases by a factor of 2 going from silicon dioxide to silicon at least down to 500 eV.

To put a true depth scale on such data was impossible prior to this present work. Presented are two different ways we have attempted to apply such a depth scale (Dowsett M G *et al.*, 1998b and 1998c). At 300-500 eV, the erosion rate on the undipped wafer probably starts at around twice that for bulk Si (because it is oxidised), then decreases to the stationary value. The only data previously available (Wittmaack K, 1996a) suggests that the dipped wafer may erode almost 10 times faster than bulk Si (although probably for sub-nm "depths") and decrease to the bulk level over 1 nm or so. From the data in Figure 13 of Ref. [K. Wittmaack, 1996a] we have attempted to calibrate the depth scale for the dipped wafer more realistically by assuming that the

silicon sputter yield varies linearly with ion dose between its initial and final values so that the depth z is given by:

$$z = \Omega_{Si} \int_0^{\phi} Y(\phi')\, d\phi' \qquad (5.1)$$

where

$$Y(\phi) = Y_0 + \frac{\phi}{\phi_{eq}}(Y_\infty - Y_0), \quad \phi \leq \phi_{eq};$$
$$Y(\phi) = Y_\infty, \quad \phi > \phi_{eq}$$

and Ω_{Si} is the silicon atomic volume, ϕ is the primary ion dose, ϕ_{eq} is the dose required for equilibrium, and Y_0 and Y_∞ are the initial and final sputter yields (Wittmaack K, 1996a).

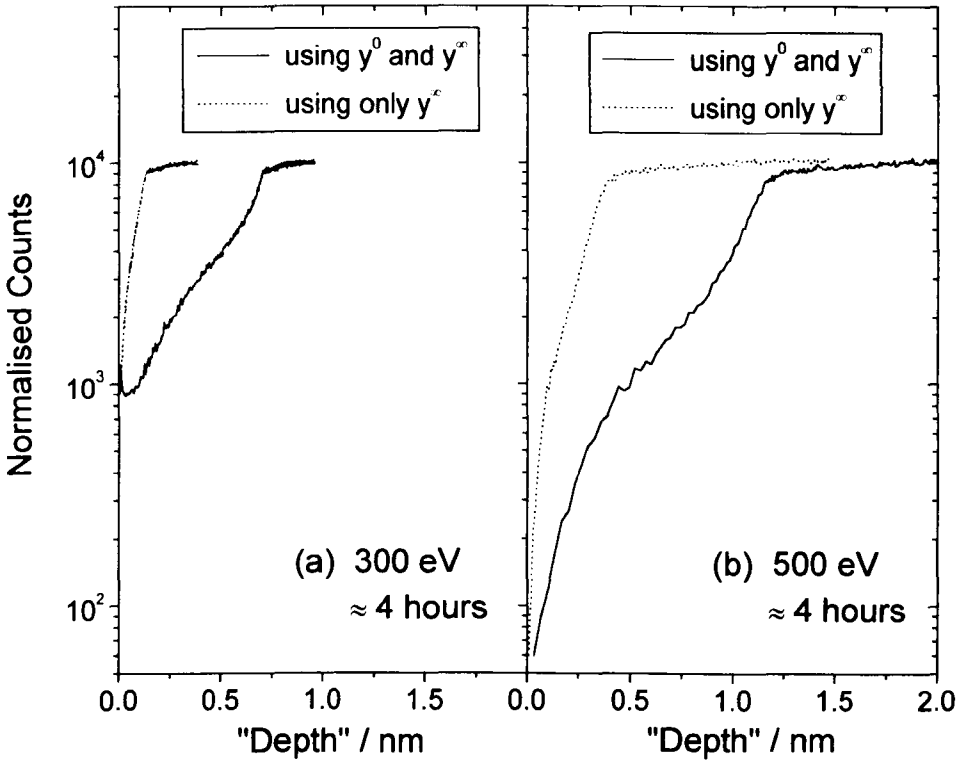

Figure 5.8: Si^+ Surface transients from the 4 hour exposed surface with depth calibration taking account of varying erosion rate across the transient region (Sputter yield data from Ref. [Smith N S, 1996]).

These data are shown in Figure 5.8. The 300 eV data still reach equilibrium in significantly less than 1 nm, even when there is minimal surface oxide, this is consistent with extrapolation of the equilibrium depth from higher energies (Wittmaack K, 1996a).

Figure 5.9 shows the equilibrium dose ϕ_{tr}, the apparent transient width z_{app} and the true transient width z_{tr} as a function of beam energy, where $z_{app} = \dot{z}_{bulk}\phi_{tr}$ and $\dot{z}_{bulk}$ is the steady-state erosion rate (Smith N S, 1996 and Gibbons R). The $\dot{z}$ are erosion rates in units of depth of silicon eroded per unit ion dose. The true width, *i.e.* the depth of silicon sputtered to achieve steady state is calculated from $z_{tr} = z_{app} - \Delta z_c$ where Δz_c is the energy dependent shift (Wittmaack K, 1996b) measured for the centroid of boron or silicon delta-layers in silicon (~ 0.9 nm/keV/O_2^+). This calculation is based on the hypothesis that the erosion rate comes to equilibrium as the ion yields achieve steady state. Since ϕ_{tr} was the same for all species observed at a given energy, there is no ion-specific ambiguity here.

The apparent transient width at low beam energies for the undipped sample is marginally less than for the dipped sample. Results of this and other studies show that the transient dose is independent of oxidation at the surface (although the signal behaviour is not), provided that the true transient width is greater than the oxide thickness. Below 500 eV, z_{tr} is indeed less than 1 nm, and amounts to just 0.4 nm (slightly less than the silicon lattice parameter) at 300 eV. Figure 5.9 shows that while there is only a 4-5 fold decrease in equilibrium dose on decreasing the beam energy from 2.5 keV to 300 eV, this corresponds to an approximate 30 fold decrease in the apparent transition depth. Although we do not yet know how the matrix erosion rate varies across the pre-equilibrium region, these data support estimates (Wittmaack K, 1996a) that the initial sputter yield Y_0 greatly exceeds that in the bulk Y_∞ by up to a

factor of 10 at low energies. Figure 5.10 shows the ratio of average sputter yield of dipped silicon in the pre-equilibrium region, Y_{ave} to Y_{∞} varies as a function of energy.

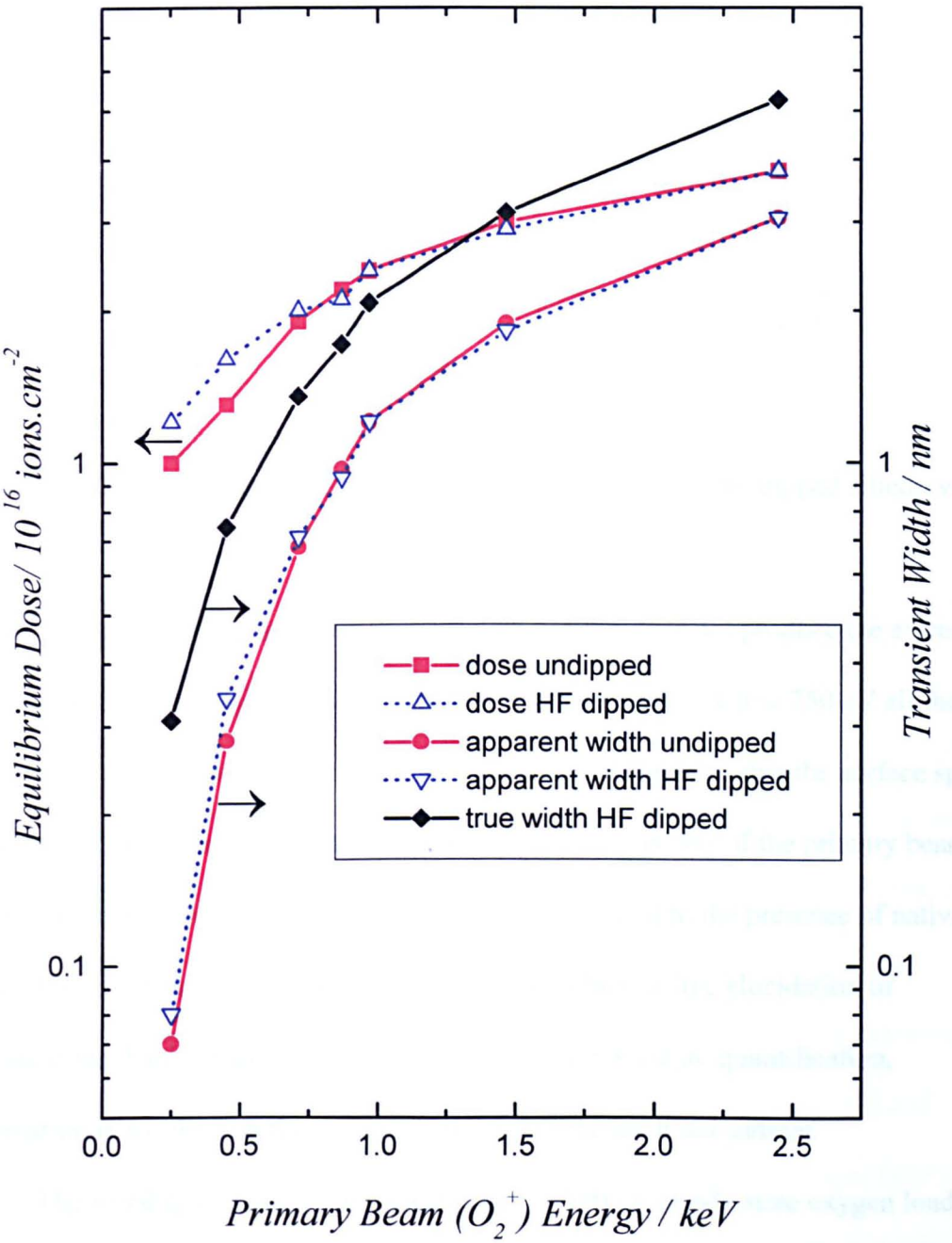

Figure 5.9: Equilibrium dose and apparent and true transition widths vs. beam energy.

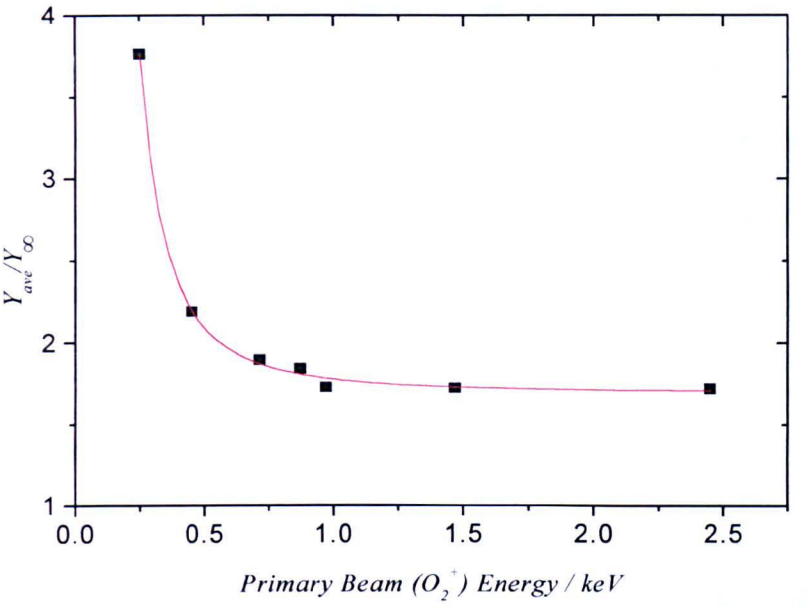

Figure 5.10: Ratio of average transient to bulk sputter yields for dipped silicon vs. beam energy.

Sub-keV normal incidence analysis with oxygen does not produce the extreme surface transients and spikes typical of higher beam energies. Below 750 eV all the matrix transients rise monotonically from a low level, suggesting that the surface spike is influenced by the energy deposition and/or penetrating power of the primary beam and the top monolayer of the sample, and not solely related to the presence of native oxide. Further study of this behaviour may be important for the elucidation of ionization mechanisms in SIMS. It is obvious that for accurate quantification, information is required on the surface chemistry of the analysed sample.

The worst case calculation indicates that at 300 eV steady state oxygen loading of the sample is achieved for less than 1 nm of silicon erosion, and therefore the ion yields and erosion rates should be constant thereafter.

The above data was collected on crystalline silicon. Further, recent data suggests (Dowsett M G, 1998a) that the surface damage occurring during implantation may alter the surface oxidation and transient shape, but not the equilibrium dose.

The change of erosion rate in the pre-equilibrium region is an important parameter, experiments to measure this at 500 eV are in progress, in a combined study using the techniques of MEIS and SIMS.

5.1.2. Sample History and its Effects.

Silicon used in semiconductor devices forms a native oxide when a fresh surface is exposed to air. The rate of oxide formation, and its ultimate thickness, depends on the surface preparation of the wafer, the quality of the air, the ambient temperature, and the duration of the exposure. The rate of oxide formation, typically follows a parabolic growth pattern, and can be highly sensitive to impurities on the silicon surface (Gräf D *et al.*, 1990). Ultra-low energy implants can be injected through the native oxide, which then may modify the diffusional properties of the implant. While this behaviour has always been present its effects were insignificant till recently, both because of the range of implants, and the analysis energy used in SIMS depth profiling. However, for modern keV and sub-keV implantation technology, the effects can be significant both in the process and during the analysis. The comparison of SIMS data from different process batches will be complicated by differences in wafer ageing both between manufacturing batches and between analyses. There are also implications for reference materials used in ultra-shallow profiling which will also age in a similar manner. It seems that the top few nm in a SIMS profile might only be interpretable with a detailed

knowledge of the surface chemistry, due in part to the presence of native oxide and its effects on the ion yield and erosion rate.

The transient behaviour of silicon and oxygen related signals were recorded for a normally incident O_2^+ beam at two primary beam energies of 300 and 500 eV. The samples were a phosphorous doped (35-65 Ω cm) float zone (100) silicon wafer ≥ 7 years old, and the same wafer dipped in 5% HF solution in de-ionized water until the surface dewetted perfectly. The latter surface was not subsequently rinsed to avoid any reaction with de-ionized water. These are referred to as undipped and dipped respectively. The dipped wafer surface was allowed to age in laboratory air for varying periods prior to analysis

Figure 5.11 shows the differences observed in the Si^+ surface transients as a function of wafer age. Data at both 300 and 500 eV are responsive to the level of native oxide, but its presence does not significantly affect the equilibrium dose. The depth scale is again from bulk silicon erosion rates. After 11 days in air the wafer surface has not finished changing. This is consistent with behaviour observed elsewhere for air exposed wafers (Gräf D *et al.*, 1990).

Initial results obtained using only the 500 eV O_2^+ analysis conditions were obtained on ageing the dipped wafer for a significantly longer period of time up to 37 days, unfortunately the data were not collected under ideal analysis conditions. After 37 days in air the wafer surface had not finished changing, with the number of ions detected continuing to increase with air exposure time, especially in the region where the dose ≤ 5E15 ions cm^{-2}. This clearly demonstrates the strong ion yield dependence on oxygen concentration in the transient region.

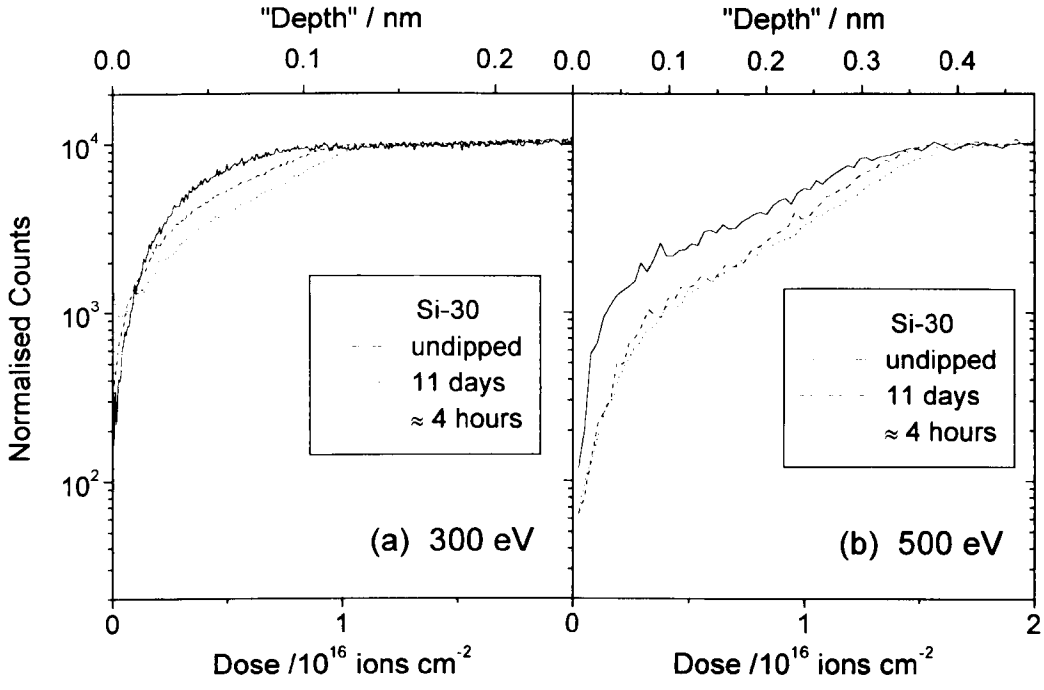

Figure 5.11: 300 eV and 500 eV Si^+ transients from the 7 year old wafer and from surfaces exposed to air for ~4 hours and 11 days.

5.1.3. Determination of the Transient Shift.

The results mentioned previously for the true or corrected width of the transient region, are based on the widely accepted theory that the energy dependent shift observed in the peak and centroid position of delta layers, is due solely to the enhanced erosion rate in this region (Wittmaack K and Wach W, 1983). Whereas, more recently it has been proposed (Barlow R D *et al.*, 1992) that the actual shift measured is dependent on the feature-to-surface and feature-to-crater bottom distances. The results presented in the rest of this chapter will prove this latter hypothesis.

In this section are presented results of the author's attempts to determine the actual size of the transient region, and hence the transient shift for a MBE grown

material. It is well known that the apparent transition depth and related profile shifts can be reduced by lowering the beam energy. If the magnitude of the profile shifts are to be determined accurately, one needs to know the original location z_o of a suitable feature e.g. a delta layer. Typically this value is not known with the desired accuracy of $\pm$ 0.5 nm. Many groups (Clegg J B, 1987; Barlow R D *et al.*,1992; Dowsett M G, 1992; Wittmaack K, 1996a and Smith N S *et al.*,1997) have previously tried to derive z_o by performing measurements on single delta doping distribution as a function of beam energy. However in this work samples containing multiple boron delta doped layers were used. It is known from this and other work (Wittmaack K, 1996a) that the apparent centroid and apparent peak positions for boron deltas have essentially the same intercept z_o if plotted against beam energy. Provided any systematic errors are beam energy dependent, it can be assumed that the true depth $z_\delta \equiv z_o$. This strategy has been applied to two MBE grown samples containing multiple boron delta doped layers. In all cases immediately prior to analysis, the analyte surface was dipped in a 5 % HF solution in de-ionized water until the surface was fully hydrophobic. Therefore, all profiles started on a surface with similar conditions, and the measured parameters such as transient widths will be comparable.

Most of the previous studies at normal incidence, have tended to use samples containing single delta layers, limiting their usefulness. This also probably explains the large differences reported in the literature for the energy dependent profile shifts. Boron delta layers were chosen because it has been shown to be a well behaved impurity, which does not undergo significant unidirectional transport phenomena i.e. segregation.

The first sample (25.47) was analyzed using a normally incident O_2^+ beam at six primary beam energies 230 eV $\leq E_p \leq$ 10 keV on EVA 3000. The apparent transition width was taken as the position where the $^{30}Si^+$ intensities reached 95% of the

equilibrium level. These positions were determined by fitting the function shown in equation 5.2 through the data, A_1, A_2 and K were fitting parameters and z was the depth. To improve the quality of the fit, the surface peak was excluded from the fit. We show in figure 5.12 the apparent surface transient widths for normally incident O_2^+.

$$y = A_1 - A_2 exp^{(-KZ)} \qquad (5.2)$$

Also included are similar data for float zone silicon. We can see that the apparent surface transient width reduces from over 10 nm to 0.5 nm as the primary beam energy decreases from 10 keV to 230 eV. In the sub-keV regime, the float zone results differs significantly from the MBE result, giving even narrower transients. The reason for this is not known at present - but a likely cause is the high boron concentration on the surface of the MBE grown wafer due to segregation effects. It is important to note that based on this data one would expect the result for preamorphized silicon implants to be different again - especially if as suspected the surface became loaded with atmospheric oxygen when removed from the implanter. It was shown in the previous section that the presence and thickness of the native oxide, can have a small effect (10-20%) on the equilibrium dose.

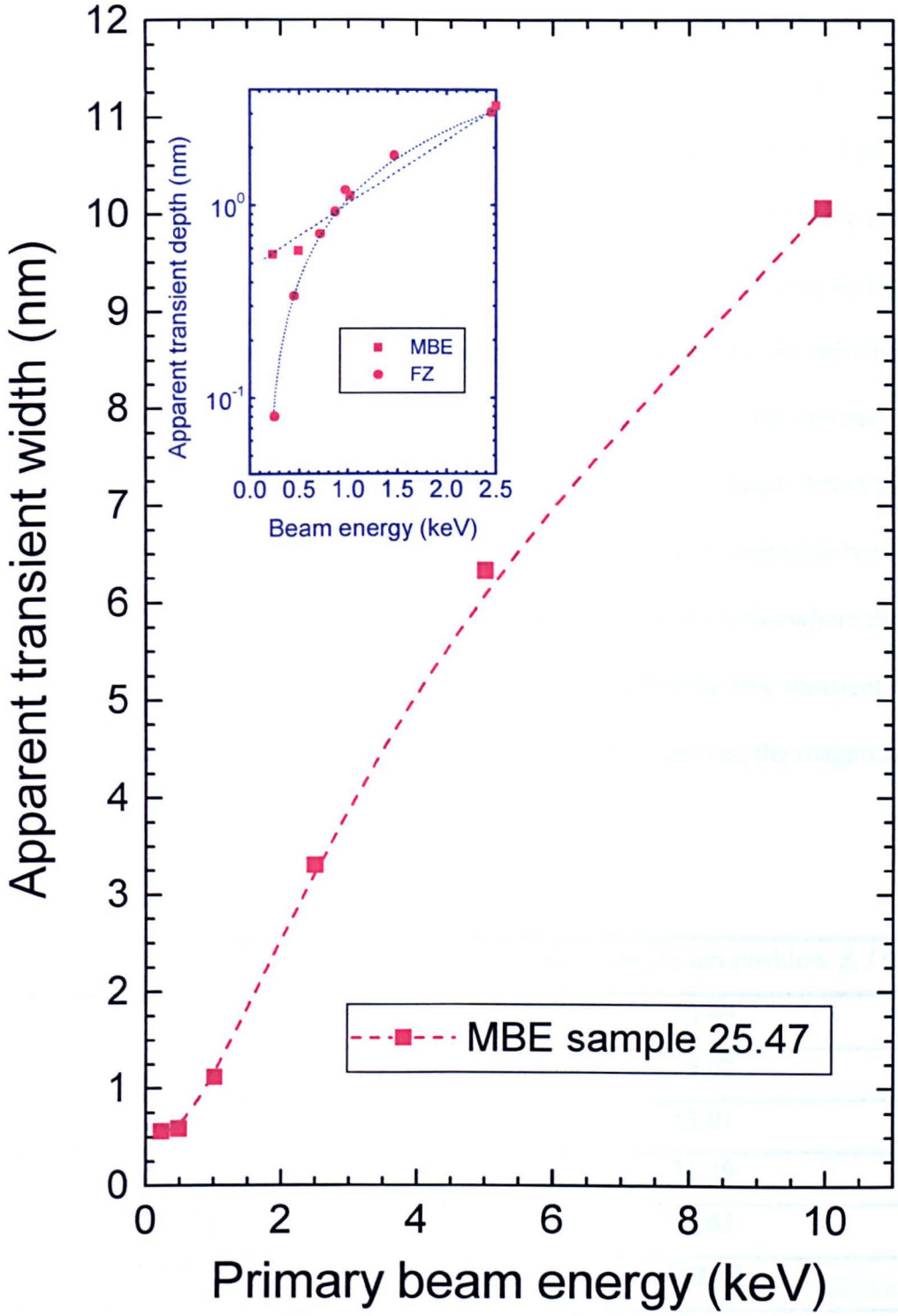

Figure 5.12: Apparent surface transient widths as a function of primary beam energy.

The procedure for calculating the true transient width and hence actual transient shift is briefly outlined below.

At each of the six primary beam energies used the apparent centroid and apparent peak maximum positions of each of the 10 delta layers in the sample were determined. For each delta layer the centroid and peak maximum positions were plotted against primary beam energy, and the relevant z_o values (see table 5.1) determined by fitting the data with a polynomial. At each energy using the frame numbers (which are proportional to dose) and z_o values of the first two delta layer centroids beyond the transient region, the real erosion rate between the delta layers is calculated. From the first delta layer centroid beyond the transient region, whose apparent depth has been corrected to its true value, the real erosion rate is applied back to the point where the $^{30}Si^+$ intensities reached 95% of the equilibrium level, this is then the true transient width, and hence the actual transient shift can be calculated. However, the magnitude of the transient shift calculated

True peak centroid position, z_o / nm	True peak maximum position, z_o / nm
16.72	16.99
34.69	35.02
52.82	53.01
71.10	71.19
89.54	89.63
107.76	107.87
126.07	126.26
144.40	144.63
162.60	162.62
180.71	180.83

Table 5.1: z_o values for sample 25.47.

by this method will also be affected by any other changes in erosion rate during sample analysis e.g. that due to surface roughening (found to be considerable under some oblique angles of incidence), or changes in the primary beam current (minor). The spacing between the peak maxima and peak centroids decreases continuously with decreasing beam energy, ranging from 1.6 nm at 10 keV to approximately -0.2 nm at E_p=0.

Figure 5.13 shows the apparent and true transient widths for the MBE grown silicon wafer for normal incidence O_2^+. We can see that true surface transient width reduces from over 23 nm to 1.0 nm as the primary beam energy decreases from 10 keV to 230 eV. This large value obtained at 10 keV is nicely illustrated in figure 5.14 as the transient region extends well beyond the first delta layer in sample 25.47 which is at a depth of 16.7 nm. Also the true surface transient width is at least twice the size of apparent surface transient width, and generally at least 30 % larger than the calculated value obtained previously. Both the apparent and true transient widths follow power law dependencies shown below:-

$$Ztr_{app} = 1.47Ep^{0.85} \qquad (5.3)$$

$$Ztr = 3.35Ep^{0.85} \qquad (5.4)$$

Unfortunately the 230 eV data values obtained here, seem abnormally large, due to a very gradual increase in the ion counts from the 80 -100% equilibrium value rather than a more typical rapid increase.

In a recent review on transient phenomena (Wittmaack K, 1996a), values for the apparent and true transient depths of 2.5 ± 0.5 nm and 5.5 nm respectively were reported, for a 2 keV O_2^+ beam at normal incidence, these values are in close agreement to those obtained here.

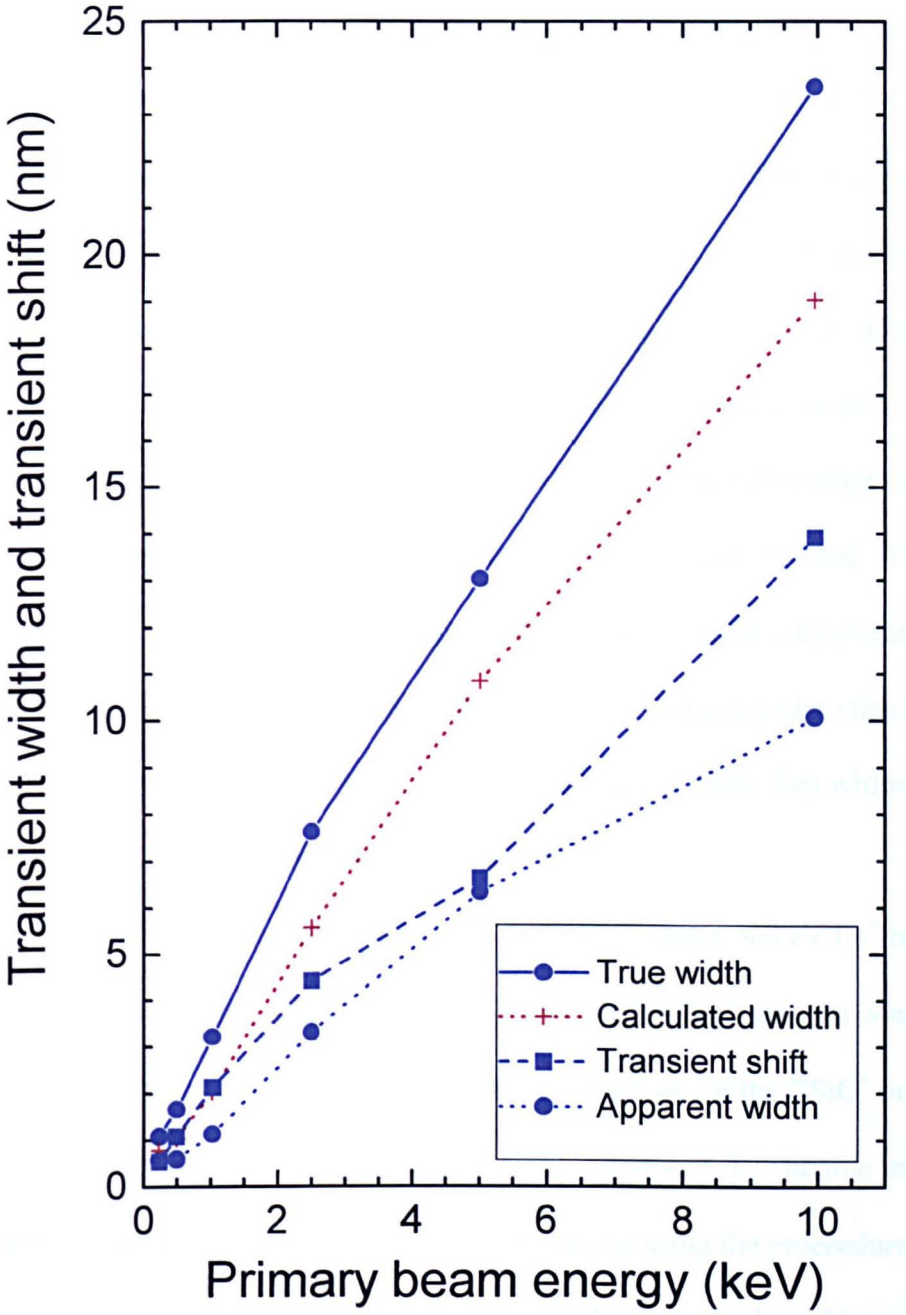

Figure 5.13: Apparent, calculated and true transient widths and transient shift for sample 25.47 as a function of primary beam energy. The O_2^+ beam is at normal incidence.

Figures 5.14 (a) and (b) show the apparent and true depth scales for the first 3 boron delta layers in the MBE grown sample 25.47 obtained at 490 eV and 9.96 keV. The O_2^+ beam is at normal incidence. In Figure 5.14 (a) several advantages of profiling at ultra-low energy are immediately obvious, the rapid establishment of equilibrium, less atomic mixing resulting in higher depth resolution and observation of the true profile shape (the unusual shape at the front of the peaks is due to boron diffusion during growth). On closer examination the significant decrease in boron ion yield within the transient region is also observed. The misalignment of the boron delta layers is due to the differences in the size of the transient shift, due solely to the faster erosion rate in the transient region and on correcting for these values figure 5.14 (b) is obtained. The first boron delta layers are still somewhat misaligned, due to the changing ion yield in the transient region and also due to the linear depth scale correction proceedure used. This clearly demonstrates the problem with obtaining accurate quantifable data within the transient region, and at 10 keV this extends beyond 23 nm.

Sample 25.47 was also analyzed on EVA 2000 FL, using a 500 eV O_2^+ beam at 5 different angles of incidence in the range 0 - 60°, under ultra-high vacuum conditions. The apparent transition width z_{trapp} was taken as the position where the $^{46}SiO^+$ or $^{72}Si_2O^+$ intensities reached 95% of the equilibrium level, using equation 5.2. The true transient width, z_{tr} and the actual transient shift Δz_{tr} were determined using the proceedure outlined previously, and the results are shown in figure 5.15. A number of interesting observations can be made from the results shown in figure 5.15.

As the angle of incidence moves from normal incidence to more oblique angles, the size of all three parameters studied increases dramatically. However, at angles up to 40° the actual transient shift remains small < 0.5 nm. At angles of incidence > 40° the rapid increase in actual transient shift is associated with the development of surface

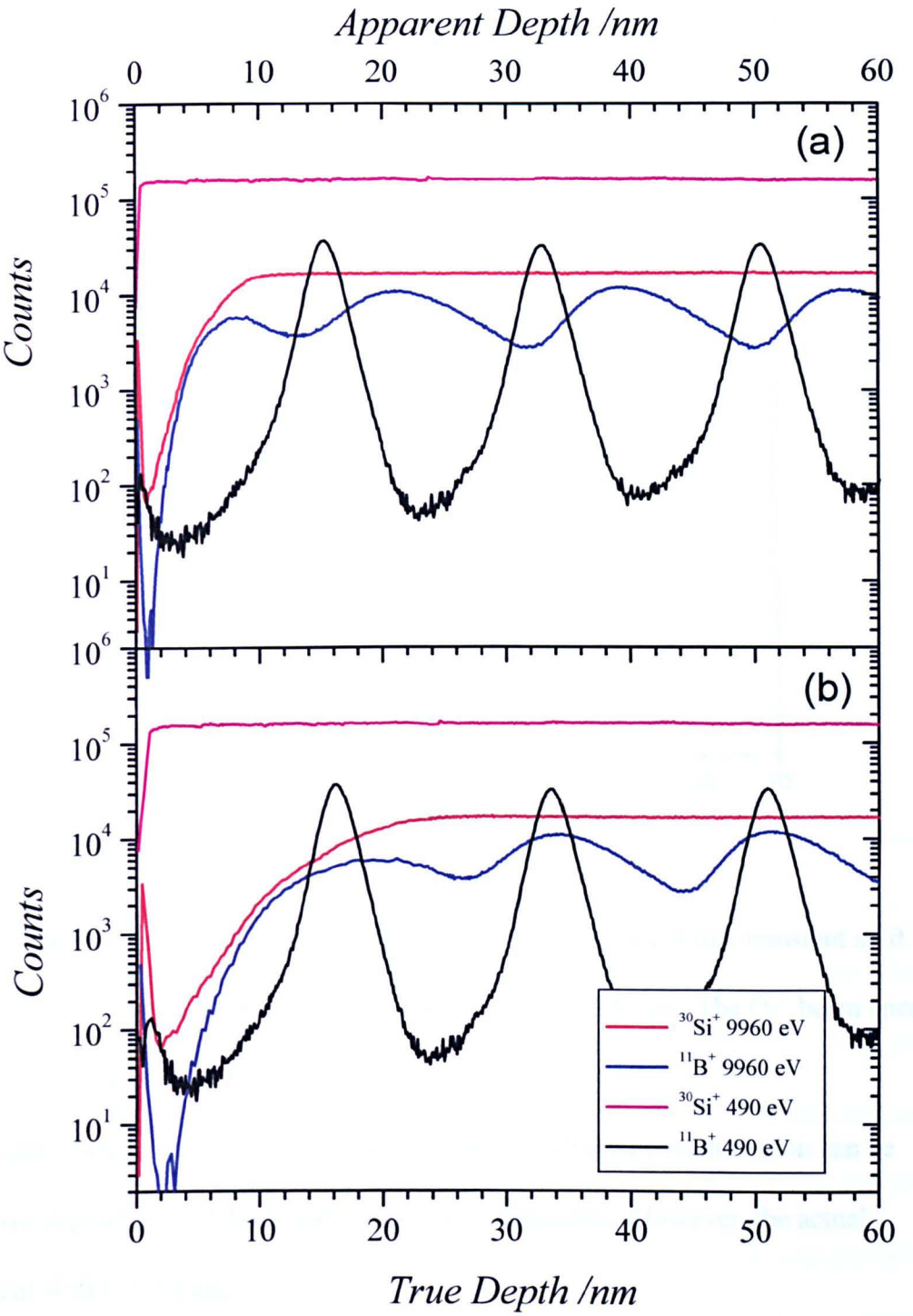

Figure 5.14: (a) Apparent and (b) True depth scales for MBE sample 25.47 obtained at 490 eV and 9.96 keV. The O_2^+ beam is at normal incidence.

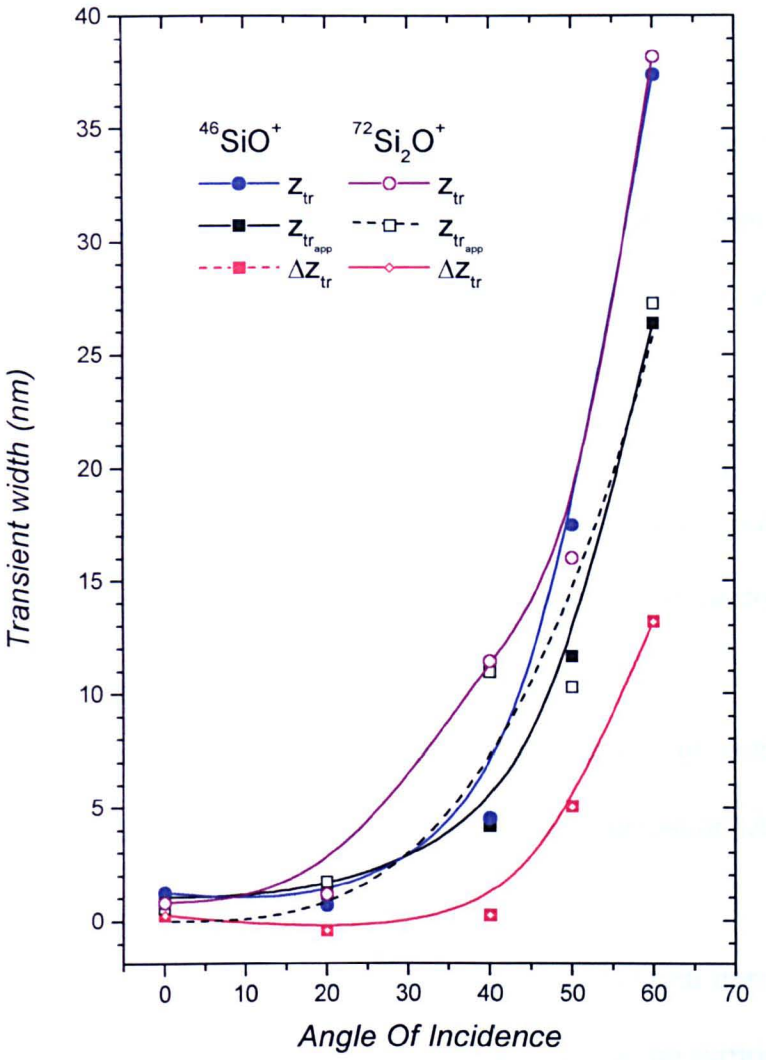

Figure 5.15: Apparent and true transient widths, along with the true transient shift for sample 25.47 as a function of angle of incidence. The O_2^+ beam energy was 500 eV.

topography (see chapter 6). At angles > 20° the size of the transient region can be different depending on which matrix species is monitored. However, the actual transient shift is the same.

5.2 The Terminal Shift

Wittmaack and Wach (1983) were the first to observe that the apparent depth of a feature (implant or delta layer) is energy dependent, they termed the slope of the plot of apparent feature depth verus energy, the differential shift. This shift or error in the depth scale quantification process, is due to three principal causes:

I. The application of a constant erosion rate.

II. The incorrect assumption (especially when reactive primary ions are used) that the measured crater depth, corresponds to the depth of matrix eroded (Barlow R D *et al.*, 1992).

III. The internal redistribution of the impurity due to a combination of atomic mixing, kirkendale currents (density renormalization effects) and segregation (Armour D G *et al.*, 1988).

This shift is particularly noticeable when using oxygen at near normal incidence, due to the formation of the oxidized altered layer. While it is of no surprise that the differential shift is highly species dependent (Dowsett M G *et al.*, 1992; Barlow R D *et al.*, 1992), a wide range of values have been reported for boron in silicon. The original data of Wittmaack and Wach (1983) reported a differential shift of -0.67 nm/keV/O_2^+ for boron in silicon, whereas Dowsett *et al* (1994) reported sample dependent values of between -1.3 - 1.6 nm/keV/O_2^+, supporting earlier work (Barlow R D *et al.*, 1992) that the actual shift measured is dependent on the feature-to-surface and feature-to-crater bottom distances. The values determined by Dowsett *et al* (1994) are also significantly larger than the later value -0.9 nm/keV/O_2^+, determined by Wittmaack (1996b) and used to calculate the transient widths in section 5.1.1. Some of this difference could be

explained by the fact that Dowsett used peak maxima of the delta layers, which are known to undergo larger shifts than the peak centroids used by Wittmaack.

In a fully quantified SIMS profile the objective is to relate a particular ordinate in impurity concentration to its true depth within the (silicon) matrix. Leaving aside problems due to atomic mixing for the moment, we have already shown that two erosion rates (bulk and average transient) are required for this. These are almost universally obtained from surface profilometry of the SIMS crater. We now show that such measurements contain at least two possible sources of systematic error which become significant for shallow profiles. Since optical and other crater measurements will also contain similar errors due to the same causes, but of different magnitude, the material below is generally useful.

Assuming that it is not significantly modified by exposure to air, the crater bottom is covered by a layer comprising of a mixture of probe and matrix atoms. If roughening has occurred, this will also remain on the crater bottom. Assume that a profilometer measurement is made from the unmodified starting surface to the surface of this layer. It differs from the depth of matrix eroded for two reasons:

(i) The matrix density (matrix atoms cm^{-3}) is modified by the presence of the implanted probe atoms. For example, for silicon fully saturated with oxygen from an O_2^+ beam, the stoichiometry is close to SiO_2, and the volumetric swelling of the matrix is around a factor of 2.2. If all the probe atoms were removed, and the silicon atoms were repacked at their original density, the crater would be deeper. This new depth gives the true position of the last ordinate in matrix channel, provided there is no roughening. (Whether the matrix density is increased or decreased in general will depend on the details of the probe species/matrix reaction. For example, if the matrix and probe were an alkali metal and oxygen, the spacing between alkali metal atoms

would be reduced compared to their metallic spacing - shrinkage as opposed to swelling.)

(ii) A profilometer stylus tip is typically 12 μm in diameter. This will ride over the crests of any roughening, resulting again in an underestimate of the true amount of matrix sputtered.

In the course of this work the authors noticed a third effect which is more subtle because it is impurity dependent: Suppose the primary beam induced mass transport is not solely due to random cascade mixing, but involves some preferential migration of the impurity into, or away from the altered layer (Dowsett M G *et al.*, 1992). A delta layer would be observed to be shallower or deeper respectively than its true depth, as would the dopant intensity from any broader distribution.

It is important to determine whether or not these effects are significant. If we consider any impurity profile, it is clear that a depth calibration based on a constant erosion rate will leave the first ordinate after the transient out of position by the amount of the transient shift, and the last ordinate out of position by the terminal shift, the difference between the true and measured crater depths added to any migratory shift. In an early experiment to measure this latter effect at high beam energies (Clark E A et al., 1990) a method based on stopping a profile at the peak of a delta layer was used, this method assumed that the peak corresponded to the true depth of the feature. Because the asymmetry of the SIMS response is energy dependent, the peak position is itself displaced from the true position (the centroid of the response where random cascade mixing is the dominant mass transport mechanism (Littmark U and Hofer W O, 1980)) by an energy dependent shift. In this work a different method was used: Assume that the true depth z_δ of a feature such as a delta layer is known by some means. Then if $z(E)$

is the apparent depth of (say) the centroid of any delta at a given energy E, the total energy dependent offset between the true and apparent positions is:

$$\Delta z_{tot}(E) = z_\delta - z(E). \qquad (5.5)$$

This profile shift comprises dose dependent fractions of the transient shift Δz_{tr} due to changing erosion rate in the transient region and the terminal shift Δz_{te} due to the beam oxidation induced swelling of the crater base and directional relocation.

$$\Delta z_{tot}(E) = f_1(\phi)\Delta z_{tr}(E) + f_2(\phi)\Delta z_{te}(E) \qquad (5.6)$$

where $f_1 \to 1$ and $f_2 \to 0$ as $\phi \to \phi_{tr}$, and $f_1 \to 0$ and $f_2 \to 1$ as $\phi \to \phi_{cr}$.

The ϕ_{cr} is the total dose used to erode the SIMS crater. If Δz_{tot} is plotted vs. ϕ_δ for a particular energy, then

$$\Delta z_{tot}\big|_{\phi=\phi_{tr}} = \Delta z_{tr} \qquad (5.7)$$

and

$$\Delta z_{tot}\big|_{\phi=\phi_{cr}} = \Delta z_{te} \qquad (5.8)$$

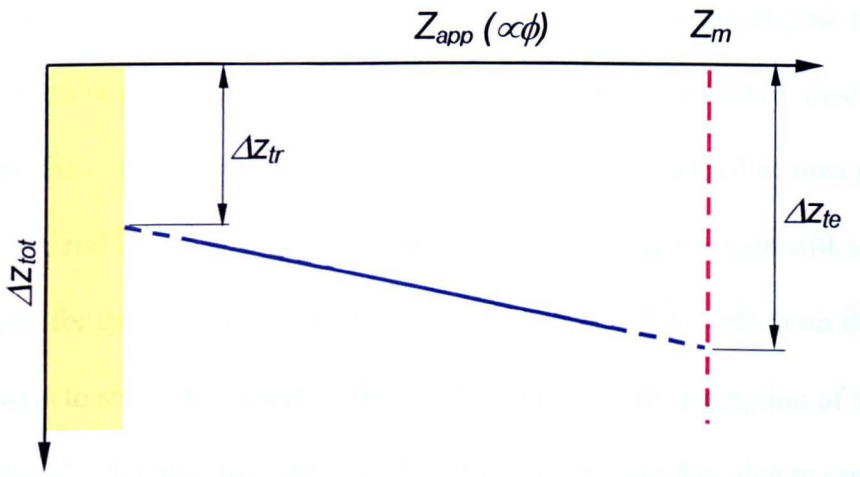

Figure 5.16: Expected shift behaviour, total shift against apparent depth.

Equation (5.8) gives the (beam energy dependent) correction required to convert the measured crater depth to the total thickness of silicon eroded plus the offset from directional relocation. In effect, if the impurity were to segregate into the altered layer, the impurity depth scale is extended beyond the depth of silicon eroded. The problem is to find a sample where z_δ is known accurately. It is known from this and other work (Wittmaack K, 1996b) that the apparent centroid and apparent peak positions for boron deltas have essentially the same intercept z_0 if plotted against beam energy. Provided any systematic errors are beam energy dependent it can be assumed that $z_\delta \equiv z_0$. This strategy has been applied to the two MBE grown samples containing multiple boron delta doped layers. In all cases immediately prior to analysis, the analyte surface was dipped in a 5 % HF solution in de-ionized water until the surface was fully hydrophobic. Therefore, all profiles started on a surface with similar conditions, and the measured parameters such as transient widths will be comparable.

The first sample (25.47) was analyzed using a normally incidence O_2^+ beam at six primary beam energies 230 eV $\leq E_p \leq$ 10 keV on EVA 3000. At each of the six primary beam energies used the apparent centroid and apparent peak maximum positions of each of the 10 delta layers in the sample were determined. For each delta layer, the centroid and peak maximum positions were plotted against primary beam energy, and the relevant z_o values determined by fitting the data with a polynomial. The results for the centroid positions are shown in figure 5.17, which on first inspection appears to show the expected linear behaviour, with the exception of the data obtained at 500 eV. To minimise any possible errors in the data, i.e. due to errors in crater depth measurement, or changes in the erosion rate during collection of the data, theoretical values of the peak centroid position were calculated (using the equations from the polynomial fit). The difference between the z_o values and the theoretical values was

then calculated for each delta layer, and plotted against the apparent depth at each E_p. The expected linear behaviour is shown in figure 5.16, assuming that there are two components to any feature shift i.e. that due to the enhanced transient erosion rate, and a shift due to swelling of the crater bottom due to retained probe atoms (and/or oxygen atoms if an oxygen flood is been used). However, the results obtained show anything but a simply linear relationship, especially at the higher energies studied. A typical example obtained at 2.5 keV is shown in figure 5.18. The data at each energy was fitted with an exponential linear curve fit function of the general form.

$$Y = a_1 e^{-X/a2} + a_3 + a_4 X \qquad (5.9)$$

The linear region at each energy was extrapolated to the measured crater depth, to calculate the terminal shift. The results obtained in the energy range $230\ \text{eV} \leq E_p \leq 5\ \text{keV}$ are shown in figure 5.19, no result was obtained at 10 keV because in the plot of measured shift against apparent depth there was no linear region. The results in figure 5.19 shows that the terminal shift correction can have a serious impact on the depth calibration for low energy shallow profiles. It extends the total depth of a boron profile from a measured 20 nm crater by ~10% if a 500 eV beam is used, and would be of the same order as the measured depth when the beam energy reaches 5 keV. For boron, the magnitude is almost identical to the total thickness of beam synthesized oxide.

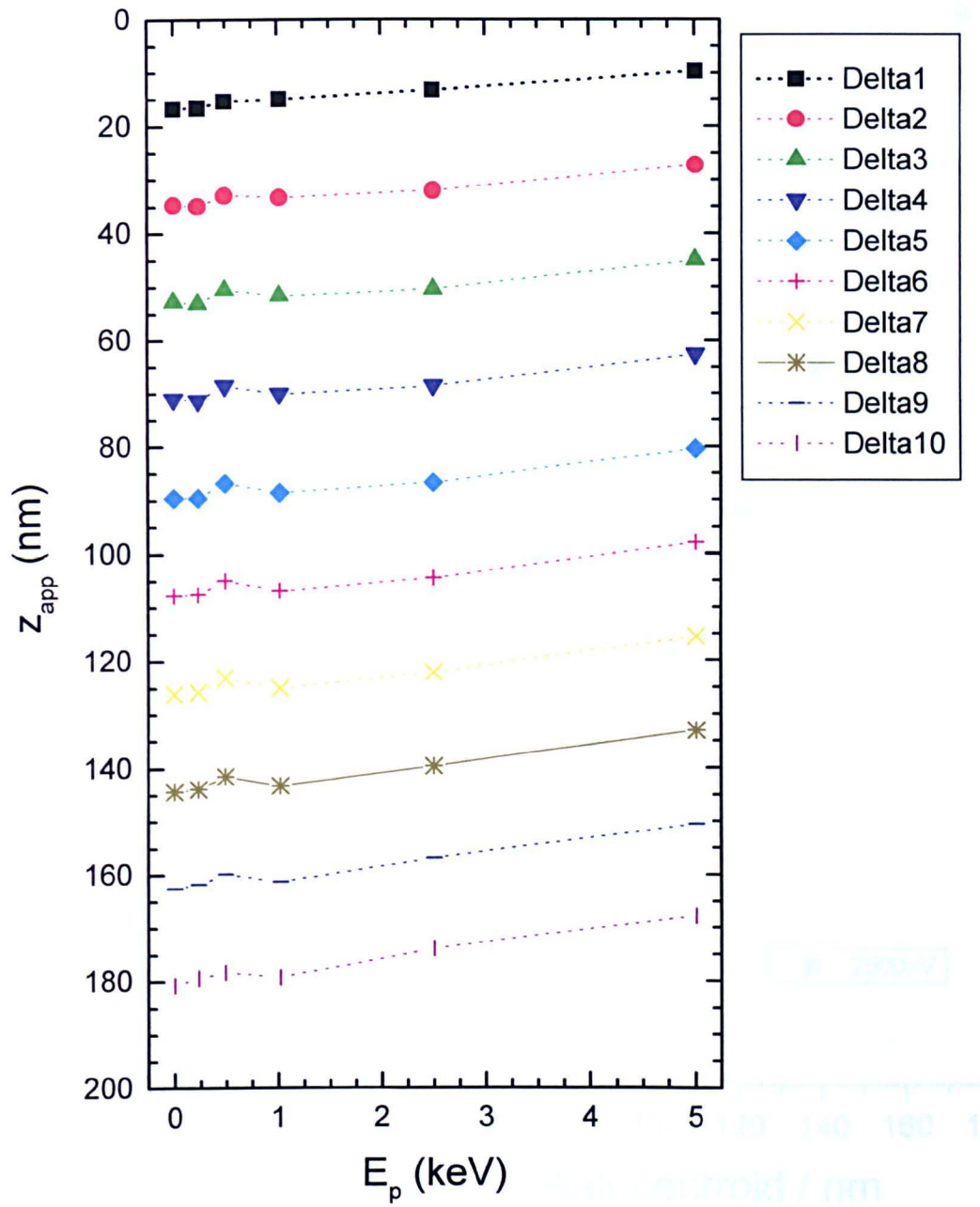

Figure 5.17: Apparent depth for the boron delta layers in sample 25.47, as a function of primary beam energy.

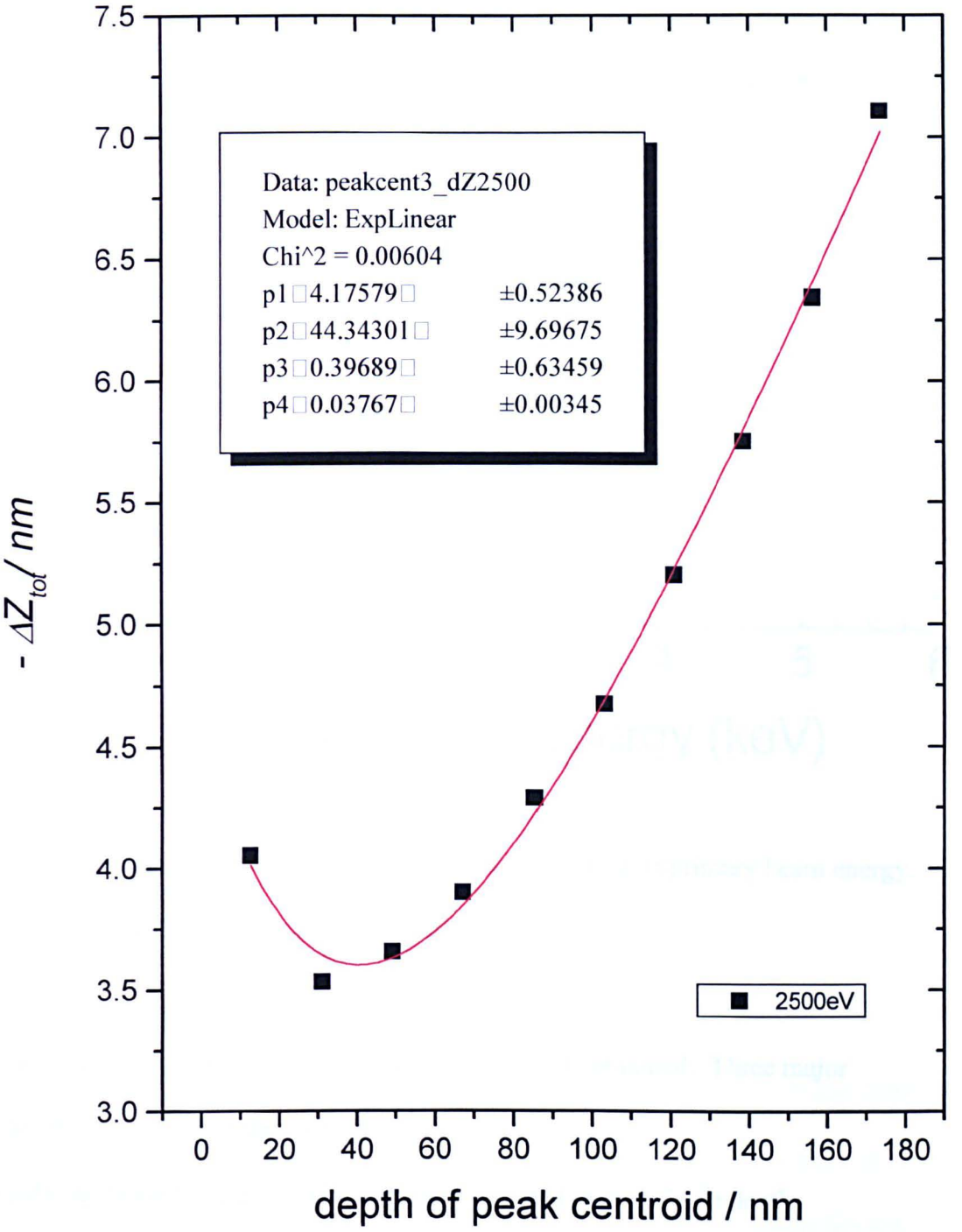

Figure 5.18: Determined total shift against apparent depth.

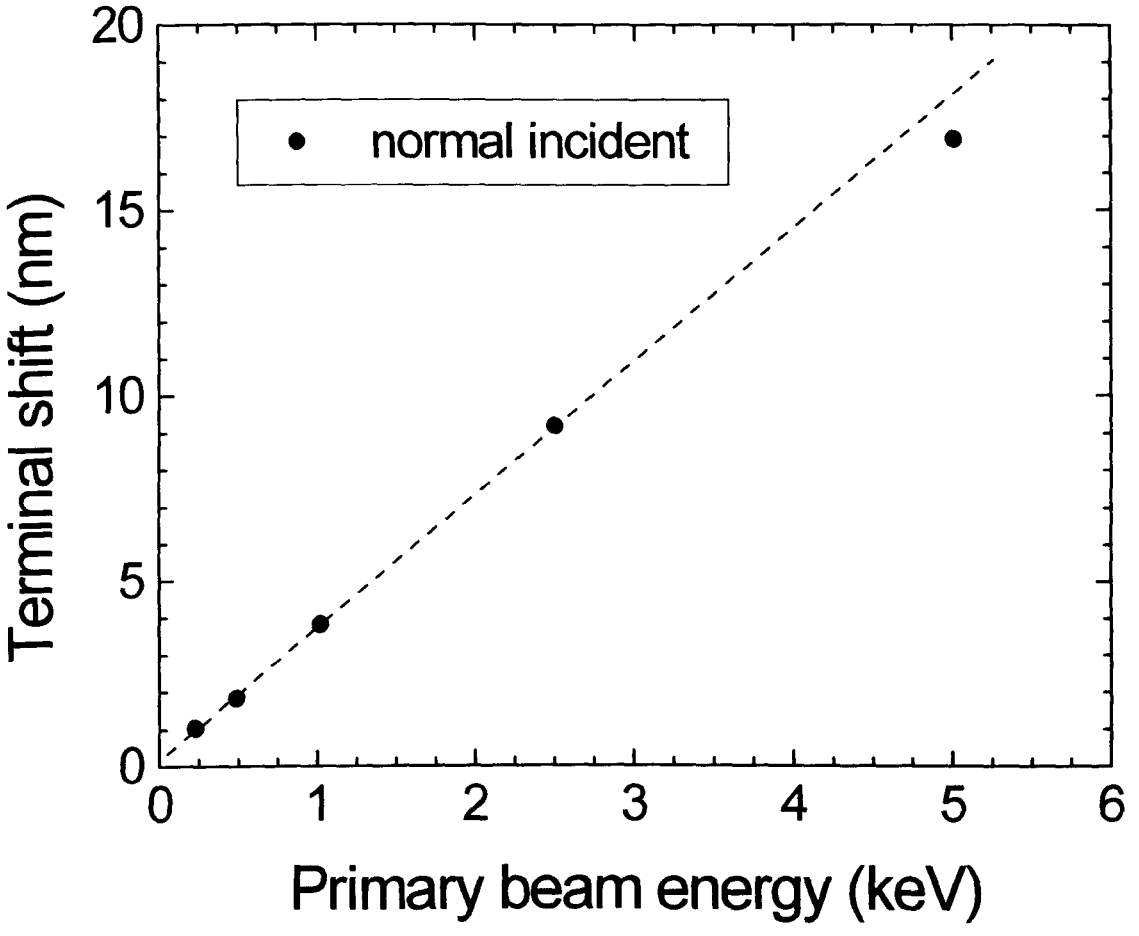

Figure 5.19: Terminal shift for boron in silicon as a function of primary beam energy. The O_2^+ beam is at normal incidence.

Figure 5.20 shows a summary of the actual results obtained. Three major observations, emerge from the data:

1. A SIMS depth profile cannot be accurately calibrated from a single depth measurement, even when combined with a single shift, as the shift required is dependent on the apparent depth.
2. The erosion rate approaches steady state asymptotically, and does not appear to stabilize with the ion yield. At E_p= 5 keV the erosion rate is still gradually changing at a depth of 70 nm. At $E_p \leq 1$ keV the extra profile shift induced is a fraction of a nm.

3. For boron, there is clearly an offset between the measured crater depth and the depth of origin. That is the centroid of a boron delta appearing to be at the base of the crater corresponds to a real feature deeper in the material by 3.6 nm/keV/O_2^+. This is partly because of the induced oxidation of the crater bottom leaves its surface above the level corresponding to the true depth of silicon eroded, but may also be due to the upward migration of boron into the altered layer.

If the data contained in figure 5.20 is replotted as shown in figure 5.21, the values of differential shift against the relative depths of the boron delta layers in sample 25.47 are obtained. The values for differential shift obtained in the energy range 230 eV $\leq E_p \leq$ 10 keV give good agreement with those previously published up to relative crater depths of 0.5. The typical peak concentration of a boron implant used in the previous studies also lie in this region if the total implant is profiled, the same can be said for the majority of the boron delta layers used. It is also known that the differential shift for a peak maximum is substantially different from that of a centroid (Wittmaack K, 1996b). The terminal shift values also show a non-linear energy dependence of the form shown in equation 5.10.

$$\Delta Z_{te} = 3.85\, E_p^{0.92} \qquad (5.10)$$

All the terminal shift values obtained to date as shown in figures 5.29 and 5.30 (with the exception of the 4 keV data obtained on sample 59.25), are very similar in magnitude to those reported by Dowsett (2000), for the altered layer thickness formed using O_2^+ bombardment at normal incidence. This strongly suggests there is some upward migration of boron into the altered layer.

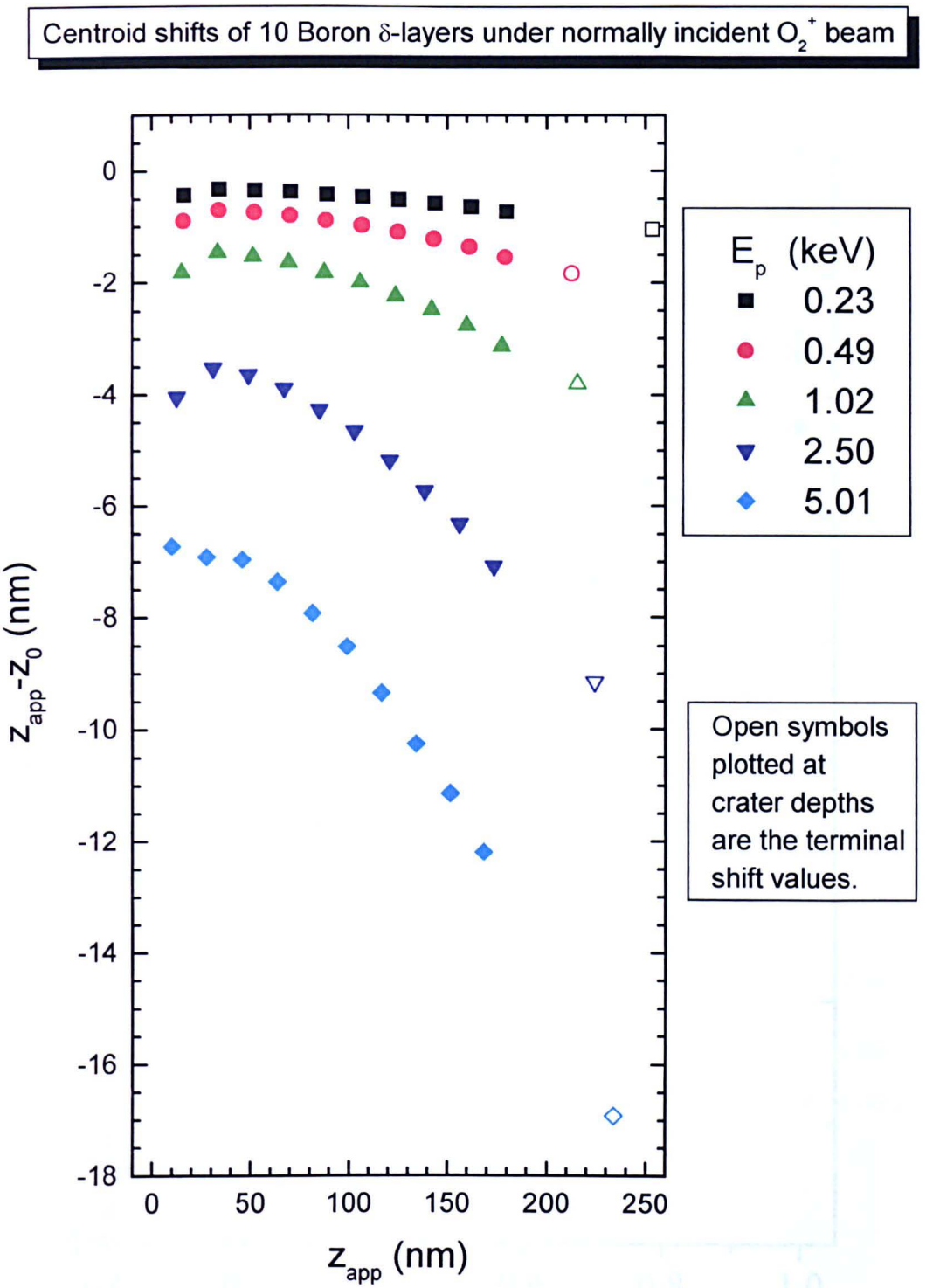

Figure 5.20: Profile shift measured for the boron delta layers in sample 25.47. The open symbols show the terminal shift of 3.6 nm/keV determined from the experiment.

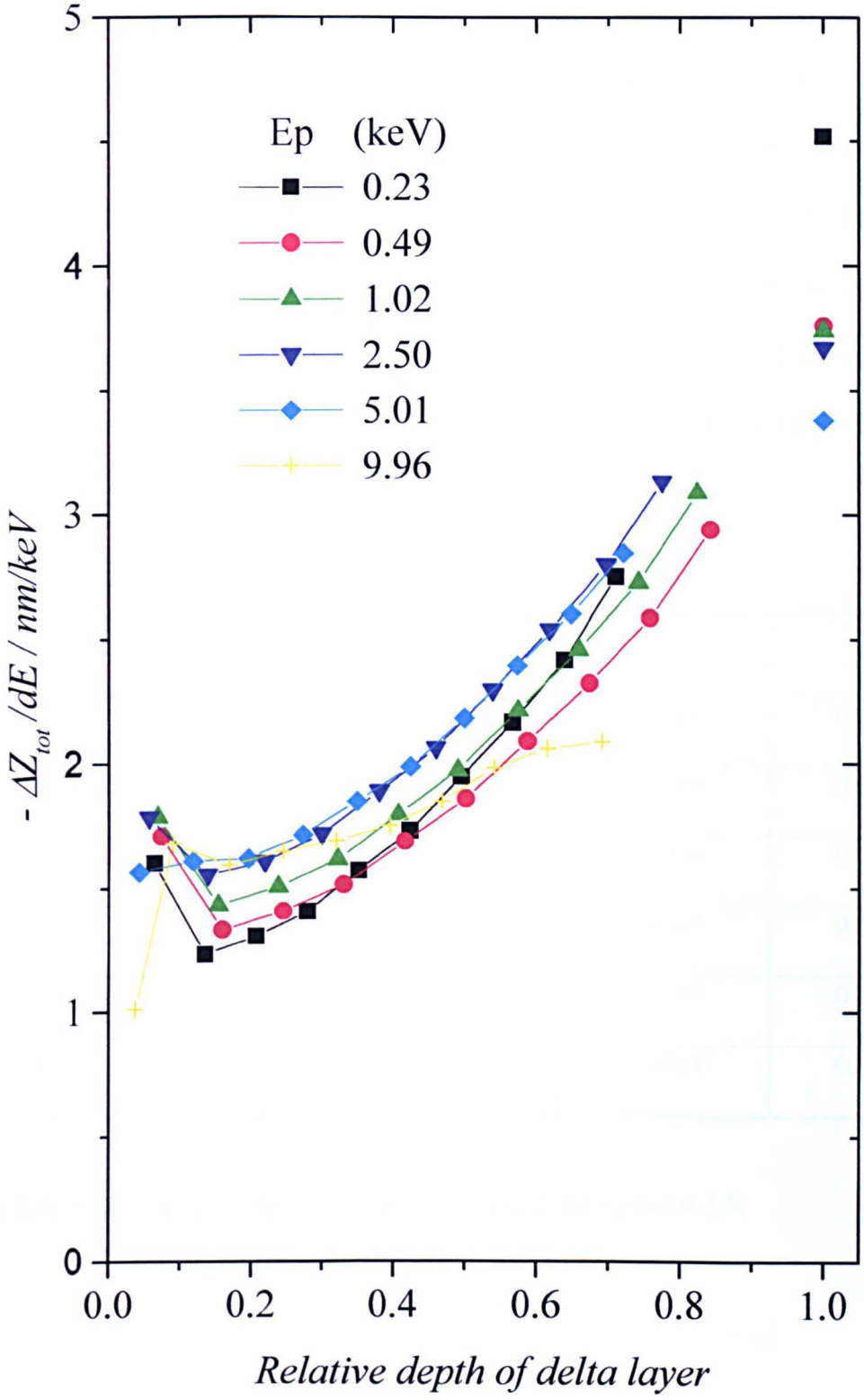

Figure 5.21: The differential shift as a function of feature depth as determined for sample 25.47. The open symbols show the terminal shift values as a function of E_p.

As mentioned previously the peak centroid data at each energy could be fitted with an exponential linear curve fit function of the general form shown in equation (5.9). The values of the individual parameters are shown in table 5.2 where $Y=\Delta z_{tot}$ and $X=z_{app}$. These values have been used to correct the depth scale of the raw data obtained on sample 25.47, followed by an area normalization, as shown in figure 5.22. It clearly shows that this procedure can be used with good agreement ± 2 nm across the full energy range studied, provided the data is beyond the transient region. However, as the observed shift for a feature at a given energy is also dependent on the depth of the profiled crater, their general applicability is limited in this form.

E_p / keV	a_1	a_2	a_3	a_4
0.23	0.5745	17.1169	0.1600	0.0029
0.49	1.1198	17.9495	0.3381	0.0062
1.02	1.9690	19.9025	0.6926	0.0127
2.50	3.3373	28.7677	1.5017	0.0305
5.01	6.7035	62.8510	0.8103	0.0644
9.96	6.3028	31.0357	8.9015	0.0488

Table 5.2: Values of the fitting parameters obtained for equation 5.9.

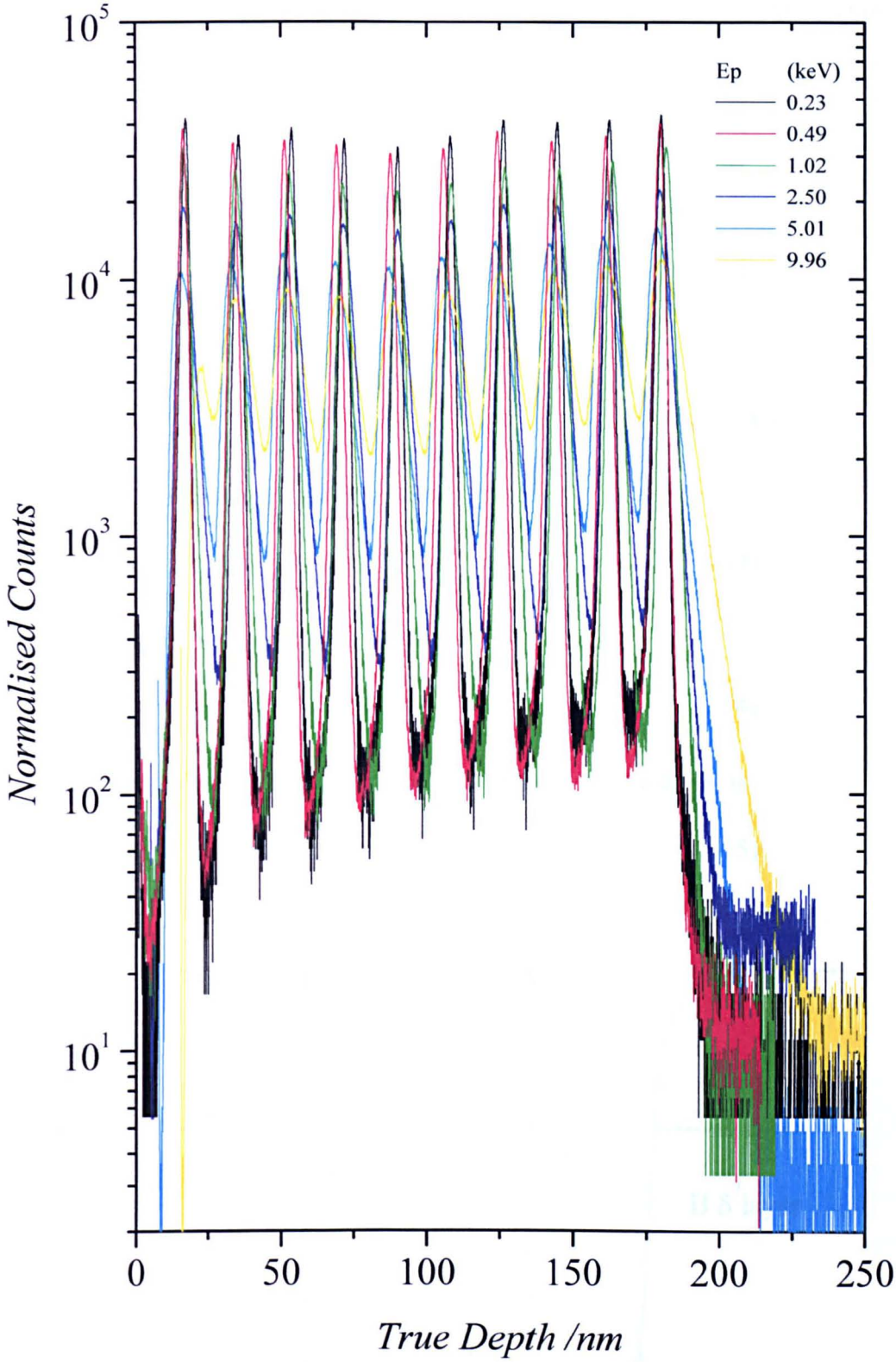

Figure 5.22: Area normalised $^{11}B^{+}$ profiles of sample 25.47, against corrected depth.

However, it is now possible to describe a general correction procedure required to obtain an accurate depth scale for normal incidence profiling using a measured crater depth z_m (see figure 5.23):

The effective end of the depth scale z_B for the dopant is

$$z_B = z_m + \Delta z_{te} . \tag{5.11}$$

An apparent erosion rate $\dot{z}_{app}$ is calculated from

$$\dot{z}_{app} = z_m / \phi_{cr} . \tag{5.12}$$

The true width of the transient region is then:

$$z_{tr} = \dot{z}_{app} \phi_{tr} + \Delta z_{tr} \tag{5.13}$$

and the profile dopant related evolution rate is

$$\dot{z}_B = (z_B - z_{tr}) / (\phi_{cr} - \phi_{tr}) . \tag{5.14}$$

Finally, the true depth z of any ordinate at a beam dose ϕ where $\phi > \phi_{tr}$ is

$$z = z_{tr} + \dot{z}_B (\phi - \phi_{tr}) . \tag{5.15}$$

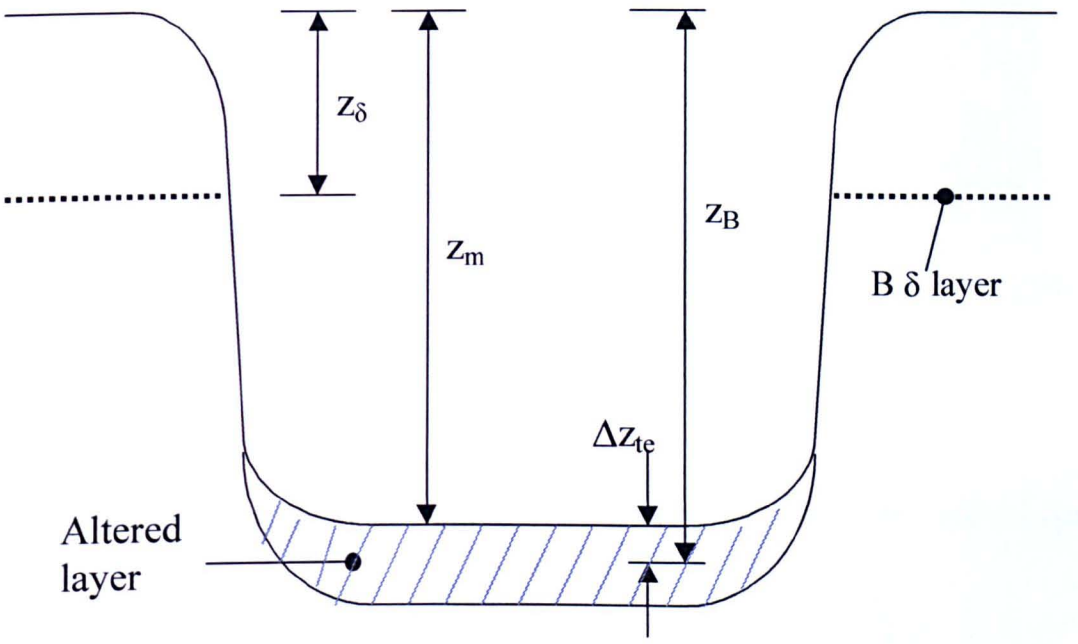

Figure 5.23: Schematic of the depth parameter notation.

This second universal depth correction procedure, has also been applied to the raw experimental data obtained on sample 25.47, followed by an area normalization, as shown in figure 5.24. While the agreement ± 3.5 nm across the full energy range studied is not quite as good as the first procedure used in figure 5.22, it should be more widely applicable in the energy range 230 eV ≤ E_p ≤ 5.01 keV. The residual errors from using both depth correction procedures are shown in figure 5.25.

To further investigate the non-linear relationship of ΔZ_{tot} with apparent depth, due to the erosion rate approaching steady state asymptotically, and confirm the magnitude of the terminal shift, a second sample 59.25 was studied. Sample 59.25 was analyzed using a normally incidence O_2^+ beam at seven primary beam energies 230 eV ≤ E_p ≤ 4 keV on EVA 2000FL. A profile of sample 59.25 obtained at 3 keV is shown in figure 5.26. The first 2 boron delta layers in this profile are merged and distorted in this profile, as they are in the transient region of the profile.

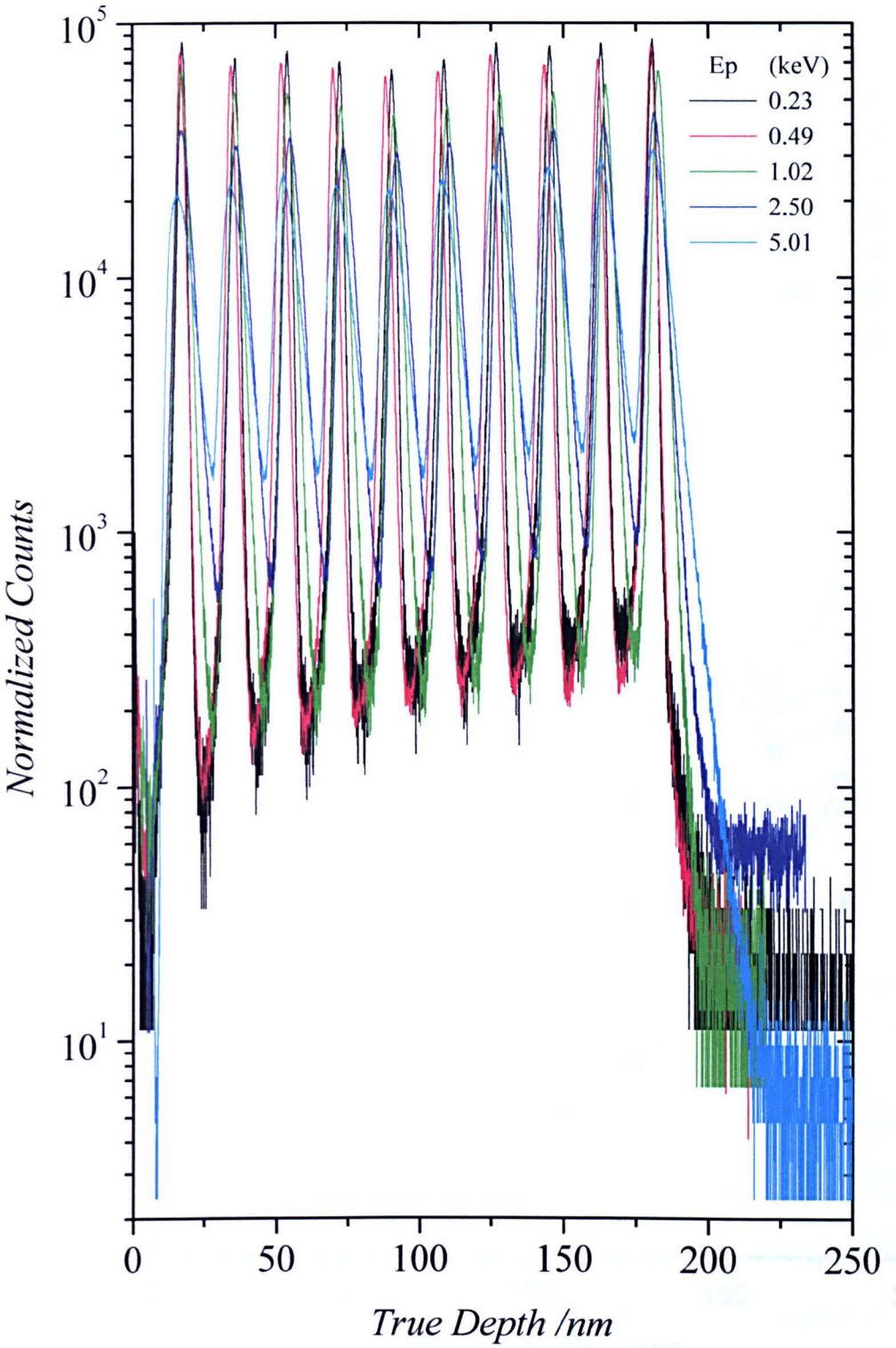

Figure 5.24: Area normalised $^{11}B^{+}$ profiles of sample 25.47, against corrected depth using the second universal depth correction procedure.

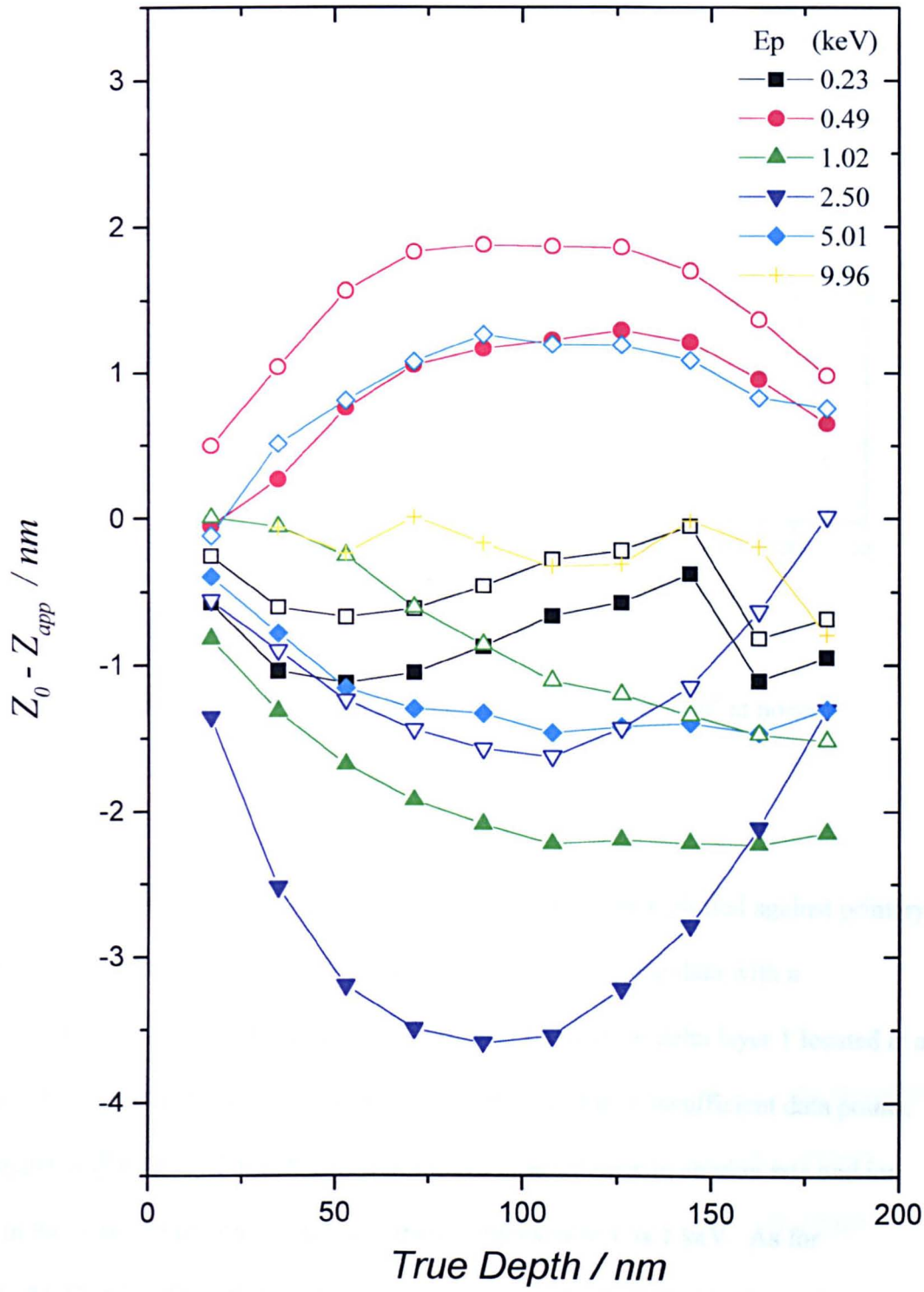

Figure 5.25: Residual errors from both depth correction procedures, solid symbols for the universal linear data and open symbols for the exponential linear curve fit data.

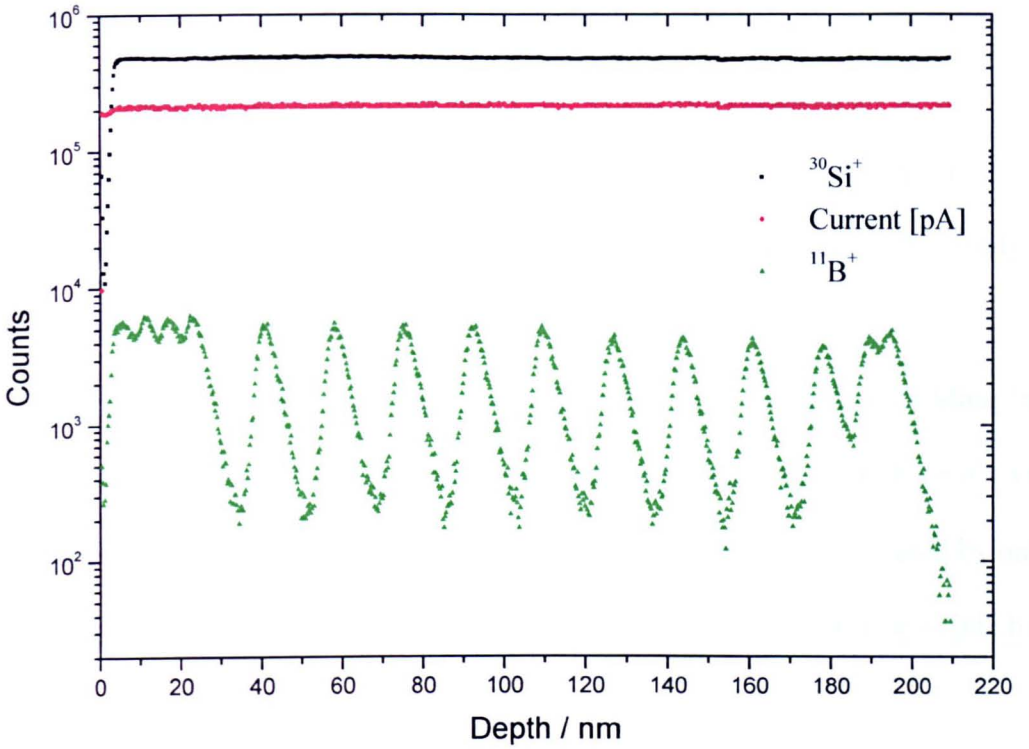

Figure 5.26: Depth profile of sample 59.25 obtained with 3 keV O_2^+ at normal incidence.

For each delta layer the apparent centroid positions were plotted against primary beam energy, and the relevant z_o values determined by fitting the data with a polynomial. This is with the exception of the data obtained for delta layer 1 located at a depth of 4.6 nm, this had to be fitted with a straight line due to insufficient data points. The shape of delta layer 1 was highly deformed by the changes in erosion rate and ion yield in the transient region, at primary beam energies as low as 1 keV. As for sample 25.47 the difference between the Z_0 values and the theoretical value was calculated for each delta layer, and plotted against the apparent depth at each E_p. A typical result obtained at 2 keV is shown in figure 5.27, which is completely different from that obtained previously with sample 25.47, *c.f.* figure 5.18. Delta layers 1 - 5

along with 15 and 16, which are spaced approximately 5.5 nm apart appear to show larger shifts, than those spaced 17.5 nm apart (i.e. delta layers 6 - 13), across the entire energy range studied. Part of this extra shift (~50%) can be accounted for by the induced error in determining the centroid position of the delta layer over less orders of magnitude. At 2 keV the relevant orders of magnitude of separation are 1.5 *c.f.* only 0.25 for the closer spaced delta layers.

Very recently research at Warwick university by Dr. B Guzmán de la Mata, has shown that when delta layers are this closely spaced, depth resolution can have a severe effect on the apparent centroid position. If the boron delta layers are separated by one order of magnitude (like at a beam energy of 250 eV), the effect can still be as much as 0.2 nm.

The measured shift for delta layers 6 - 13, in the depth range 45 - 166 nm shows a strong linear relationship with depth, over the entire energy range studied, as can be observed in figure 5.28. The shifts are slightly larger than those observed with sample 25.47, and the general trend is distorted by the different spacings of the individual delta layers. The magnitude of this distortion increases with energy. Unfortunately, due to the delta layer spacing and locations, there is no conclusive evidence, to prove or disprove the asymptotic erosion rate changes observed in sample 25.47. This information may become available by deconvolving the data, however this has not been done at present. This linear region at each of the seven primary beam energies was extrapolated to the measured crater depth to calculate the terminal shift, the results obtained are shown in figure 5.29.

The value of the terminal shift obtained at 4 keV, appears to be considerably smaller than expected, this maybe due to the particular polynomial fitting procedure used in Microcal Origin 4.1, which always passes through the last data point.

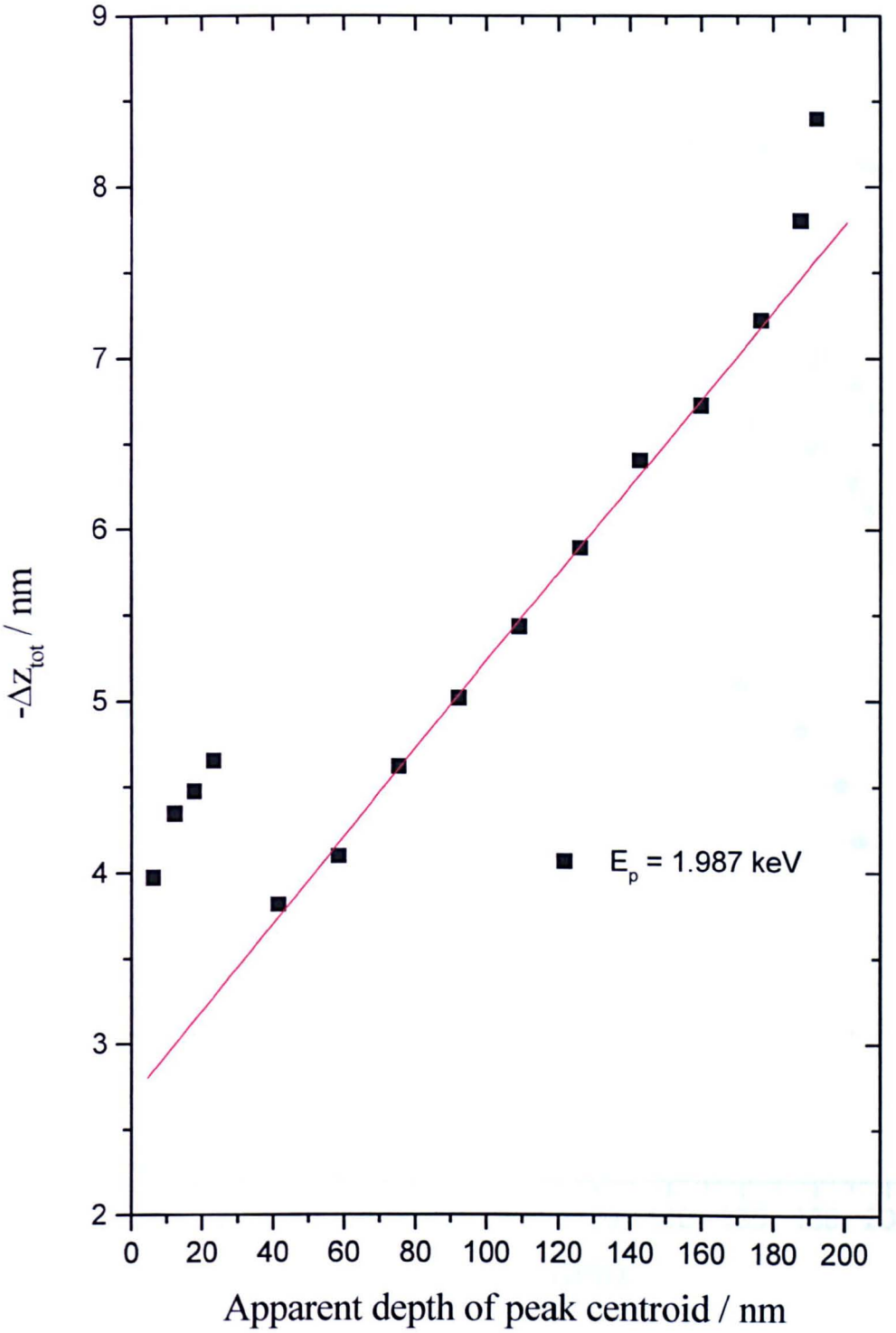

Figure 5.27: Determined total shift against apparent depth, for sample 59.25 at 2 keV.

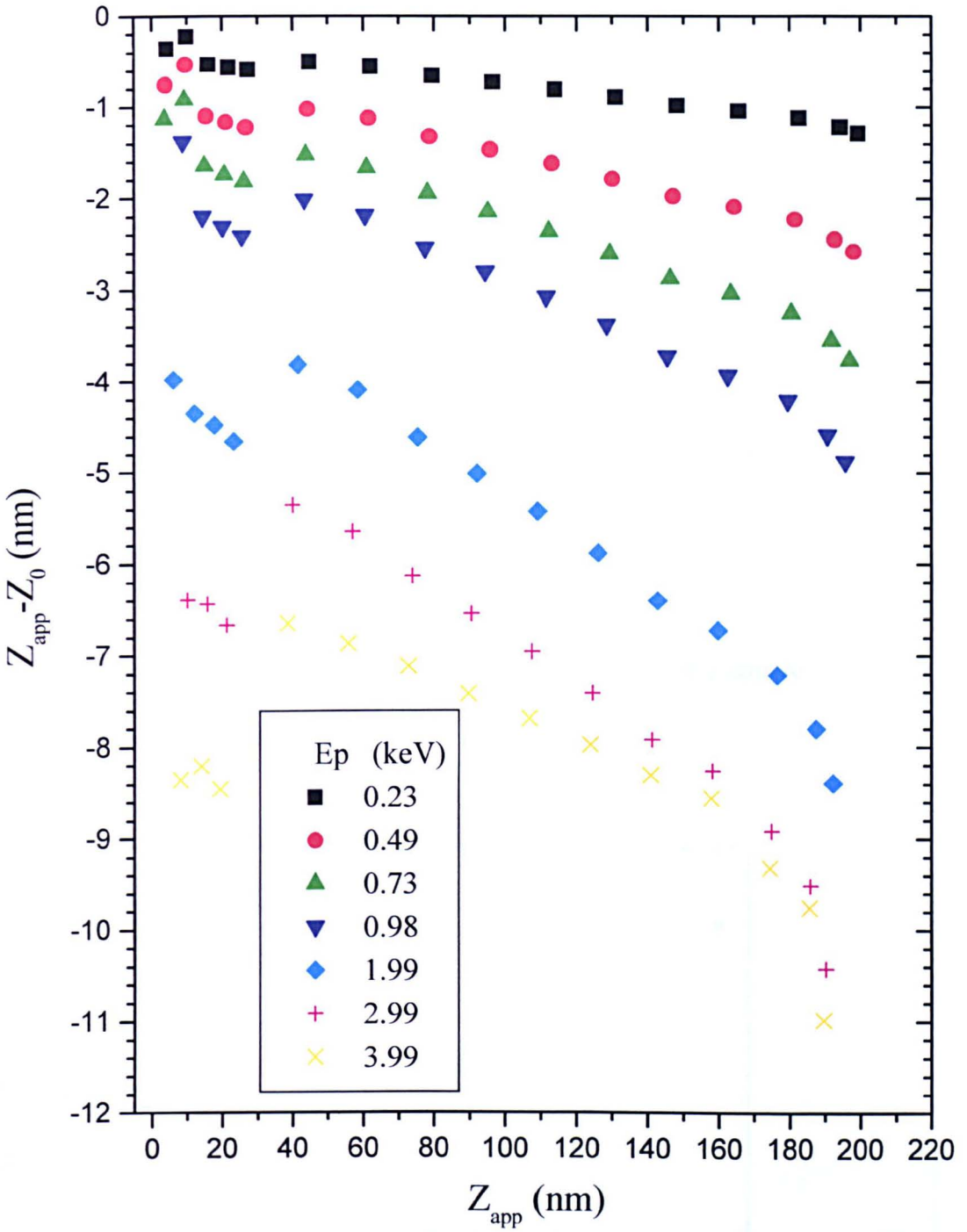

Figure 5.28: Profile shift measured for the boron delta layers in sample 59.25. The O_2^+ beam was at normal incidence.

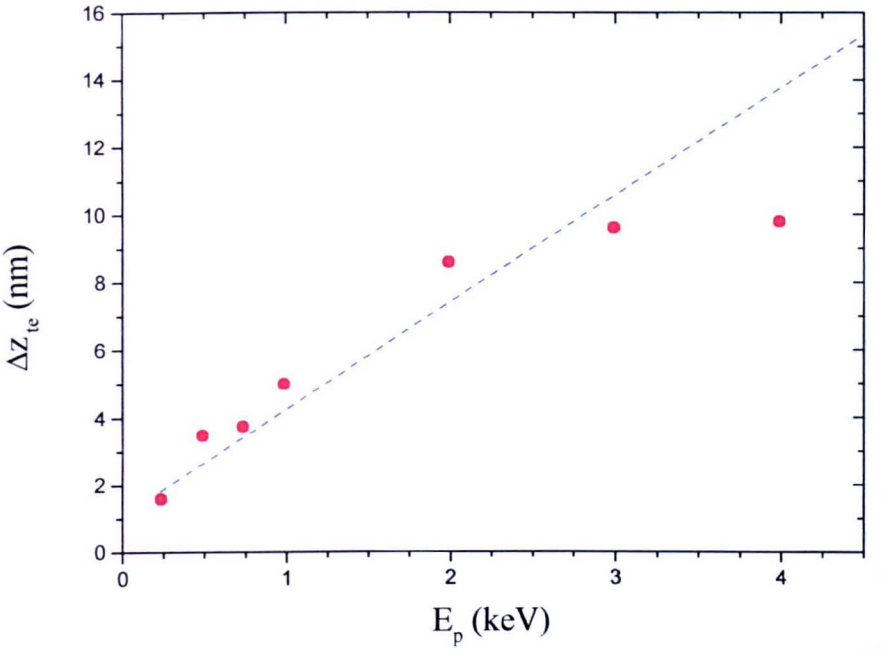

Figure 5.29: Terminal shift for boron in silicon as determined using sample 59.25, as a function of primary beam energy.

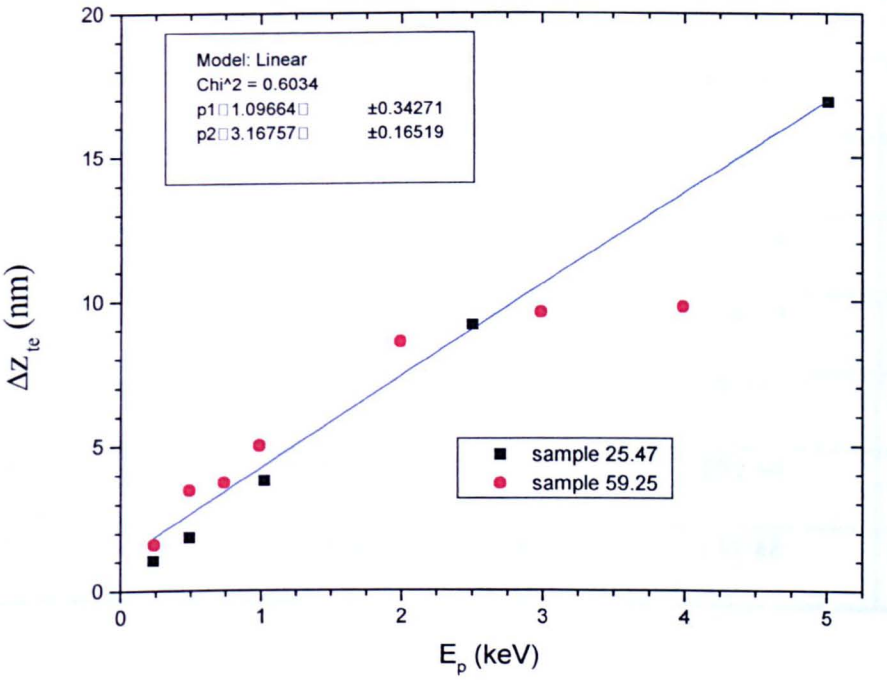

Figure 5.30: Terminal shift for boron in silicon as determined using samples 25.47 and 59.25 , as a function of primary beam energy.

A summary of the data from samples 25.47 and 59.25 is shown in figure 5.30, along with the line of best fit (the data point obtained at 4 keV was excluded from the fit).

To provide further data on the terminal shift, an undipped piece of sample 59.25 was profiled to different depths using a normally incidence O_2^+ beam at 3 keV on the Atomika 4500 instrument at Warwick. A summary of the results obtained are shown in table 5.3, which shows the mean observed shift of the last delta layer is 6.57 nm, and there is no obvious relationship between the size of the observed shift and the depth of the deepest delta layer. The observed shifts are all significantly smaller than the expected shift of 9.6 nm for a dipped piece of sample 59.25, although the HF dipping

Crater number	Crater depth / nm	Depth of deepest centriod / nm	Depth of deepest centriod / %	z_0 of deepest centriod / nm	Observed shift / nm
2	48.3	38.77	80.28	45.18	6.41
3	101.9	91.56	89.86	97.22	5.65
4	209.3	194.52	92.94	200.54	6.02
5	126.1	107.30	85.09	114.59	7.29
6	103.0	90.40	87.77	97.22	6.82
7	425.8	194.53	45.69	200.54	6.01
5	126.1	124.08	98.40	131.88	7.80

Table 5.3: Summary of results obtained on a undipped piece of sample 59.25, during a terminal shift investigation. All results obtained using a normally incidence O_2^+ beam at 3 keV.

process is thought to remove approximately 1 nm of oxide. The spread in the data is also much smaller than expected, the minimum expected error in the crater depth measurement is ± 2% (with a minimum of ± 2 nm).

The apparent lack of an obvious relationship between the size of the observed shift and the depth of the deepest delta layer, was investigated further by looking at individual delta layers. Some of the results are shown in figure 5.31, which clearly shows that the deeper a delta layer is in a profile the larger is the observed shift. The terminal shift values obtained for delta's 6 and 9 were 7.3 and 6.9 nm respectively, but for delta layer 3 it was 9.7. The larger observed shift values obtained for delta layer 3 are due to some contribution from the transient shift.

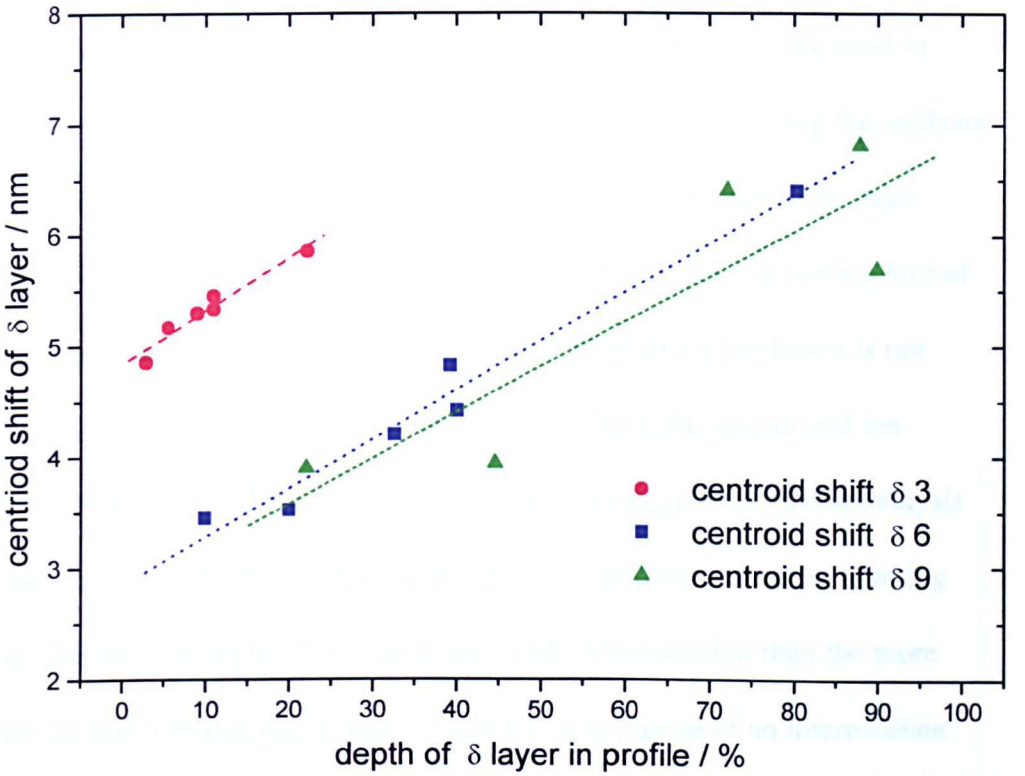

Figure 5.31: Observed centroid shifts for selected boron delta layers in a undipped piece of sample 59.25, as a function of its depth in the profile. All profiles were obtained using 3 keV O_2^+ at normal incidence.

5.3 Dual Beam Energy Profiling

The advantages of ultra-low energy SIMS i.e. a small transient region and high depth resolution, have led to the technique been widely utilized, especially for ultra-shallow implant characterization (boron and arsenic below 1 keV). In order to obtain accurate dosimetry of ultra-shallow implants, which have a very narrow, but high near-surface concentration, ion beam energies of 100-250 eV (for O_2^+) must be used.

After implantation, the dopant may only extend a few nanometers, however subsequent annealing can radically change the distribution due to the very high defect concentration, and the phenomenon of transient enhanced diffusion. SIMS is the only technique that can detect electrically inactive boron at sufficiently high sensitivity near the surface and at the position of the metallurgical junction. However, the need to detect both these parameters accurately leads to a dilemma when choosing the analysis conditions. A low beam energy is required to fully resolve the dopant in the near-surface region, which will only be a few nanometers deep, and yet can contain half of the implanted dose. However, for most of the profile, high depth resolution is not required. As the primary beam energy is reduced so are both the sputter and ion yields, as shown in figures 5.32 and 5.33, which leads to longer uneconomic analysis times and decreased sensitivity. This latter point can be important as poor counting statistics can introduce a larger error in junction depth determination than the more usual sources of depth related uncertainty. Therefore a comprise of an intermediate beam energy is often made, so that the near-surface feature is reduced to a SIMS related transient, but the total retained dose and junction depth can be measured. Profiles obtained under the comprise conditions can lead to incorrect interpretation of

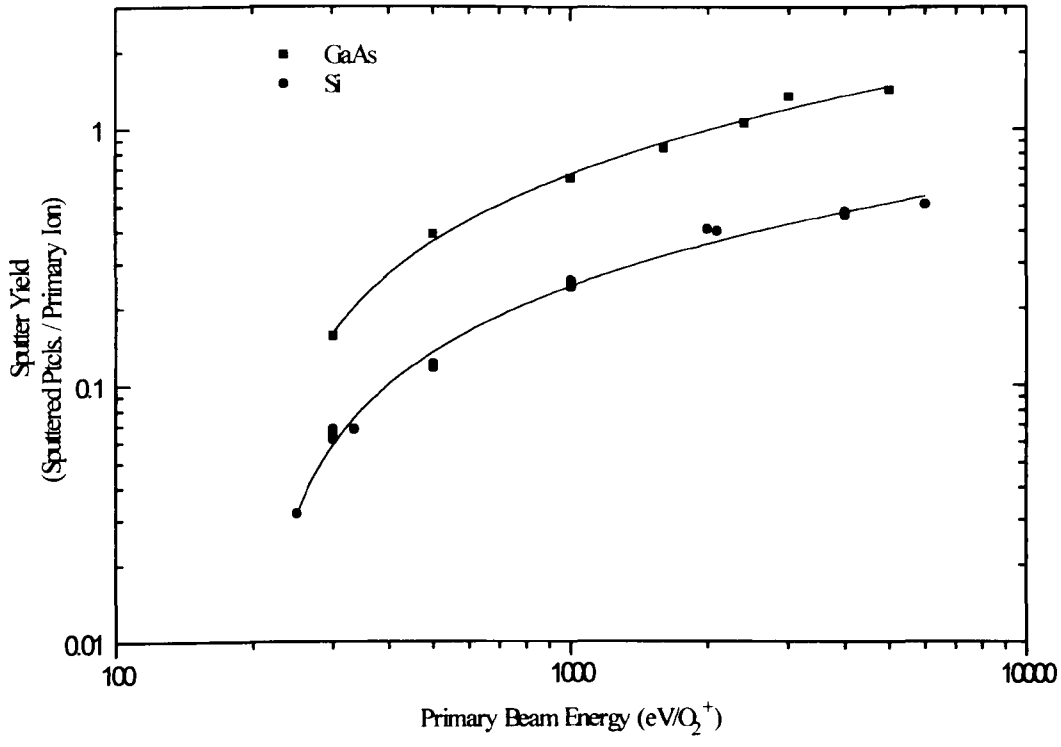

Figure 5.32: Silicon and gallium arsenide normal incidence sputter yields, as a function of primary beam energy. The O_2^+ beam is at normal incidence. Data from reference Smith (1996).

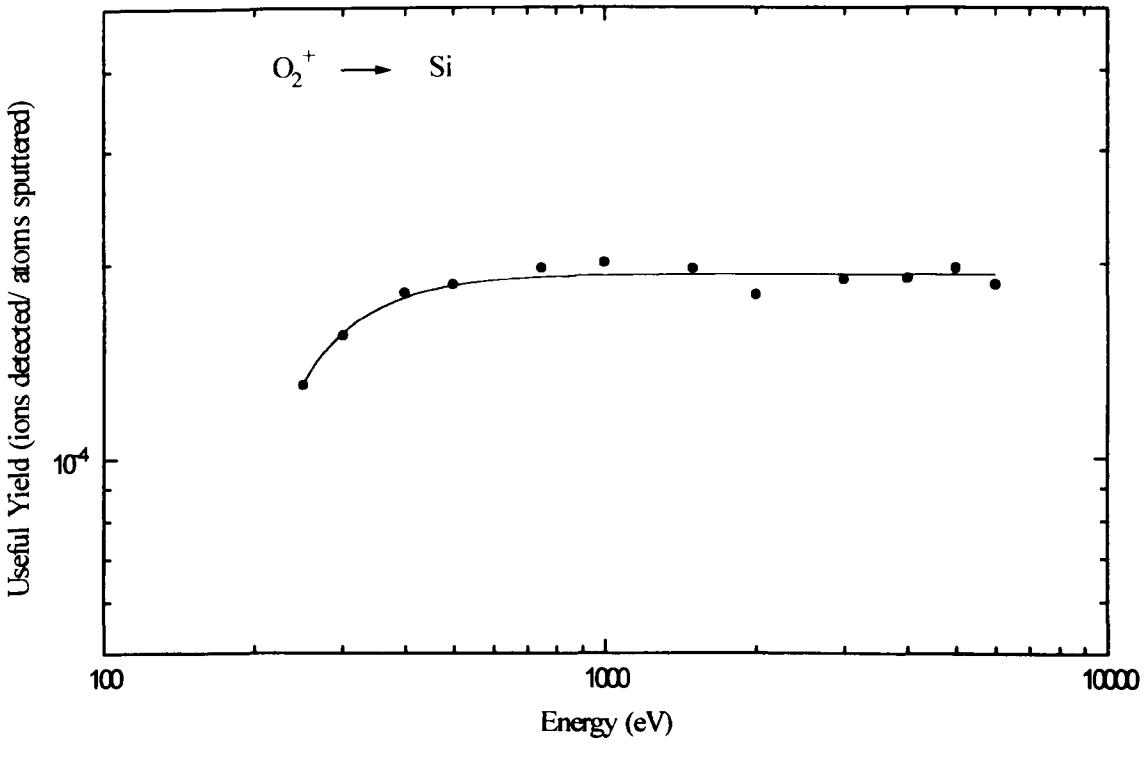

Figure 5.33: Useful silicon ion yield, as a function of primary beam energy. The O_2^+ beam is at normal incidence. Data from reference Smith (1996).

the implant physics, as the observed implant shape is limited by the SIMS measurement itself.

This section demonstrates the use of matching the primary beam ion energy to the requirements of the analysis, and investigates the quantification issues of changing the beam energy within a single depth profile.

During the measurement of ultra-shallow implants using dual beam energy profiling, we naturally start with a very low energy to minimise the unquantifable pre-equilibrium region. The beam energy is increased once the measured decay length is smaller than the limiting decay length at the second higher energy. A plot of the energy dependence of depth resolution parameters is shown in figure 5.34. The opposite case, of lowering the beam energy was also investigated, for the application of detailed analysis of deep structures and interfaces.

As was shown earlier in chapter 5.1, the depth profile recorded for boron in silicon using normal incidence O_2^+ bombardment, is shifted progressively nearer the surface as the beam energy is increased (the transient shift). Therefore it would be expected that changing the beam energy during analysis, would introduce an additional shift. If dual beam energy profiling is to become a widely employed technique, it is important to determine the magnitude of any shifts and develop a method for the accurate quantification of the complete depth profile.

Sample 59.25 containing sixteen boron delta layers was used to characterize any shifts in the profile. This sample has been carefully characterized, and the z_0 position of each delta layer is known, thus providing at least two of these layers are included the sample is self calibrating in depth. Three O_2^+ primary beam energies at normal incidence were investigated, 250 eV - for very high depth resolution and near

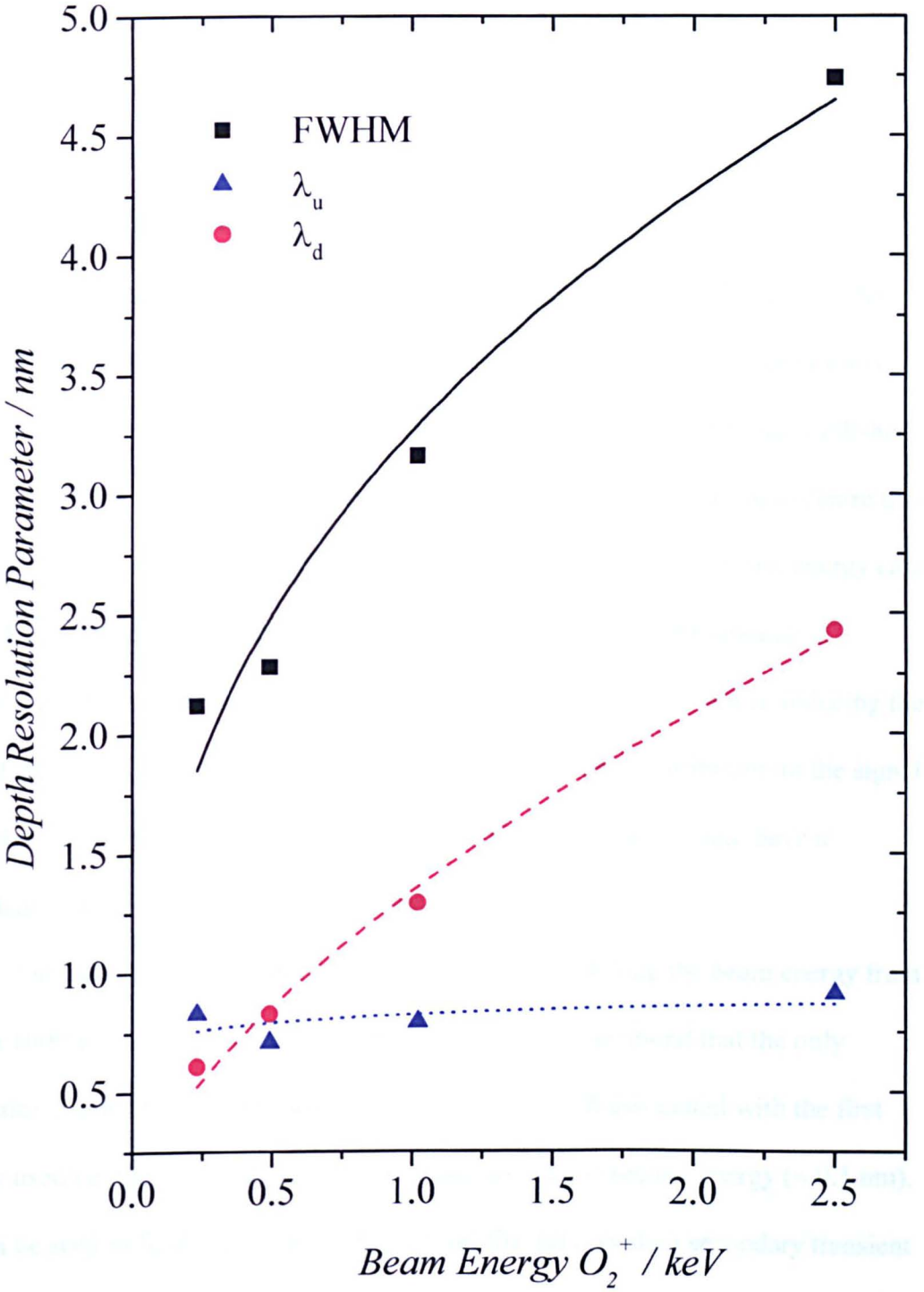

Figure 5.34: Depth resolution parameters FWHM, λ_u, and λ_d as a function of primary beam energy for normal incidence O_2^+ analysis of boron in silicon, determined using sample 25.47.

surface quantification, 500 eV - for a higher erosion rate and good depth resolution, 1 keV - for a fast erosion rate and best sensitivity. As can be seen from figures 5.32 and 5.33 increasing the beam energy above 1 keV, brings little improvement in sensitivity or erosion rate, while the depth resolution continues to degrade.

Prior to performing the measurements on EVA 2000FL the three sets of analysis conditions were optimised, and the individual settings saved. In order that the profile can be carried out in the same crater at two different beam energies it is necessary to have accurate registration of the beam position. This was accomplished by ion imaging a feature at each energy and using the scan offset control to centre the feature in the scanned area. With this information also recorded the beam energy can easily be switched, the settling time of the primary column is approximately 2 seconds, during which time the beam is blanked. A further precaution of reducing the size of the raster at the second energy was also taken, as any contribution to the signal from the crater walls, or from the surface, to the recorded profile could have a significant detrimental affect on the dynamic range.

On quantifying the depth profiles obtained by switching the beam energy from 250 to 1000 eV, 500 to 1000 eV and 1000 to 250 eV, it was found that the only correction needed to the depth scale was the transient shift associated with the first energy used i.e. there is no depth correction required at the second energy (< 0.1 nm). As can be seen in figures 5.35 and 5.36 each profile did contain a secondary transient region on switching the beam energy there is a region (typically 0.8 - 1.0 nm) where there is a change in ion yield, provided that this does not obscure a feature it can be neglected from the final result. These surprising minimal extra effects on switching the beam energy are thought to be due to the size of the altered layers being very

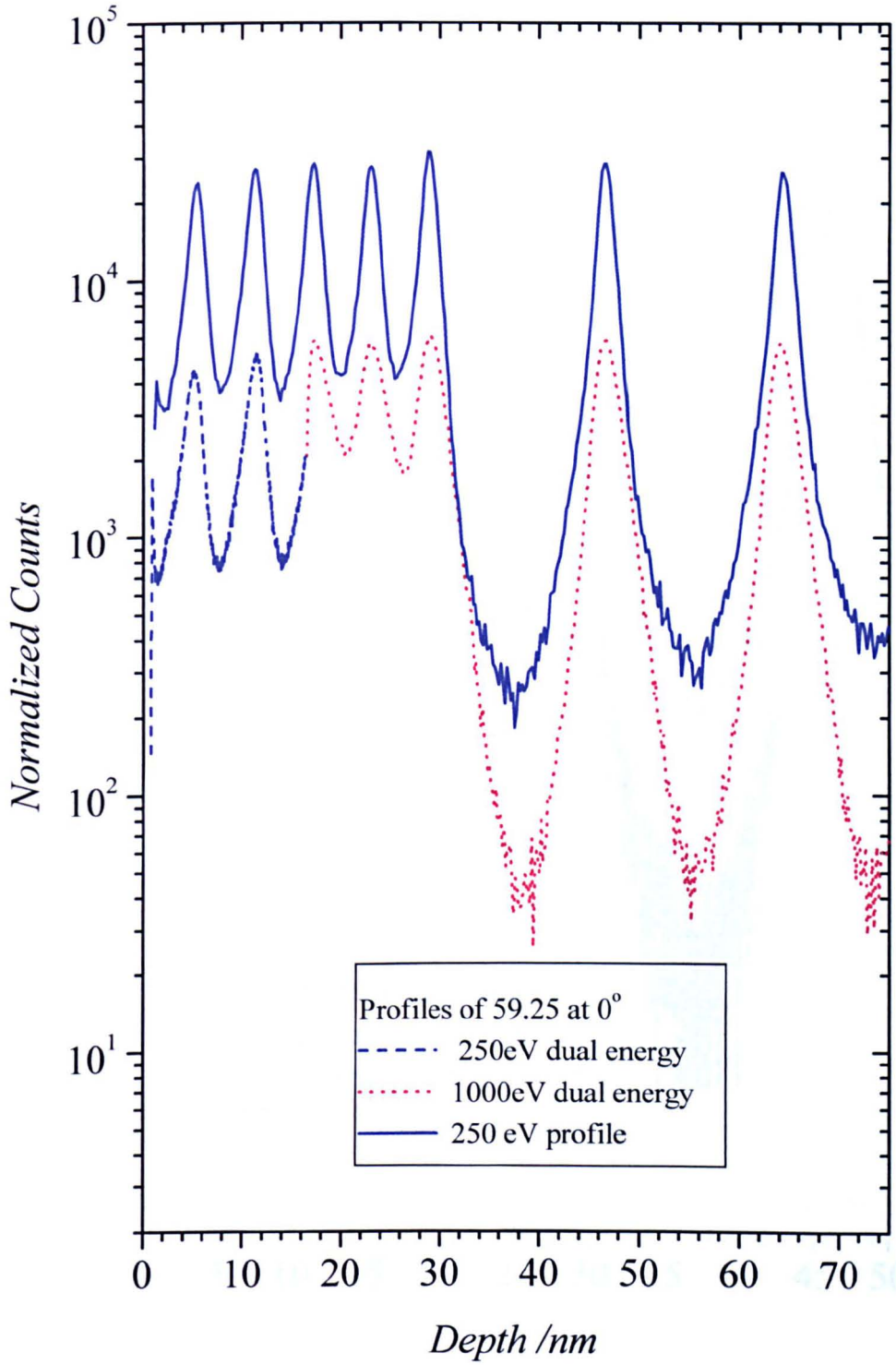

Figure 5.35: A comparison of B depth profiles for sample 59.25, obtained at normal incidence using O_2^+, (a) at 250 eV, (b) dual beam energy profile with initial and final energies of 250 and 1000 eV respectively.

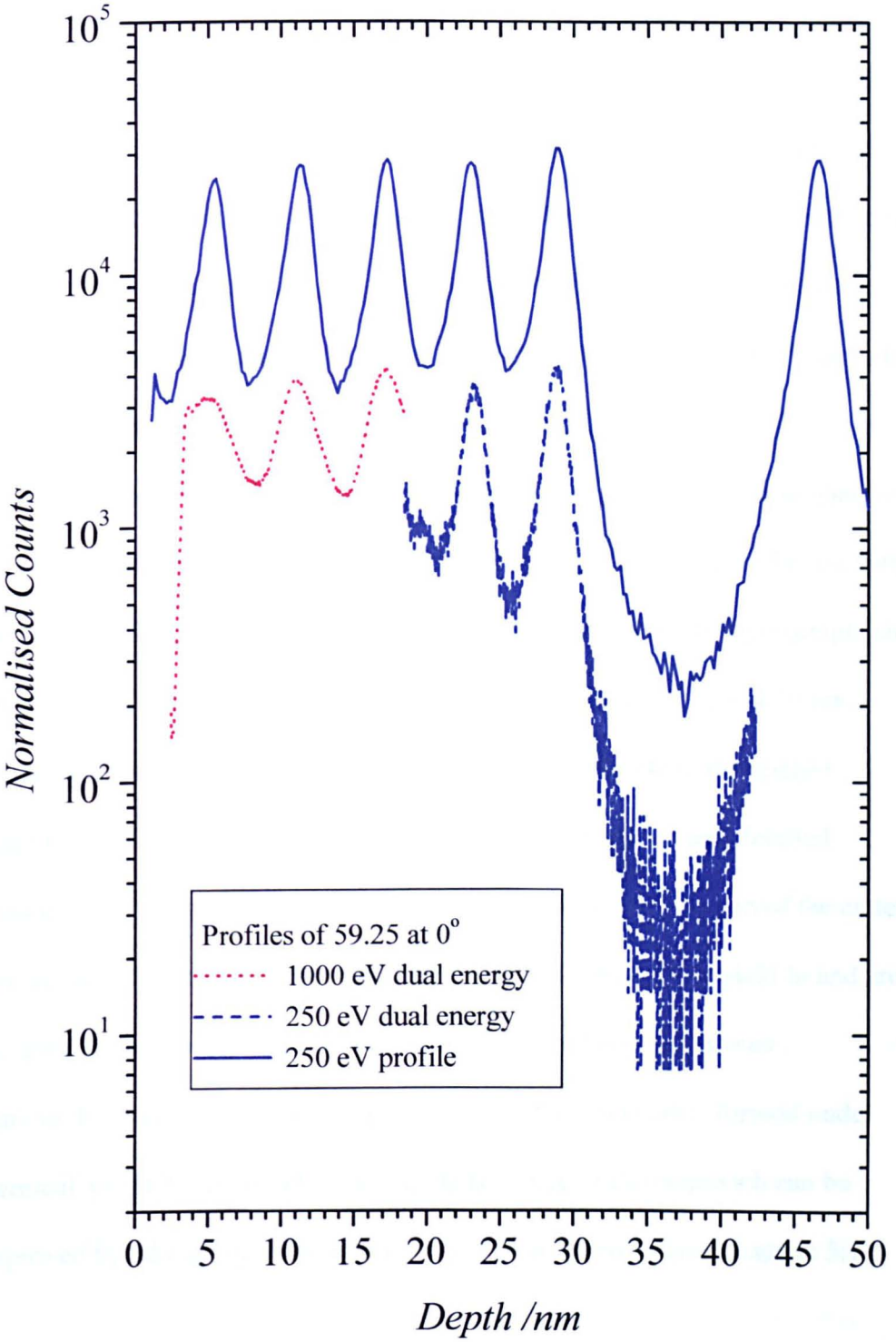

Figure 5.36: A comparison of B depth profiles for sample 59.25, obtained at normal incidence using O_2^+, (a) at 250 eV, (b) dual beam energy profile with initial and final energies of 1000 and 250 eV respectively.

similar within the analysis conditions studied. On switching the beam energy to a higher value there is a increase in the gradient of the slope in this region, and *vice versa*, this effect is clearly visible in figures 5.35 and 5.36. This effect is due to variations in the magnitude of the chemical and physical processes (i.e. mixing and segregation) occurring during the formation of the altered layer at different energies. Also plainly visible are the advantages of working at ultra-low beam energies, at 250 eV there is a significant improvement in the depth resolution parameters with more orders of magnitude of separation between the delta layers.

When using the technique of dual energy profiling to analyse ultra-shallow implants, the shallow part of the profile (formed at low energy) cannot be routinely measured by surface profilometery, with the required accuracy. In the example shown in figure 5.37, 55% and 94% of the retained dose was in the first 2 and 10 nm respectively in the 250 eV profile. Two methods are available to the analyst.

1. Requires accurate measurement of the primary beam current and detailed knowledge of the actual crater size, and sputter yields, so the depth of the crater can be calculated. For even higher accuracy, changes in the sputter yield in and around the transient region (see chapter 5.1) must also be taken into account.
2. Scaling the depth from an accurately measured deep(er) crater, formed under identical analytical conditions. Again the accuracy of this approach can be improved by taking into account transient shift corrections (see chapters 5.1).

Figure 5.37 demonstrates the application of this technique for routine dose determination as analysed by Dr. G. A. Cooke (2000). A 1 keV B implant (nominally 1E15 atoms cm^{-2}) annealed at 900°C for 10 seconds was analysed using 250 eV to resolve the near surface peak, followed by 1 keV to determine the diffusion tail. The

measured dose from the 250 eV and dual energy analyses are 8.41E14 and 8.17E14 atoms cm^{-2} respectively, a difference of about 3% which is within experimental error. The total analysis time was 30 minutes, significantly shorter than the 6 hours required to analyse the sample entirely with the lower energy.

The above example clearly shows the technique of dual energy profiling is ideally suited to shallow implant analysis, as both high depth resolution and high sensitivity are available in the desired parts of the profile, while the analysis time can be significantly decreased. As the trend of using lower implantation energies during the manufacture of modern semiconductors continues, it will require the use of lower primary beam energies for accurate quantification and implant shape determination. However this leads to decreases in available current, ion yields and sputter yields, leading to extended analysis times and decreased sensitivity. We foresee this technique becoming well established, and with the development of more computerised instruments, a routine analytical protocol. Significantly, this work has demonstrated that there is no need to introduce a further shift in the data when changing from a low to a high energy (or vice versa) under the range of conditions studied.

The above technique was also used briefly to investigate the internal boron distribution of sample 59.25 in the altered layer formed using 4 keV O_2^+ ions at normal incidence, and switching the beam energy to 500 eV. However, routinely switching the beam energy over this significantly larger range proved to be more problematic, mainly due to poorer reproducibility during relocation of the beam position than previously. This was probably due to small charging effects in the primary ion column, resulting in longer settling times of the ion beam position, and also the voltages used in

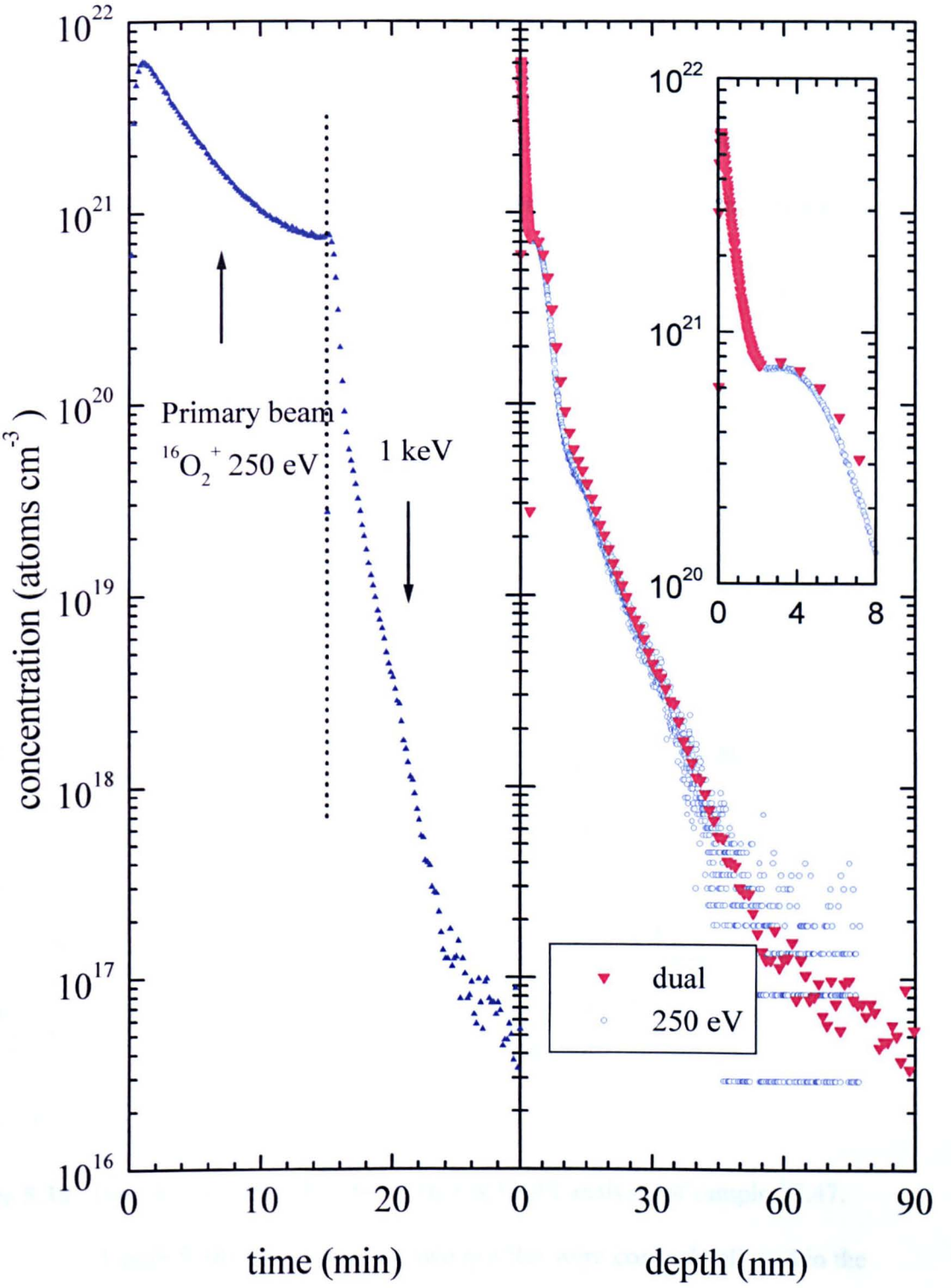

Figure 5.37: Dual beam energy SIMS analysis of a 1 keV B implant (1E15 atoms cm^{-2}) annealed at 900°C for 10 seconds.

the scan offset control are more critical. The procedure was also hindered by the fact that the ion image of the sample at the surface and at certain depths are quite similar, unlike ultra-shallow implants. These problems resulted in the recorded profile shown in figure 5.39, having a significant contribution from one of the crater walls (see dektak traces shown in figure 5.38) reducing the observed depth resolution (fewer

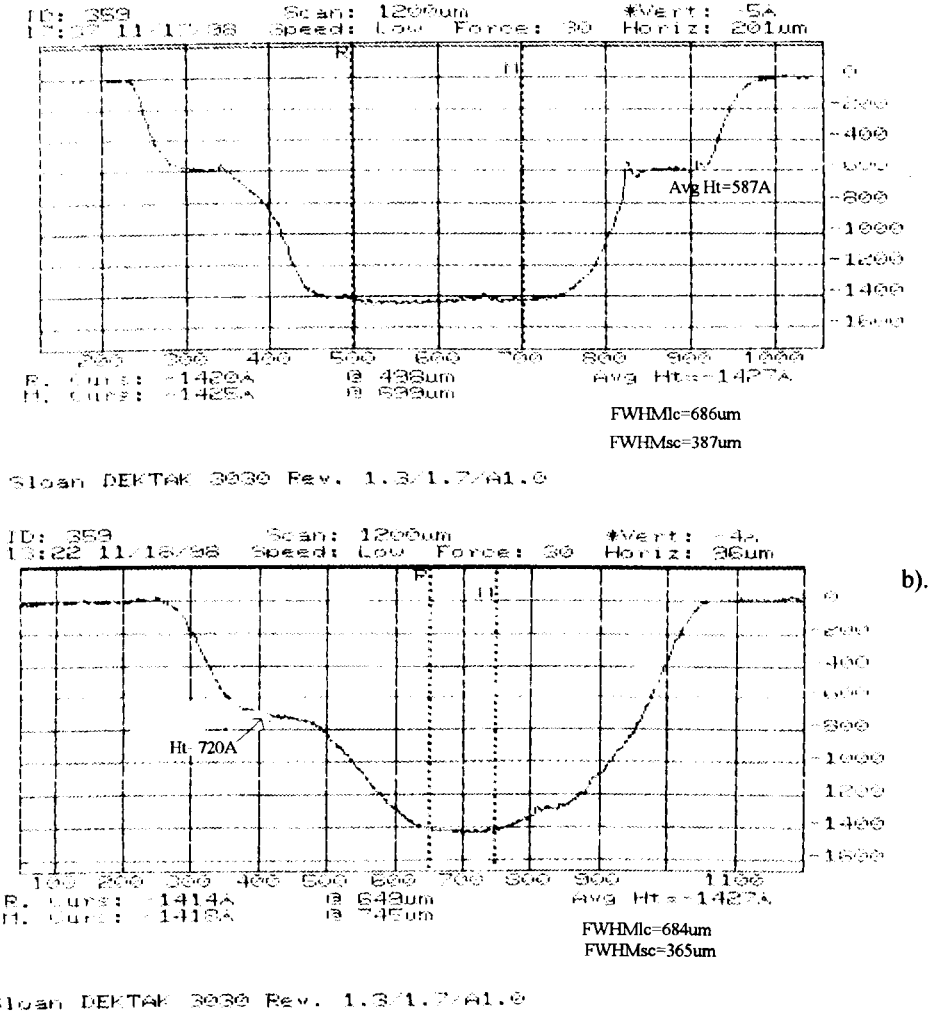

Figure 5.38: Dektak traces of a dual beam energy SIMS analysis of sample 25.47. Figure 5.38a shows how the two profiles were correctly aligned in the x-scan direction. However, figure 5.38b shows the two profiles were incorrectly aligned in the y-scan direction, resulting in the loss of depth resolution observed in figure 5.39.

orders of magnitude). However, the data was of sufficient quality to show that the internal distribution of boron in the altered layer was still of a broad delta layer, and not uniformly distributed, as suspected from the size of the terminal shift in our initial investigations of sample 25.47 (see chapter 5.2).

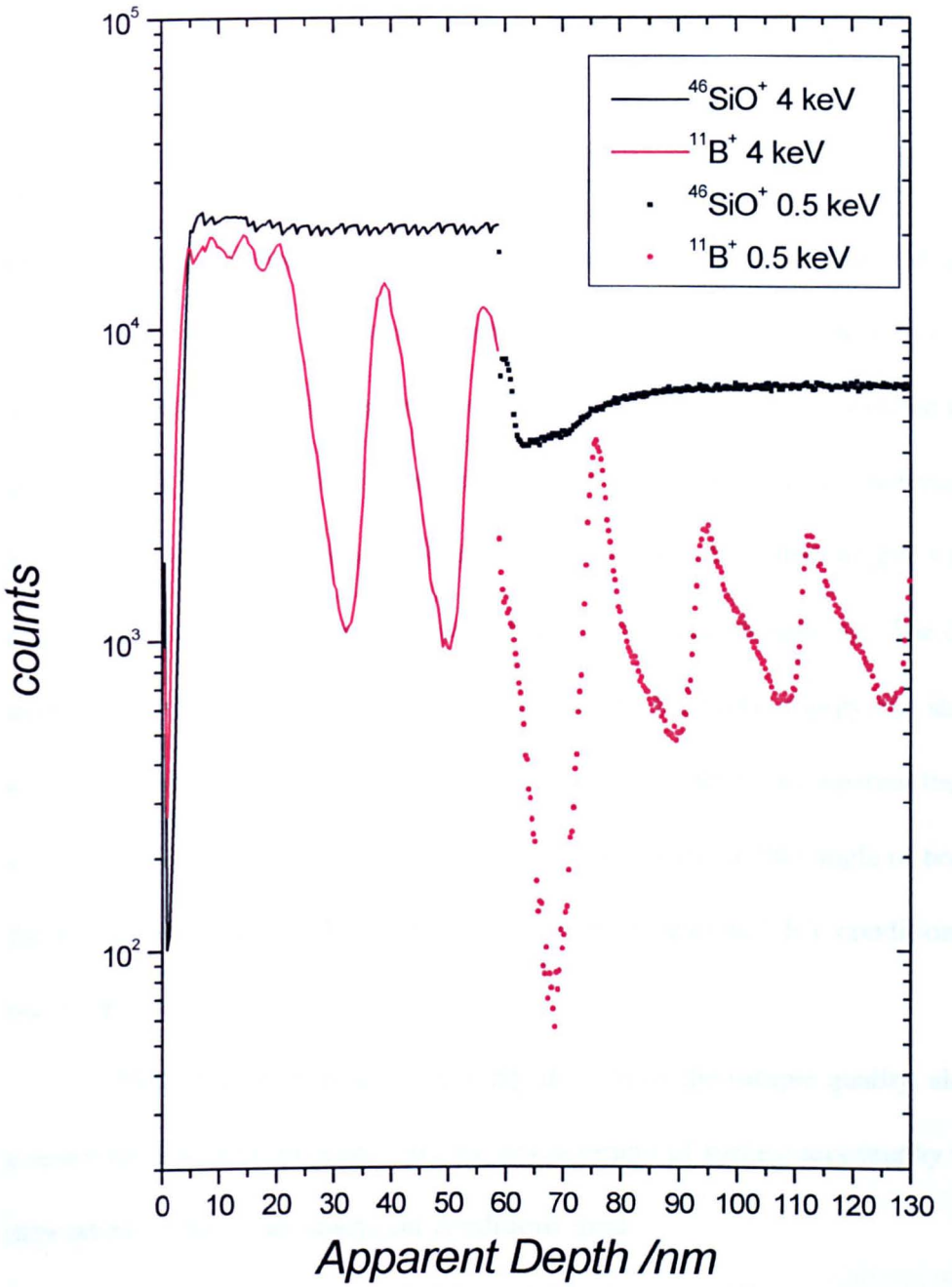

Figure 5.39: Dual beam energy SIMS analysis of sample 25.47. The dektak trace in figure 5.34a was used to correctly assign the depth scale at both 4 and 0.5 keV.

6.0 Surface Topography

High depth resolution SIMS depth profiling requires the analyzed sample to be flat on the atomic scale, as any sample unevenness or roughness will lead to a loss of depth resolution in the collected data, provided suitable analytical conditions are used. Depth resolution maybe defined in a number of different ways (Dowsett M G, 1997) *e.g.* width and inverse slope parameters, and feature separability, however the fundamental limit is governed by sample quality and the amount of atomic mixing that takes place in the altered layer due to primary ion bombardment. In order for a profile to be recorded, a sharp feature, e.g. a delta layer or an ultra-shallow implant must traverse the altered layer causing it to become disordered. The continuous remixing of material in the altered layer together with new material from deeper in the substrate gives rise to an exponential decrease in signal, characterized by the decay length, λ_d. The decay length is related to the energy of the bombarding ions, the lower the energy, the shallower the mixing region and hence the smaller λ_d and hence the ability to separate features spaced closer together. Other factors affecting the decay length are the angle of bombardment, the impurity/sample/bombarding ions combination, and the UHV conditions, e.g. the use of an oxygen flood.

Depth resolution is also adversely affected by the sample quality, along with the manner the feature is exposed, and the development of surface topography which is dependent on the exact analytical conditions used.

High resolution ultra-low energy SIMS depth profiling requires that the sample be flat on the atomic scale (any roughness will lead to a loss of depth resolution), and that the crater floor should be parallel to the buried feature so that as it intercepts the feature, it is equally exposed over the entire gated region. This leads to strict criteria

when designing SIMS instrumentation, especially in the area of scan plate design, and scan generation. To achieve this, the primary ion dose must be uniform over the crater bottom in this region, otherwise parts of a feature will be exposed before or after the bulk leading to distortion in the collected profile. This is more difficult at oblique angles of primary ion bombardment as a square raster is projected as a trapezium, and hence for optimum results a complicated correction must be introduced, generally in the scan generator.

If semiconductor growth conditions are not carefully controlled during manufacture, defects, e.g. pinholes, may be introduced into the sample, especially during the growth of high concentration features, due to impurity precipitation, or high lattice strain due to lattice mismatch. Although the defects may only represent a very small fraction of the total area, they may be preferentially eroded by ion bombardment, and due to the high dynamic range of SIMS artefacts maybe generated in the collected depth profile. The development of surface topography e.g. ripples, blisters and cones, occurs under many different analytical conditions involving ion bombardment i.e. AES where it is recognised and widely researched as a major problem affecting the technique.

6.1 The Potential effects of Surface Topography

The success of SIMS depth profiling depends on the fact that, when samples are bombarded by ion beams, there exist experimental conditions (probe energy E_p, angle of impact to normal θ_p, and species X_p) where the physical and chemical processes occurring in the near surface region achieve steady state over a useful range of primary beam dose. In this steady state regime, both the time and intensity scales are easily converted to depth and concentration through multiplication by constant factors (in the

case of the depth scale the highest accuracy also requires the addition of an offset). The main danger to accuracy in quantitative SIMS profiling is the assumption without proof that steady state has been achieved, especially where new experimental conditions become available for the first time. Under routine analytical conditions (E_p>2 keV, $0° \leq \theta_p \leq 60°$, X_p=O_2^+, Cs^+), it is now well known that the SIMS profile for a single matrix can be divided into three regions as shown in Figure 6.1(a). These are:

1. A transient or pre-equilibrium region at the surface where both the ion yield and the erosion rate may vary by more than a factor of 10 (Wittmaack K, 1996a). In this region (which typically persists for *at least* 2 nm of matrix sputtered per keV of primary beam energy for O_2^+ bombardment of silicon), contaminants and native oxide are cleaned off the surface, and probe species are progressively incorporated into the sub-surface. At some point the internal distribution of probe and matrix species achieves steady state from the instantaneous surface onwards and we enter the second, quantitatively useful part of the profile.
2. The steady-state region of the profile where the ion yields for impurities and the erosion rate of the matrix are constant. Provided the depth of the first point in this region can be found, an accurate depth scale can be established by applying a uniform erosion rate from that point onwards.
3. The roughening region of the profile (Stevie F A *et al.*, 1988). Over most of the energy and angular range of the primary beam, the steady state region is only temporary, and the profile enters a regime where the surface of the material becomes rough or rippled. Here, depth resolution is lost and the profile will also be distorted by a progressive change in ion yield as new average surface conditions become established. Normal incidence bombardment appears to be the only condition which

is generally free of this problem across the energy range (at least in silicon and gallium arsenide).

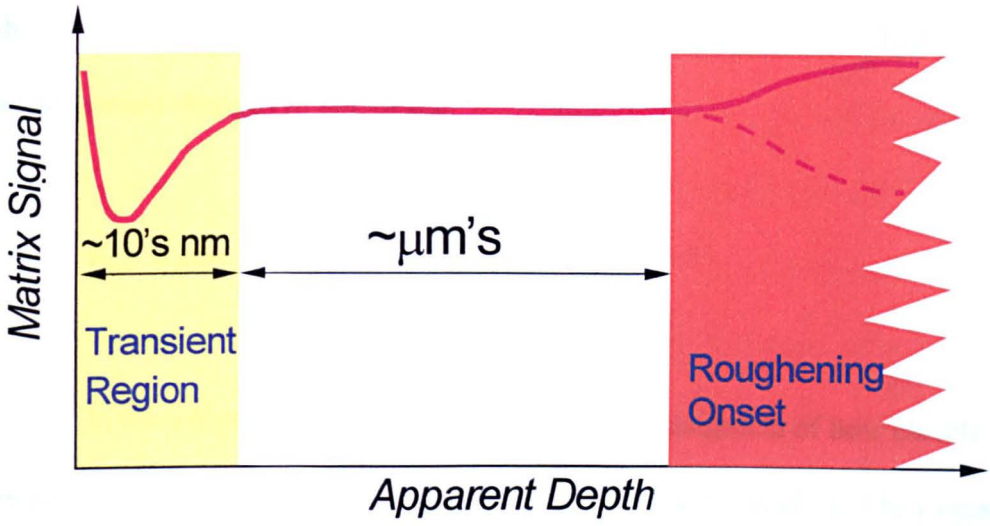

(a) "Conventional" Profile - E_p>2keV

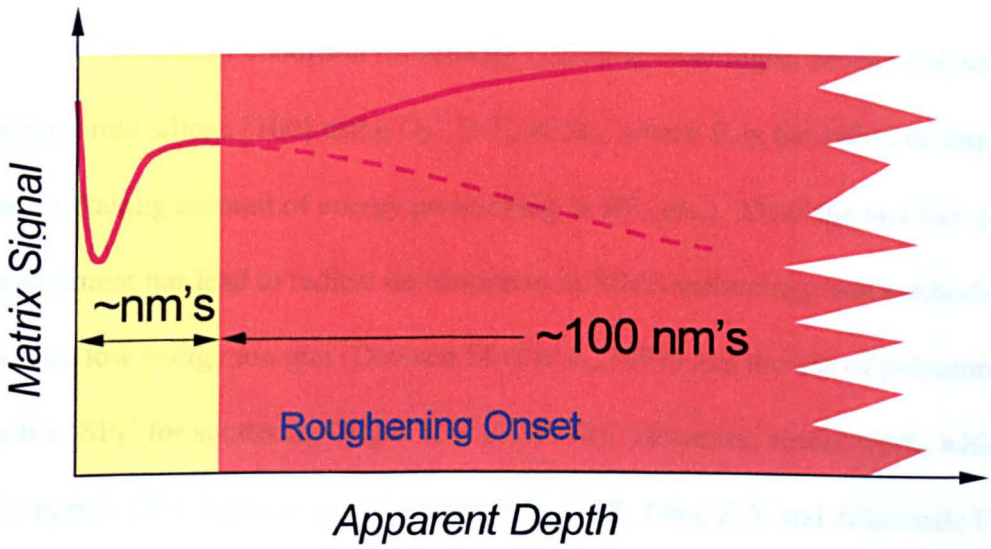

(b) Low Energy Profile - E_p<1 keV -except for θ_p=0 and other angular windows

Figure 6.1: Regions in (a) conventional and (b) low energy SIMS profiles at non-normal incidence. The red lines show typical matrix behaviour.

Any roughening will introduce errors or shifts in the depth scale whose magnitude is dependent on the size of the change in erosion rate, the depth at which roughening first occurs, and the final depth of the crater. Errors are also introduced in the concentration scale, not only due to the errors in the depth scale, but also due to the accompanied changes in ion yields.

6.2 Loss of Depth Resolution

In this chapter is presented a preliminary investigation of how closely the recently discussed ultra low energy bombardment conditions ($E_p \leq 1$ keV) match the above description (Dowsett M G and Chu D P, 1998), and comment on the extent to which the description is appropriate at any energies.

A necessary condition for directly obtaining meaningful profiles of, say, a boron implant into silicon [100] using O_2^+, is $E_p \leq 0.5E_i$, where E_i is the effective implant energy (taking account of energy partitioning in BF_2 etc.). Over the last five years this requirement has lead to radical development in SIMS technology and methods including an ultra low energy ion gun (Dowsett M G *et al.*,1997) and the use of polyatomic ions such as SF_5^+ for sputtering (Iltgen K *et al.*, 1998). However, recent work, which is still in progress (Wittmaack K and Corcoran S F, 1998; Jaing Z X and Alkemade PF A, 1998b; Mount G R *et al.*, 1998; Chu D P *et al.*, 1998), shows that for $E_p \leq 2$ keV region 2 in Figure 6.1(a) only exists for narrow *energy dependent* windows in θ_p. For other conditions the transient and roughening regions effectively coalesce as shown Figure 6.1(b). A shallow implant profile gives no warning, as to when it is distorted by these effects. The profiles of our boron delta layer sample 25.47 in Figure 6.2 show the effect

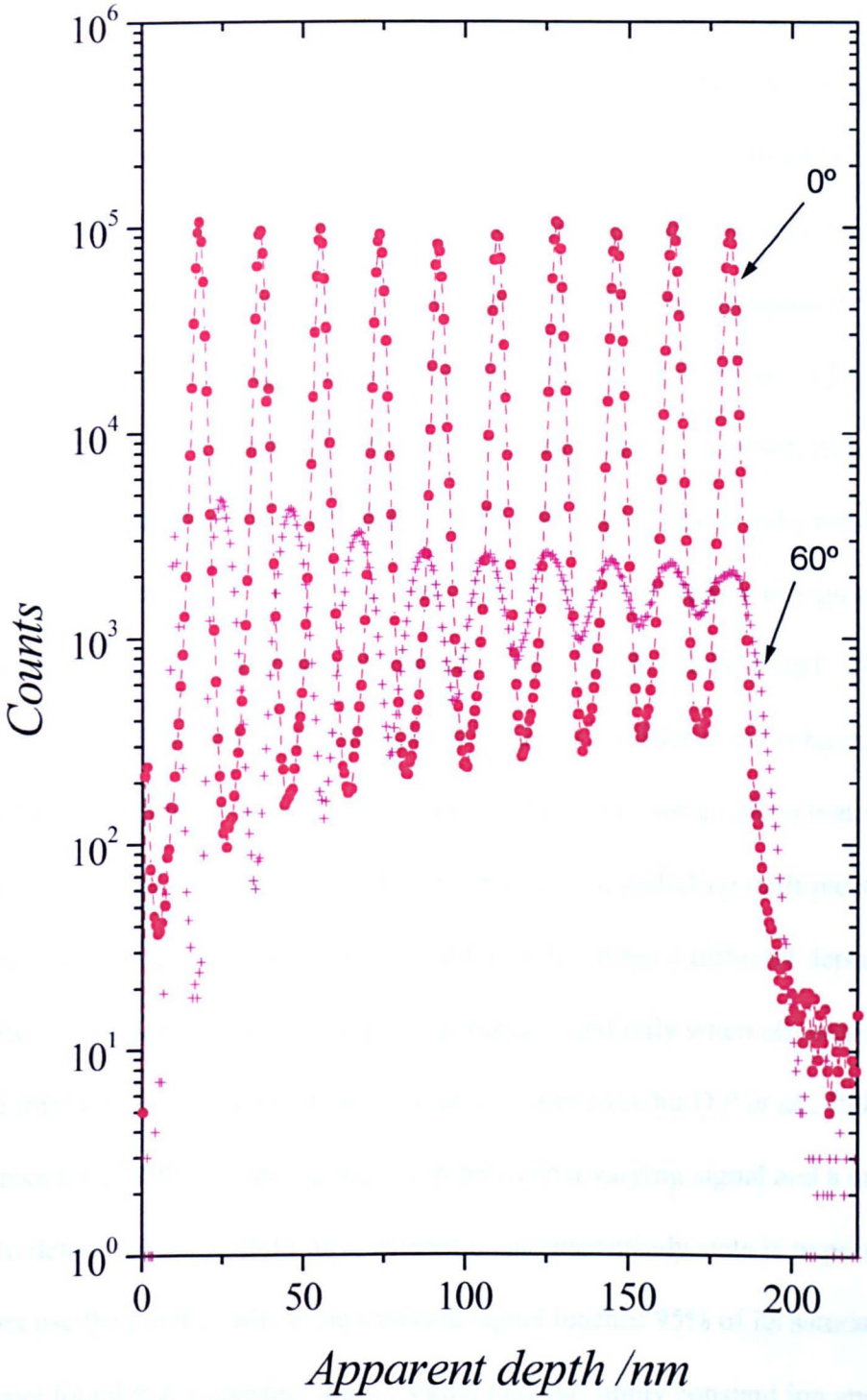

Figure 6.2: The 10 boron δ layers in silicon profiled by a 500 eV $^{16}O_2^+$ beam at normal incidence and 60° without oxygen flooding. The profile obtained at 60° was aligned so that the centroid of the last delta layer was located at the same position as that analyzed at normal incidence.

clearly. We find that θ_p= 0±5° provides a high depth resolution window across the whole energy range. Around the time of starting this investigation it was widely reported that another window exists at ~50° for E_p= 500 eV with oxygen flooding to signal saturation (Mount G R *et al.*, 1998). However, its transient region appears to be wider than that at normal incidence and the depth resolution is marginally worse, as is clearly demonstrated in Figure 6.3 followed by detailed comparisons in Figure 6.6.

As far as the low energy measurement technique is concerned, there are two key issues: Firstly, the existence of a useful steady state region needs to be established for the sample under consideration. Secondly, the width of the transient region must be measured so that the first reliable data point on the profile can be found. The most direct way of obtaining all this information might be to observe the behaviour of matrix-related transient signals (e.g. Si^+, Si_2^+, SiO^+, Si_2O^+ ... etc. for a silicon matrix). It turns out to be essential to measure several transient signals, including multiplets of the matrix atom, since the transient behaviour for each ion has a different dependence on the physical and chemical condition of the surface, and only when all matrix signals are stable might it be *assumed* that steady state is achieved (Chu D P *et al.*, 1998; Wittmaack K, 1990). Since the transition between a varying signal and a constant one is hard to determine, some definition of what constitutes steady state is required, e.g. some authors use the point at which the transient signal reaches 95% of its saturated value. We have found that a constant matrix signal may not imply constant ion and sputter yields and, furthermore, it certainly does not guarantee a constant depth resolution.

The existence of a stable region does not, in itself, imply high depth resolution — the surface may be rough, but the roughness may be in steady state. The depth resolution pertaining to a particular set of experimental conditions must be established separately.

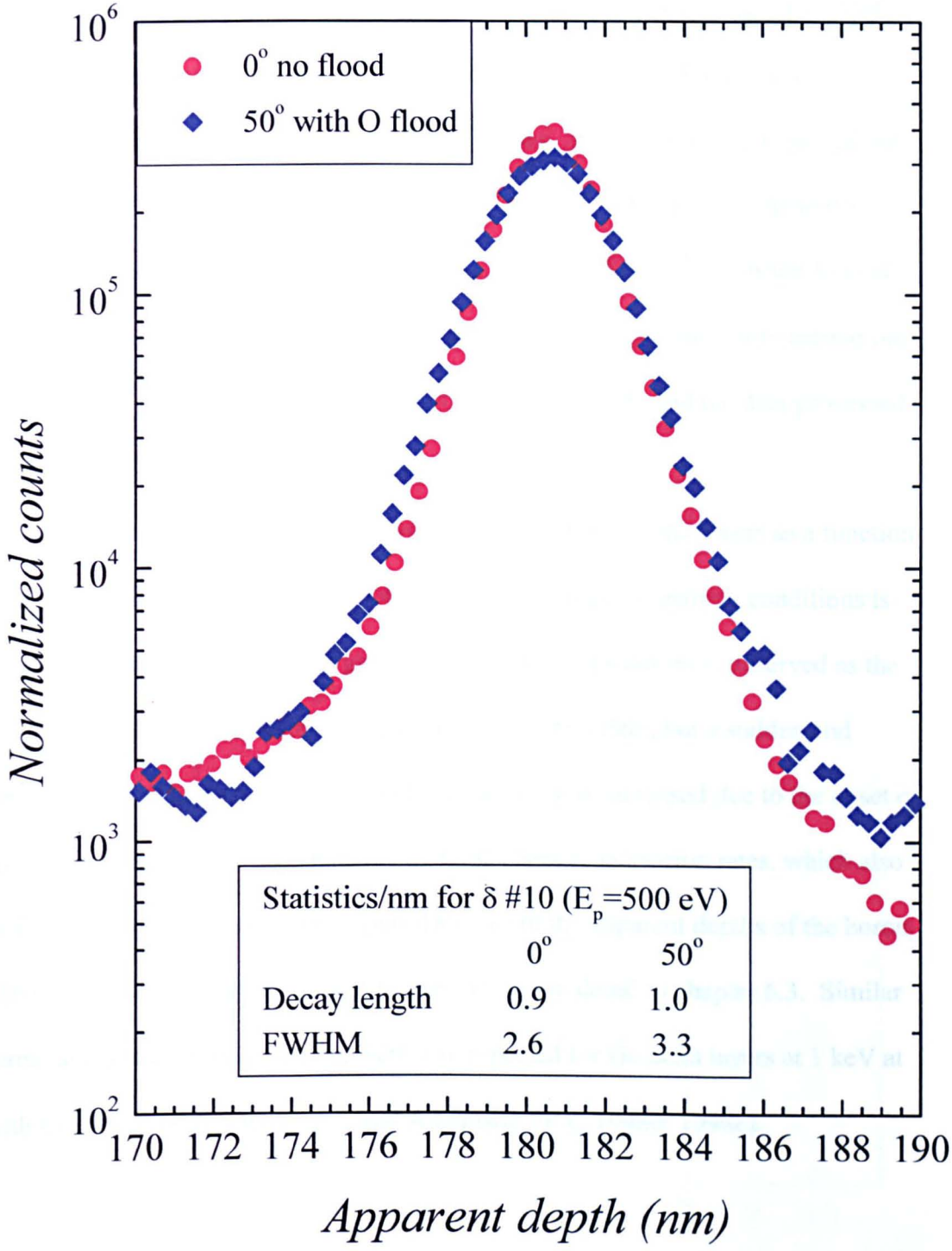

Figure 6.3: Delta #10 profiled by a 500 eV $^{16}O_2^+$ primary beam at normal incidence without oxygen flooding and at 50° with oxygen flooding. N.B. The Significant difference in profile quality, is much more obvious if the intrinsic width of the delta layer is removed from the data.

The FWHM of some closely spaced identical delta layers in a profile is normally a good indicator of the depth resolution for the corresponding depth range. Two MBE grown samples containing multiple boron delta doped layers were extensively investigated, over a wide range of analytical conditions. Experiments were carried out on four quadrupole SIMS instruments, EVA 2000FL, EVA 3000 and two Atomika 4500's, all equipped with floating low energy ion guns; the FLIG^{TM}, (Dowsett M G *et al.*, 1997). All the raw data utilizing the technique of oxygen flooding were carried out by Dr. S. B. Patel at ATOMIKA Instruments GmbH in Munich, and the data processed at Warwick.

A summary of results for FWHM of the profiled boron delta layers as a function of depth and E_p, obtained on sample 25.47 over a wide range of analysis conditions is shown in Figure 6.4. As expected a gradual loss of depth resolution is observed as the analysis energy is increased because of the atomic mixing effect, but a sudden and unpredictable loss is also found as the angle of incidence is increased due to the onset of surface roughening. This is accompanied by large changes in erosion rates, which also introduce large shifts, (up to 13 nm in only 180 nm) in the apparent depths of the boron delta layers as shown in figure 6.5 and discussed in more detail in chapter 6.3. Similar problems, due to surface roughening, were also reported for Ge delta layers at 1 keV at 60° with oxygen flooding (Jiang Z X and Alkemade PFA, 1998b; 1998c).

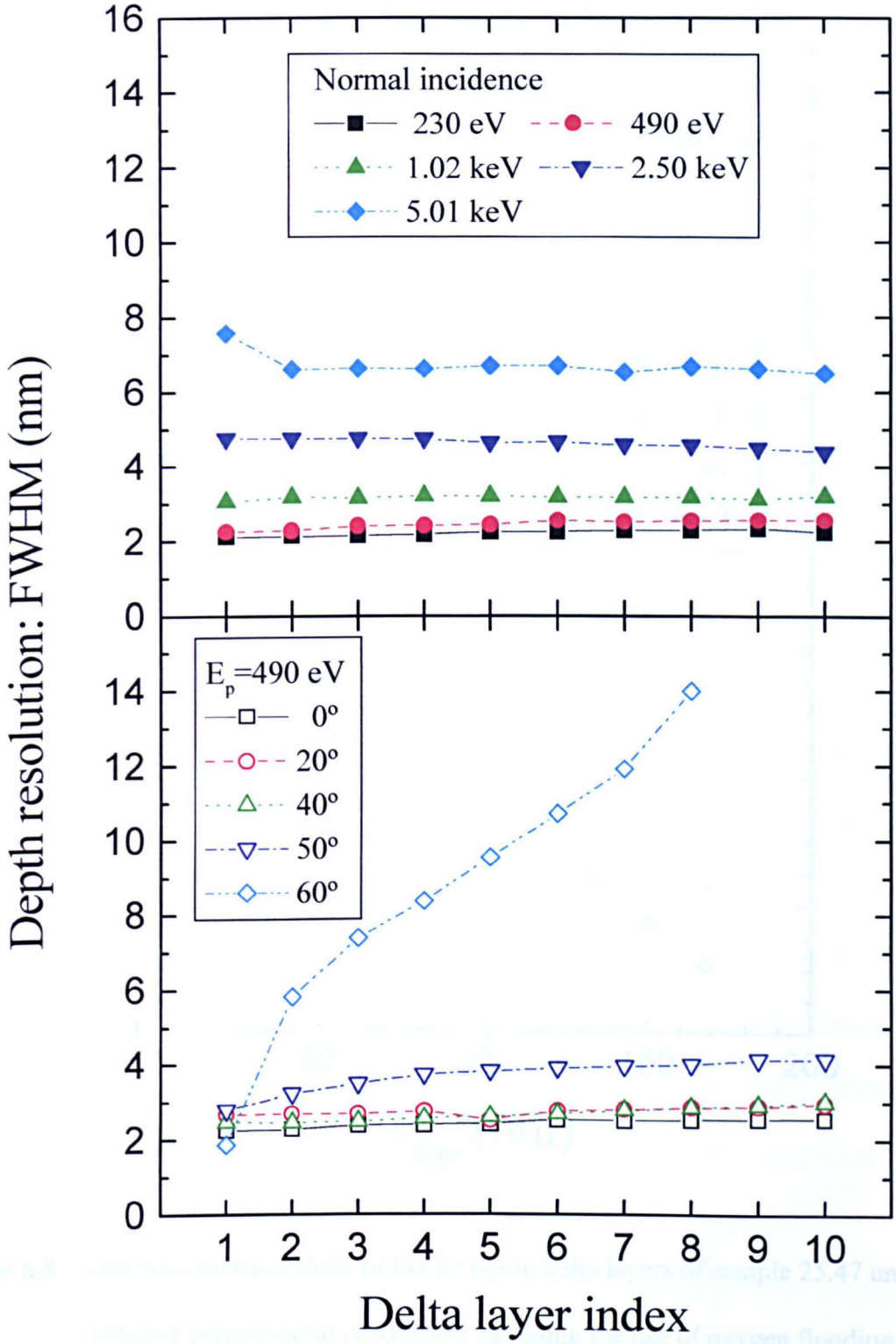

Figure 6.4: FWHM values vs. (a) analysis energy and (b) angle of incidence. Oxygen flooding was not used.

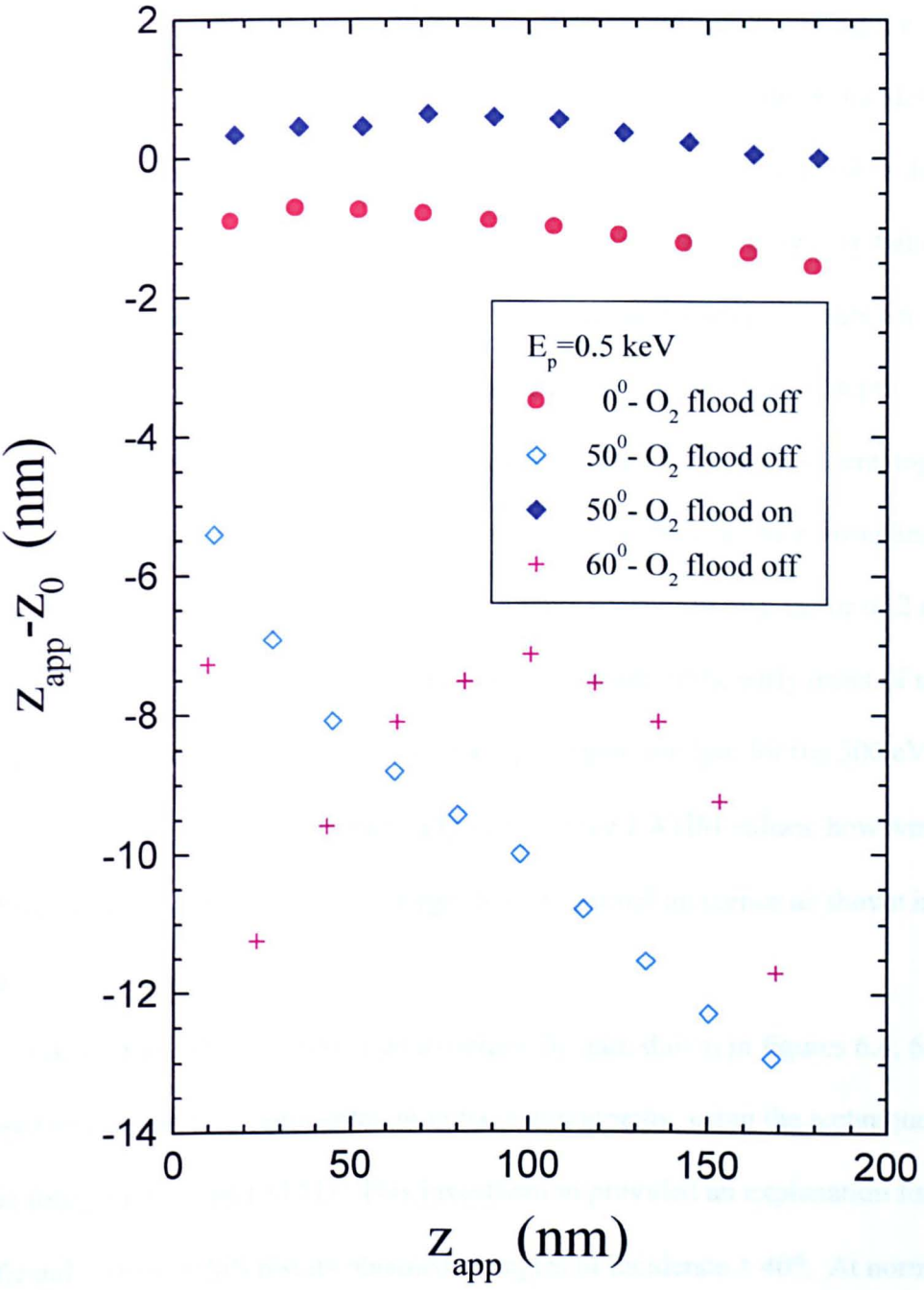

Figure 6.5: Observed centriod shifts of the 10 boron delta layers of sample 25.47 under different experimental conditions, including the use of oxygen flooding. The profile obtained at 50° with oxygen flood was aligned so that the centroid of the last delta layer was located at the same position as that analyzed at normal incidence no oxygen flood.

To compare the effect of oxygen flooding on depth resolution for a 500 eV 50° incidence profile, the FWHMs of the 10 boron delta layers are plotted in Figure 6.6 as well as the data from some normal incidence profiles. At 230 eV normal incidence, the FWHMs range from 2.1-2.3 nm. We believe the slight loss of resolution with depth in this case is due to extra diffusion of the deeper layers which were grown first and maintained at the growth temperature whilst the rest of the structure was grown. Doubling the beam energy to 500 eV, we observed as expected a loss of depth resolution of approximately 10%. On the other hand, increasing the incident angle, one would expect the corresponding FWHMs be smaller if there is no micro-roughness present. Instead, we observed a rapid decay in depth resolution by a factor of 2 and 8, respectively, in the 50° and 60° 500 eV profiles as a result of the early onset of micro-roughness described in Figure 1(b). Introducing oxygen flooding for the 500 eV analysis at 50° (and 60°) does dramatically improve the FWHM values, however, we found the values remain at least 30% larger than at normal incidence as shown in figure 6.6.

Some of the SIMS craters used to obtain the data shown in figures 6.4, 6.5 and 6.6 were investigated for bombardment induced topography, using the technique of atomic force microscopy (AFM). This investigation provided an explanation for the significantly worse SIMS results obtained at angles of incidence > 40°. At normal incidence the topography showed no structure, merely stochastic roughness of RMS 0.17 nm, as shown in figure 6.7. The rippled surface reported by other workers at higher impact energies, was observed for all cases of oblique incidence bombardment, including for the first time in the critical high depth resolution window of 500 eV at 50° (without and with oxygen flood) as shown in figures 6.9 and 6.10 respectively. As these latter figures show the use of an oxygen flood substantially reduces the ion beam

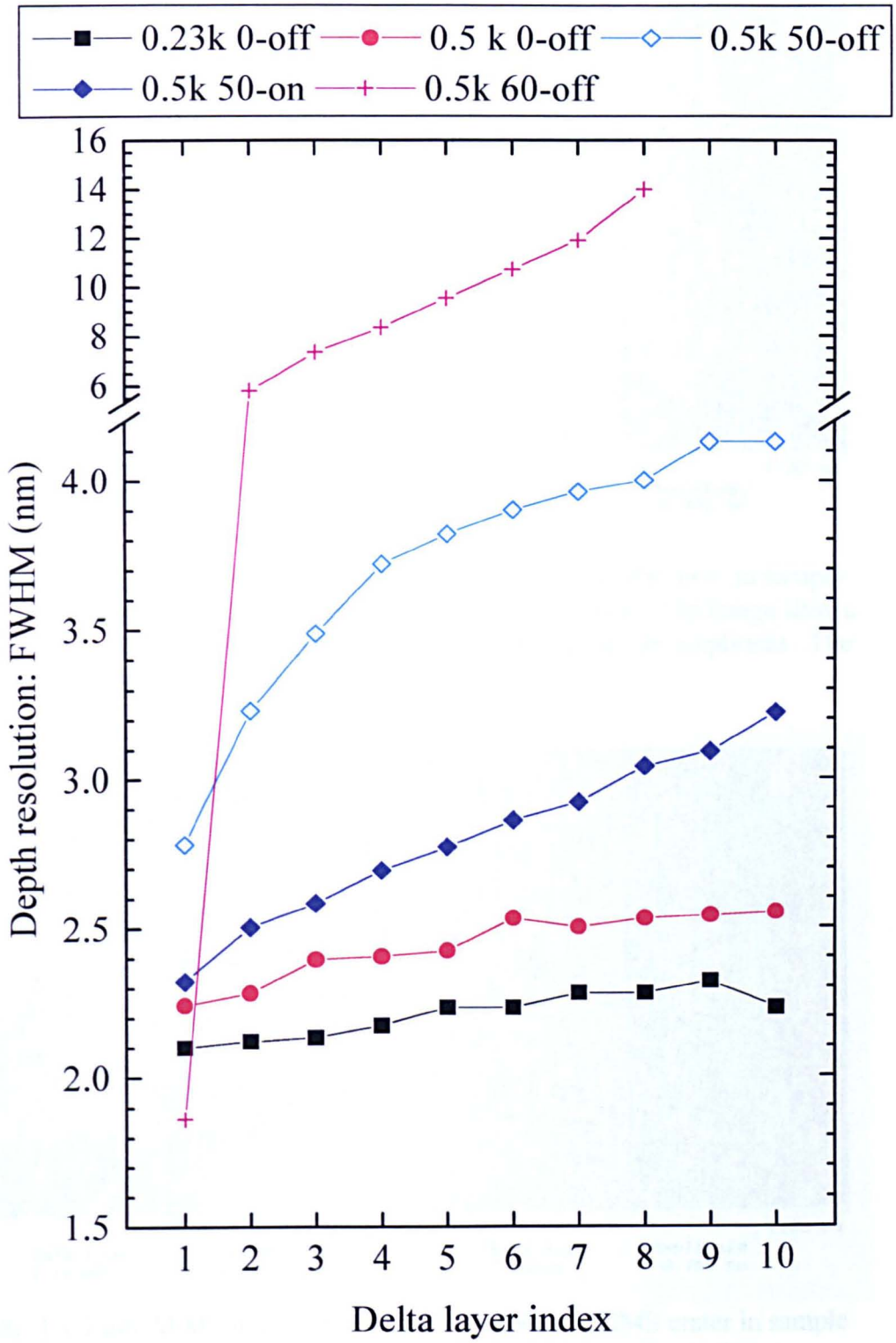

Figure 6.6: Comparison of the FWHM values under different experimental conditions including the use of oxygen flooding. On and off refer to the use of oxygen flooding.

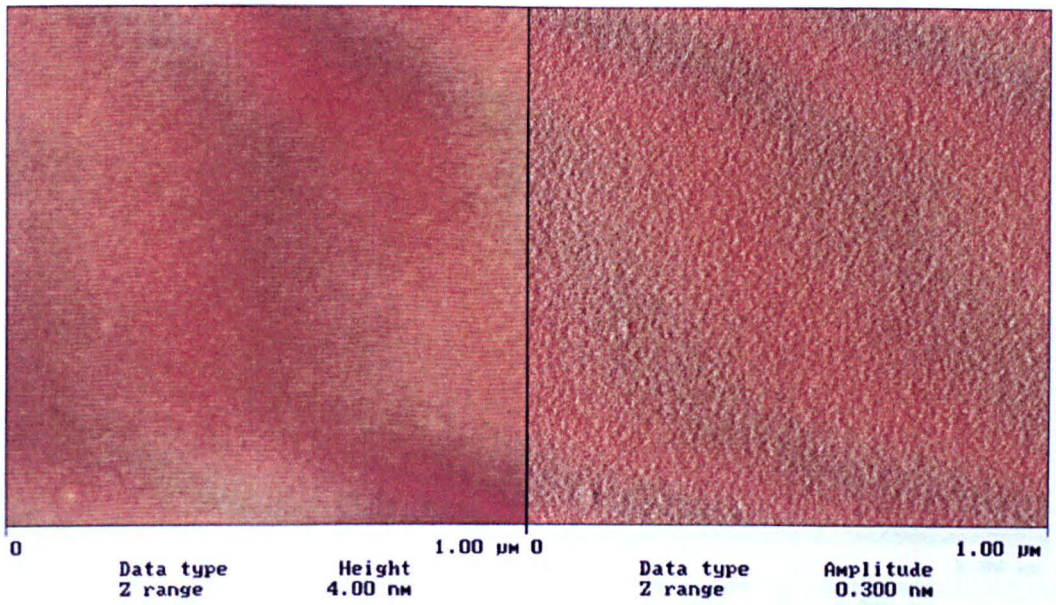

Figure 6.7: 1 x 1 µm AFM image of the bottom of a 242 nm SIMS crater in sample 25.47 profiled using 500 eV O_2^+ at normal incidence. The image shows fine scale texture which is virtually isotropic of sub-nm amplitude. The rms of the surface roughness was 0.17 nm.

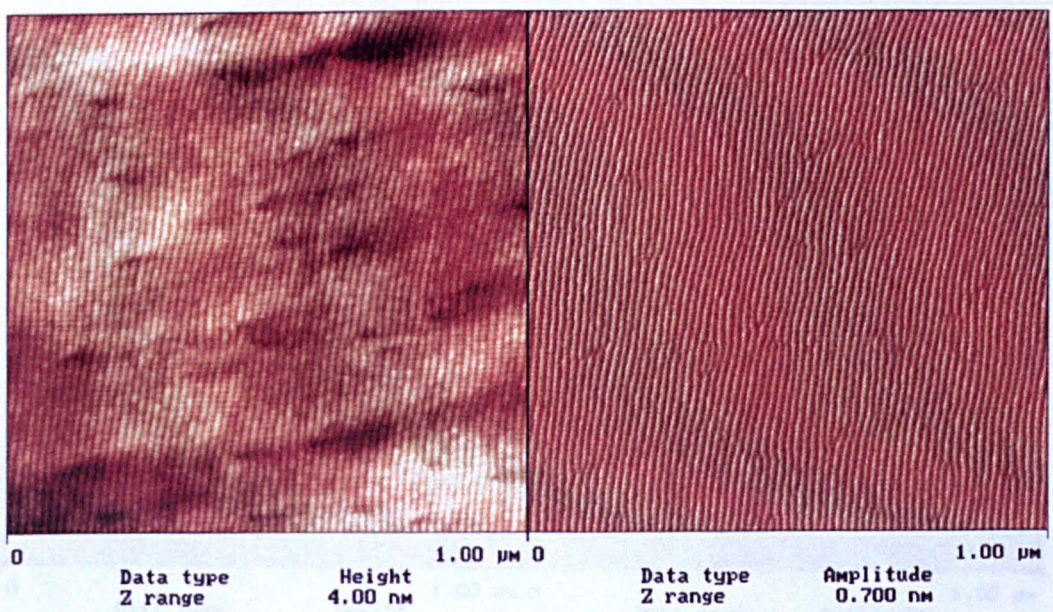

Figure 6.8: 1 x 1 µm AFM image of the bottom of a 245 nm SIMS crater in sample 25.47 profiled using 500 eV O_2^+ at 60° with oxygen flood. The image shows ripples of period 14-15 nm and peak to valley heights of 0.6-1.2 nm amplitude. The rms of the surface roughness was 0.53 nm.

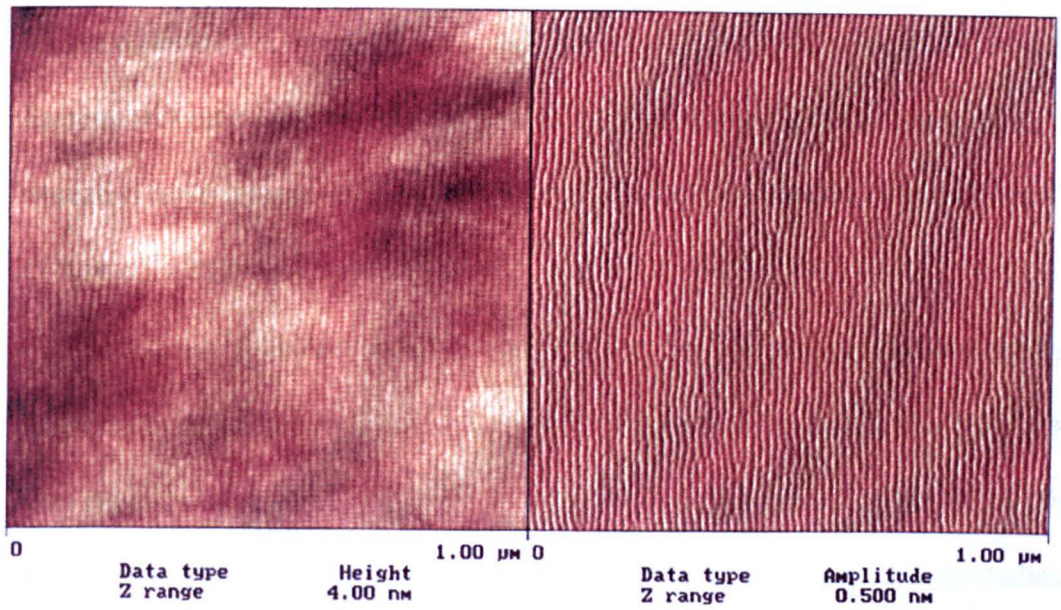

Figure 6.9: 1 x 1 µm AFM image of the bottom of a 284 nm SIMS crater in sample 25.47 profiled using 500 eV O_2^+ at 50° no oxygen flood. The image shows ripples of period 14-15 nm and peak to valley heights of 0.3-1.2 nm amplitude. The rms of the surface roughness was 0.42 nm.

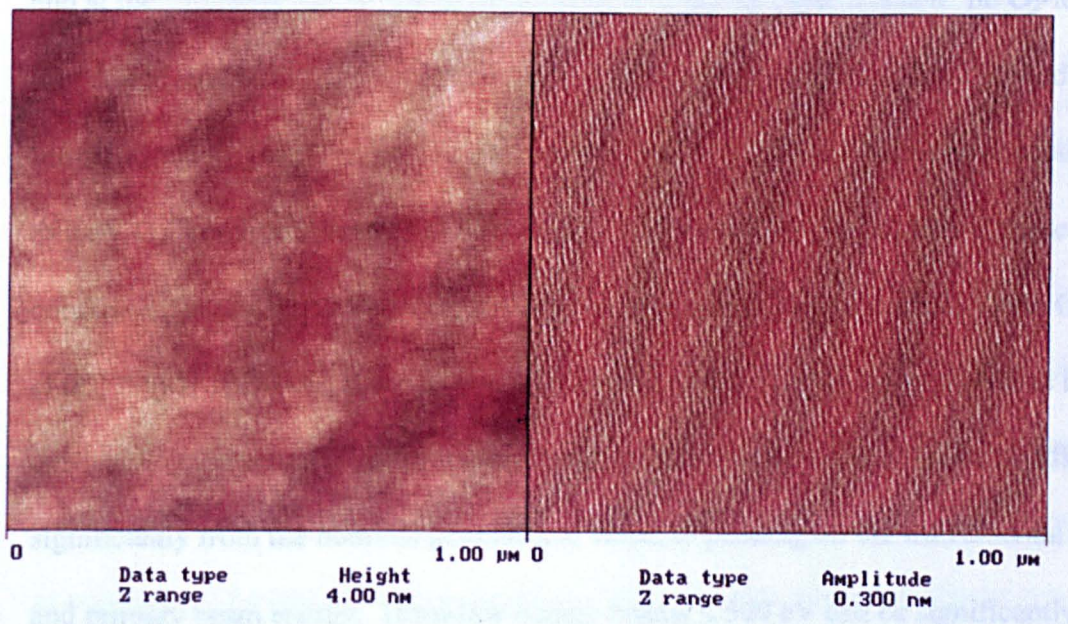

Figure 6.10: 1 x 1 µm AFM image of the bottom of a 245 nm SIMS crater in sample 25.47 profiled using 500 eV O_2^+ at 50° with oxygen flood. The image shows ripples of period 11-12 nm and peak to valley heights of 0.1-0.6 nm amplitude. The rms of the surface roughness was 0.23 nm.

induced surface roughness, but does not prevent the formation of ripples at oblique angles of incidence, when profiling with 500 eV O_2^+. At 500 eV and 60°, the ripple formation occurs early in the bombardment and is undoubtedly the cause of the observed rapid change in ion yield and depth resolution between 16 and 34 nm (Cooke G A *et al.*, 1999).

This so called 'magic angle' of 50° with oxygen flood has also been called into question by other groups around the world (Wittmaack K and Corcoran S F, 1998) and very recently by Schueler and Reich (2000), this latter group are employed by Physical Electronics, the SIMS instrument manufacturer Mount *et al.* used in their studies. In a study to identify the analysis conditions (using the same sample as Mount *et al.*) that minimize the depth scale distortions in SIMS depth profiles, on a PHI ADEPT 1010 quadrupole instrument with O_2^+ bombardment at 7 energies between 150 and 1000 eV, and at the following analysis angles 40°, 45°, 50° with O_2-leak and at 0° no O_2-leak, they found that all but one measurement exhibited constant sputter rates (beyond the transient region), over the limited depth range studied of 35 nm. The one exception was 500 eV O_2^+ bombardment at 50° with O_2-leak, this supports our findings at these conditions, over a much larger depth range of 200 nm (Cooke G A *et al.*, 1999; Ormsby *et al.*, 1999). However, some of this discrepancy could also be due to problems in determining the actual angle of incidence of the primary O_2^+ ions, as this can differ significantly from the nominal geometrical value, depending on the instrumental design and primary beam energy. Ultra-low energy beams ≤ 500 eV can be significantly deflected even by typical voltages present in quadrupole instruments. On EVA 2000FL it was found using 500 eV O_2^+ bombardment at 50° (no O_2-leak), that switching the voltage applied to the sample holder by as little as 25 V produced poor crater shapes, resulting from the beam position moving by nearly 100 μm in the y-direction, as shown

in figure 6.11. Schueler and Reich reported in their work that the nominal geometrical angle accurate to ± 2° was corrected for primary ion beam deflection due to the secondary ion extraction field, calculated using the ion optics program SIMION 3D, however the magnitude of the corrections were not reported, but by insinuation must have been larger than 2° at some of the conditions investigated.

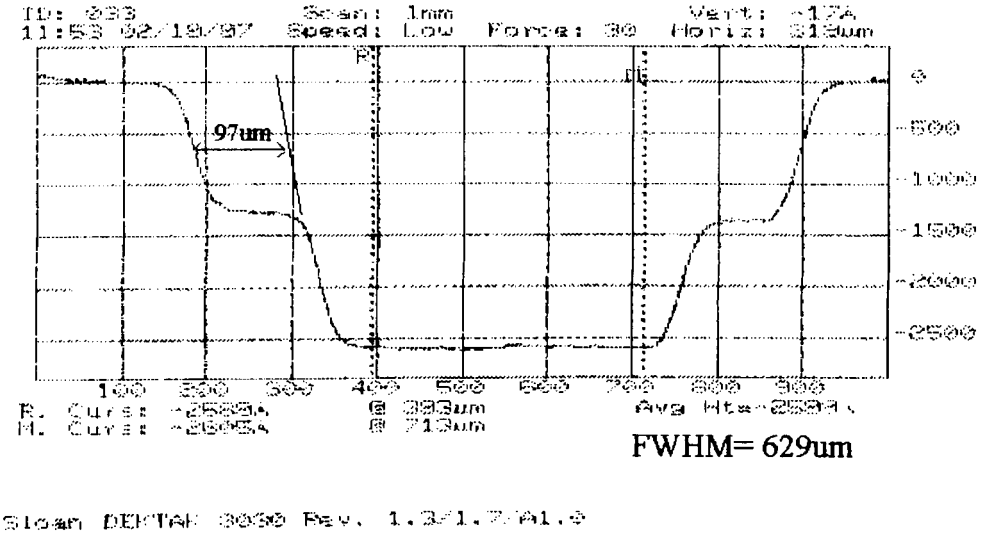

Figure 6.11: Dektak trace of a SIMS crater in sample 25.47 profiled using 500 eV O_2^+ bombardment at 50° (no oxygen leak). The appearance of a small deeper crater inside a larger crater of half the depth, is due to the primary ion beam being deflected by nearly 100 μm for half the total analysis time, induced by a difference of 25 V in the applied sample bias.

Schueler and Reich, also reported that the depth resolution at 27 nm for any given primary beam energy is better with oblique bombardment (with O_2-leak) than at normal incidence (no O_2-leak). This supports our findings that a O_2-leak improves depth resolution, but the results do not scale with the energy perpendicular to the sample as predicted. The best resolution reported was obtained at normal incidence at a beam energy of 150 eV, no results at this energy were presented for non-normal incidence, probably due to distortion of the primary ion beam under these conditions. The sample used in this and other studies (Mount G R *et al.*, 1998; Chia V K F *et al.*, 2000) appears to be of similar quality to a second sample 59.25 grown at Warwick and used to further

investigate optimum depth profiling conditions. Figures 6.12 and 6.13 show very similar depth resolution parameters for the two samples at O_2^+ energies of ≤ 500 eV, however at higher energies the quality of their SIMS profiles appear to degrade much faster than for sample 59.25. Possible reasons for these observations are differences in either the methods of depth calibration used, or in the concentrations of the boron delta layers. My results obtained at 1 keV and 45°, appear to indicate that these conditions do not develop surface roughening, however results shown later in this chapter show that this is not the case with severe problems developing at a depth of 60-70 nm.

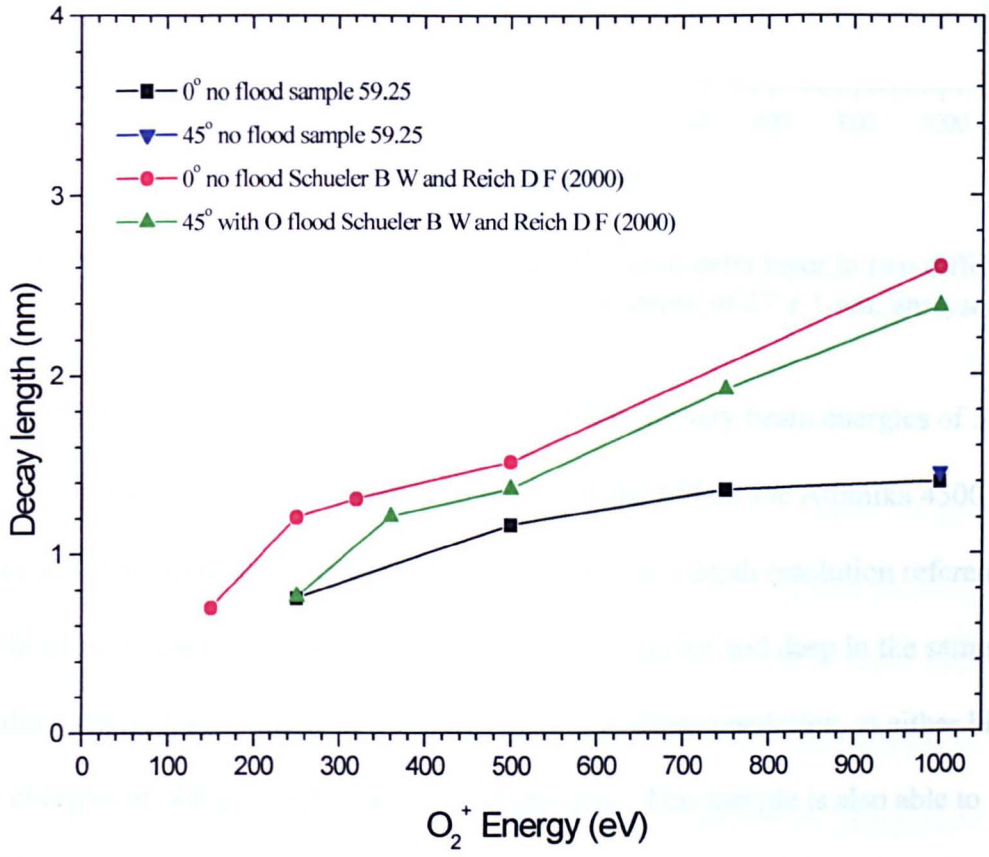

Figure 6.12: Comparison of the decay lengths for the 5th boron delta layer in two different samples, both of which are at a nominal depth of 27 ± 1 nm, analysed under varoius experimental conditions.

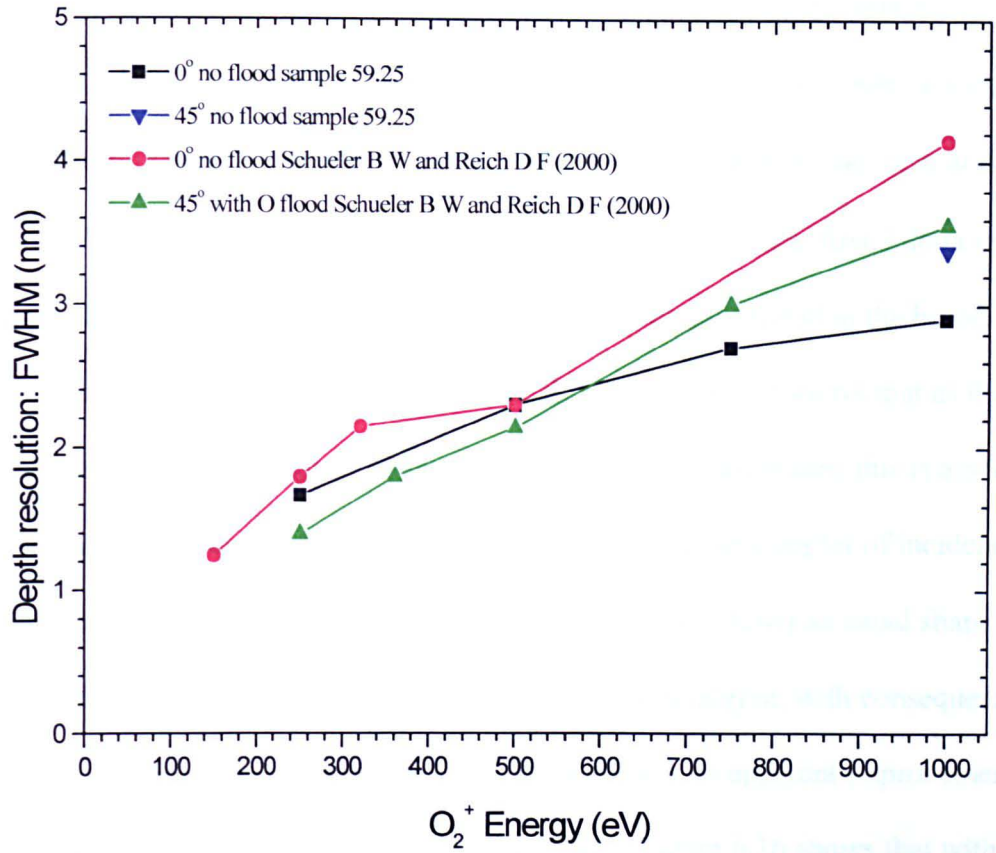

Figure 6.13: Comparison of the FWHM for the 5th boron delta layer in two different samples, both of which are at a nominal depth of 27 ± 1 nm, analysed under varoius experimental conditions.

Sample 59.25 was analyzed using an O_2^+ beam at two primary beam energies of 500 eV and 1 keV at various angles of incidence between 0 and 65° on the Atomika 4500 SIMS instrument. This sample had been specifically grown as a depth resolution reference, with the closely spaced boron delta layers at both the surface and deep in the sample, providing a more visual image of the observed loss in depth resolution, at either higher beam energies or oblique angles of ion bombardment. This sample is also able to provide more accurate information of the profile distortions occuring in the surface transient region, than the previous sample 25.47 used.

A summary of results obtained for the depth resolution parameter FWHM of the profiled boron delta layers as a function of depth and angle of incidence are shown in Figure 6.14, for a 500 eV O_2^+ ion beam. As for figure 6.4b, a sudden decrease in depth

resolution is observed at angles of incidence >40° due to the onset of surface roughening. As the angle of incidence is increased beyond 40°, the problems associated with surface roughening worsen and also occur at shallower depths, such that at 60° and 65° the FWHM parameter can not even be determined for all of the first 5 delta layers, located in the top 27 nm of the sample. This is clearly demonstrated in the boron profiles obtained at these angles and shown in figure 6.15, it also shows that as the angle of incidence increases the apparent depth of the delta layers decreases, this is associated with the larger transient region and larger transient shift at these angles of incidence, as is shown in the $^{30}Si^{+}$ signal. At 60° and 65° the $^{30}Si^{+}$ signal shows an usual shape as the chemical transient region has merged with the roughening region, with consequently changes in both the ion and sputter yields. This results in an apparent improvement in depth resolution within the top 10 nm of the profiles. Figure 6.16 shows that with the exception of 65°, the $^{30}Si^{+}$ signal remains constant beyond the transient region, and at 60° and 65° the last two boron delta layers in sample 59.25 have completely merged and become one feature.

A summary of results obtained for the depth resolution parameter FWHM of the profiled boron delta layers as a function of depth and angle of incidence are shown in figure 6.17, for a 1 keV O_2^{+} ion beam. At 1 keV a sudden decrease in depth resolution is observed at all angles of incidence >30° due to the onset of surface roughening. However, the pattern is totally different from that observed at 500 eV, the poorest angle appears to be 40° with severe roughening developing between 60-80 nm, closely

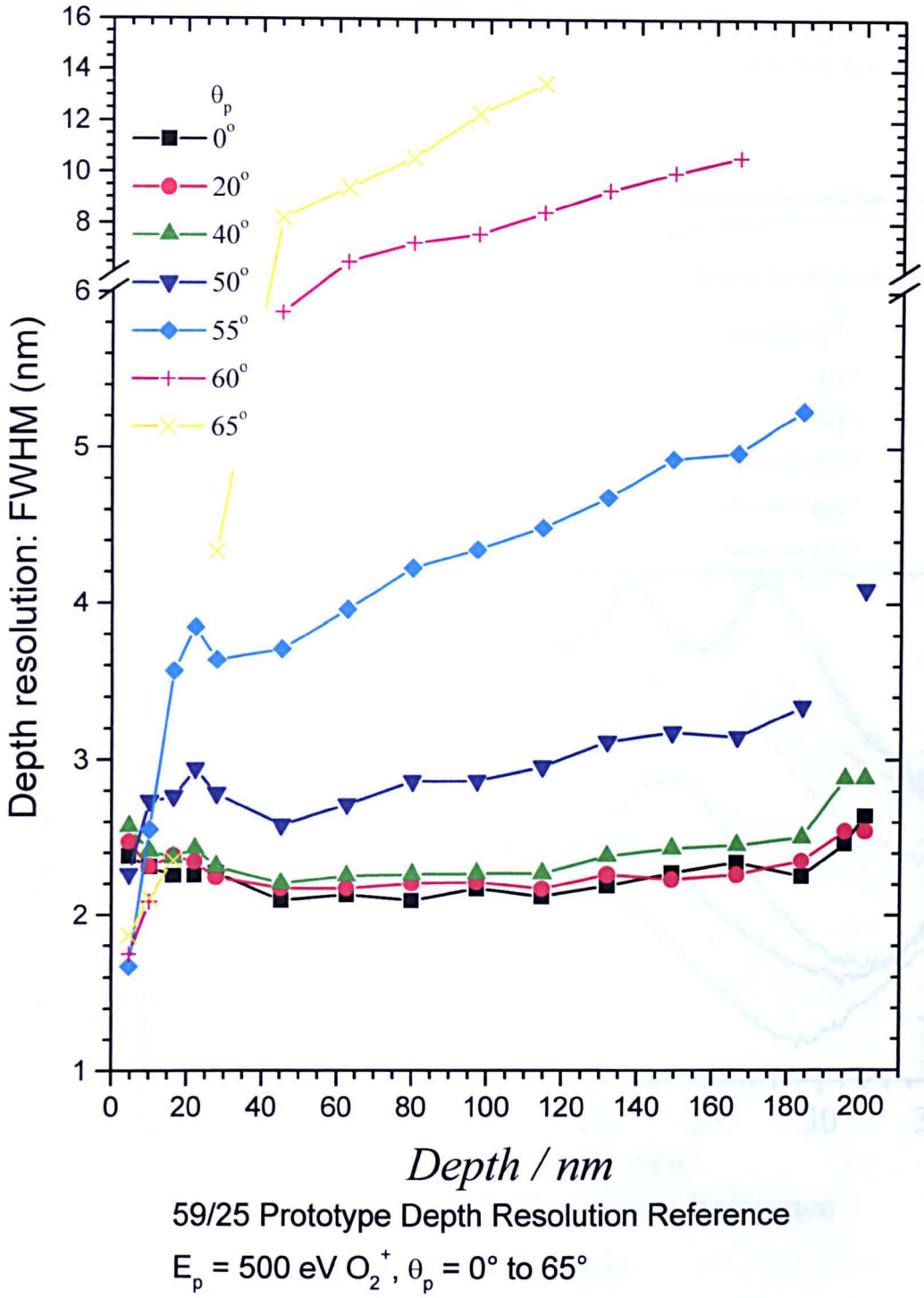

Figure 6.14: FWHM values as a function of depth determined by profiling sample 59.25, using 500 eV O_2^+ at various angles of incidence.

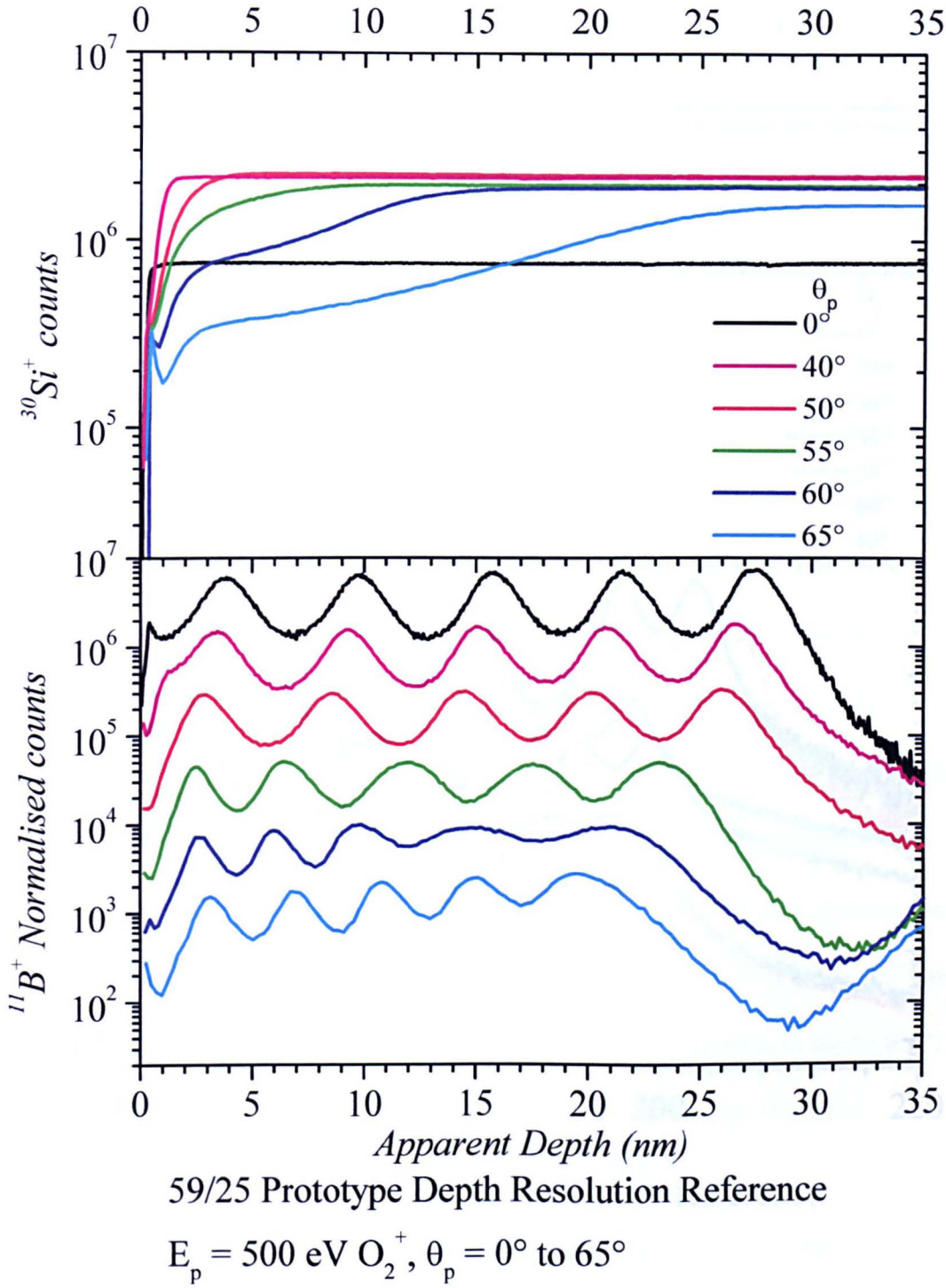

Figure 6.15: Various SIMS depth profiles obtained using 500 eV O_2^+ at various angles of incidence on sample 59.25, only the first 35 nm are shown.

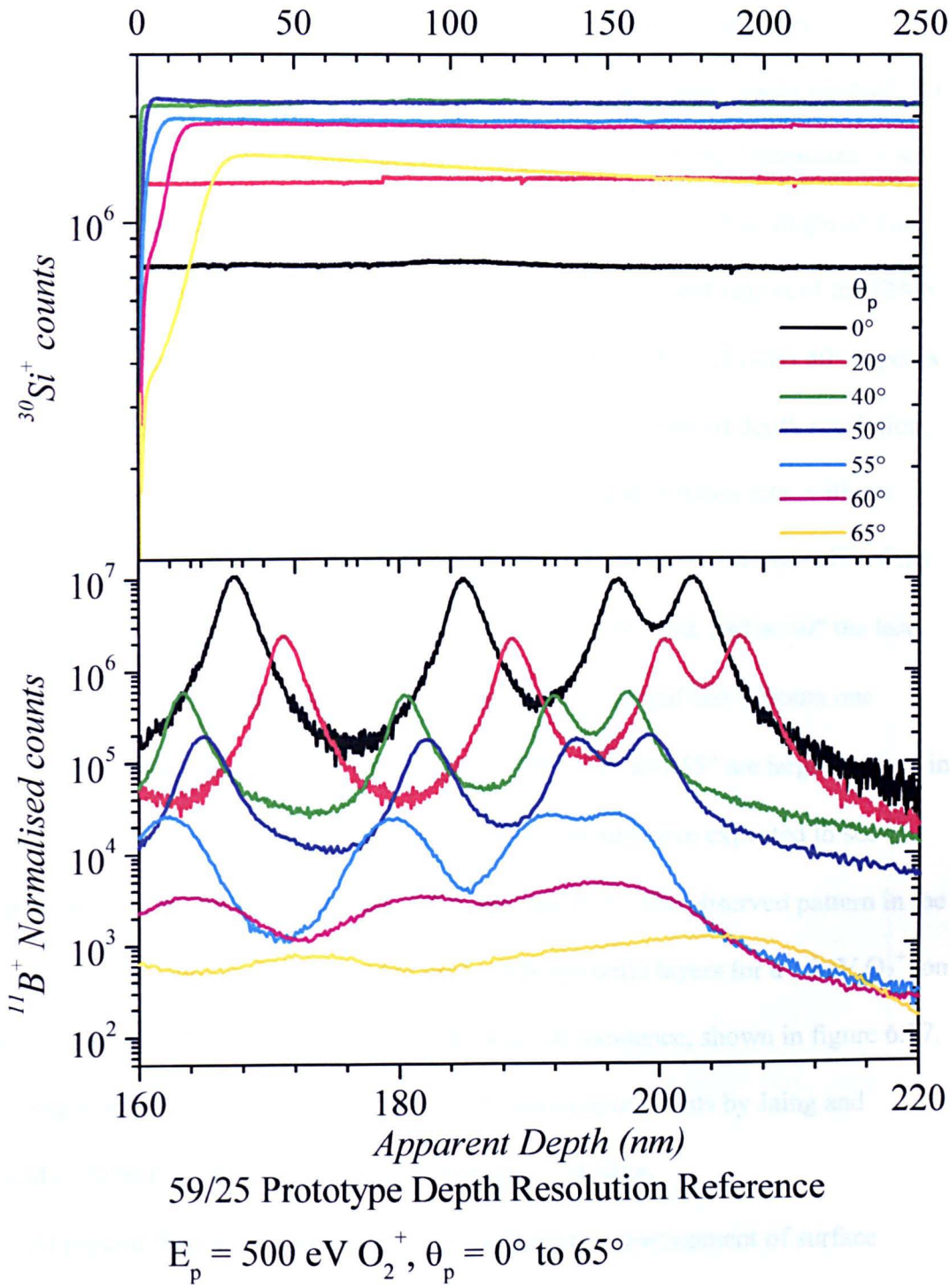

Figure 6.16: Various SIMS depth profiles obtained using 500 eV O_2^+ at various angles of incidence on sample 59.25, only the last 60 nm are shown for the $^{11}B^+$ signal. This is to show the significant loss of depth resolution over this depth range at oblique angles of incidence .

followed by 45° and 50° with severe roughening developing at approximately 100 nm, at 55°, 60° and 65° although there is an significant loss in depth resolution at approximately 80 nm, further degradation in depth resolution is much more gradual. At 1 keV, the FWHM parameter for the boron delta layers 2-5, could be determined at all the angles of incidence studied, unlike at a beam energy of 500 eV. The shape of the first delta layer in most cases is distorted as it is within the transient region of the SIMS profile as shown, in the boron and silicon profiles in figure 6.18. Although 40° appears to the worse angle of incidence to profile using 1 keV O_2^+ in terms of depth resolution, the resultant SIMS profile seems to exhibit an almost constant erosion rate, with no large shifts in the centriod positions observed, as shown in figures 6.18 and 6.19. Only at angles of $\leq 30°$ are the last two boron delta layers fully resolved, and at 40° the last three boron delta layers in sample 59.25 have completely merged and become one feature. Suprisingly, only at angles of incidence of 45°, 50° and 55° are large changes in the $^{30}Si^+$ signal observed, as shown in figure 6.19, one would have expected to see similar changes in the profiles obtained at 40°, 60° and 65°. The observed pattern in the depth resolution parameter FWHM of the profiled boron delta layers for a 1 keV O_2^+ ion beam at a depth of 200 nm as a function of the angle of incidence, shown in figure 6.17, closely resembles that reported for surface roughness measurements by Jaing and Alkemade (1998a), obtained under similar analysis conditions.

At present there is no model that fully explains the development of surface topography, under all possible ion sputtering conditions, especially one that can take into account the effect of using oxygen flooding. The observed complex behaviour at oblique angles of incidence, means that simple models cannot provide wholly accurate explantions. The evolution of surface topography during ion sputtering is a complex phenomenon, dependent on both roughening and smoothing processes. This is because

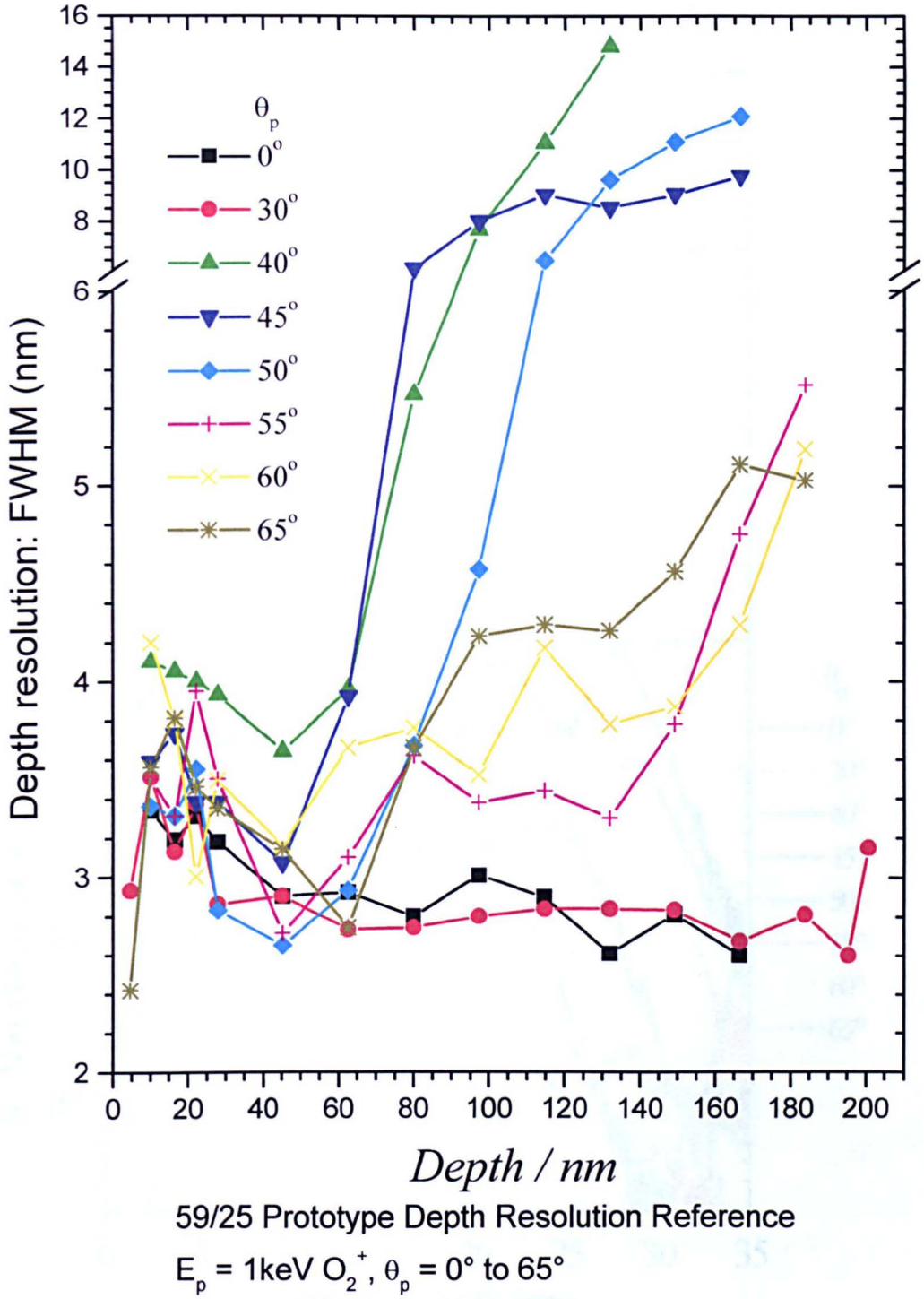

Figure 6.17: FWHM values as a function of depth determined by profiling sample 59.25, using 1 keV O_2^+ at various angles of incidence.

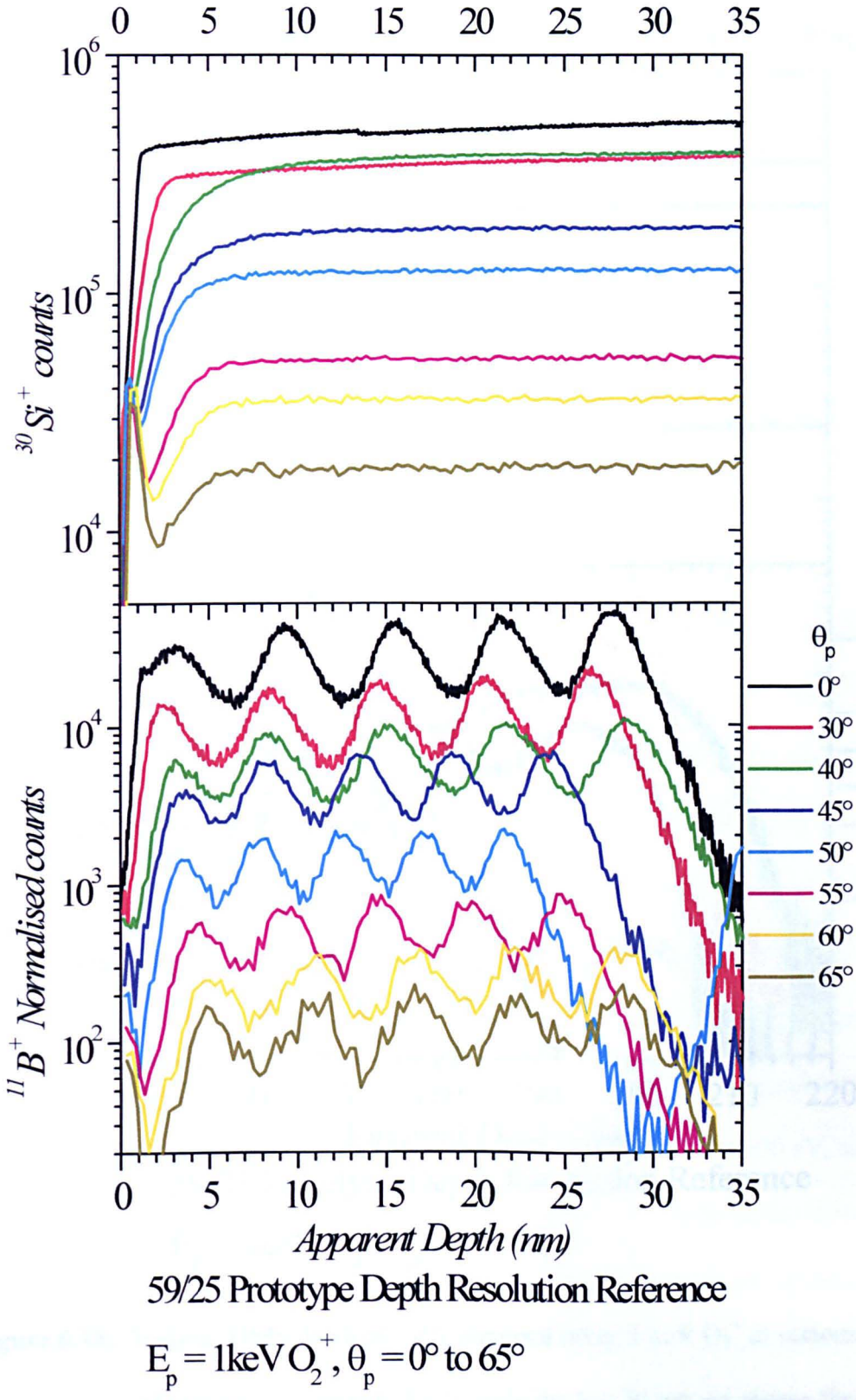

Figure 6.18: Various SIMS depth profiles obtained using 1 keV O_2^+ at various angles of incidence on sample 59.25, only the first 35 nm are shown.

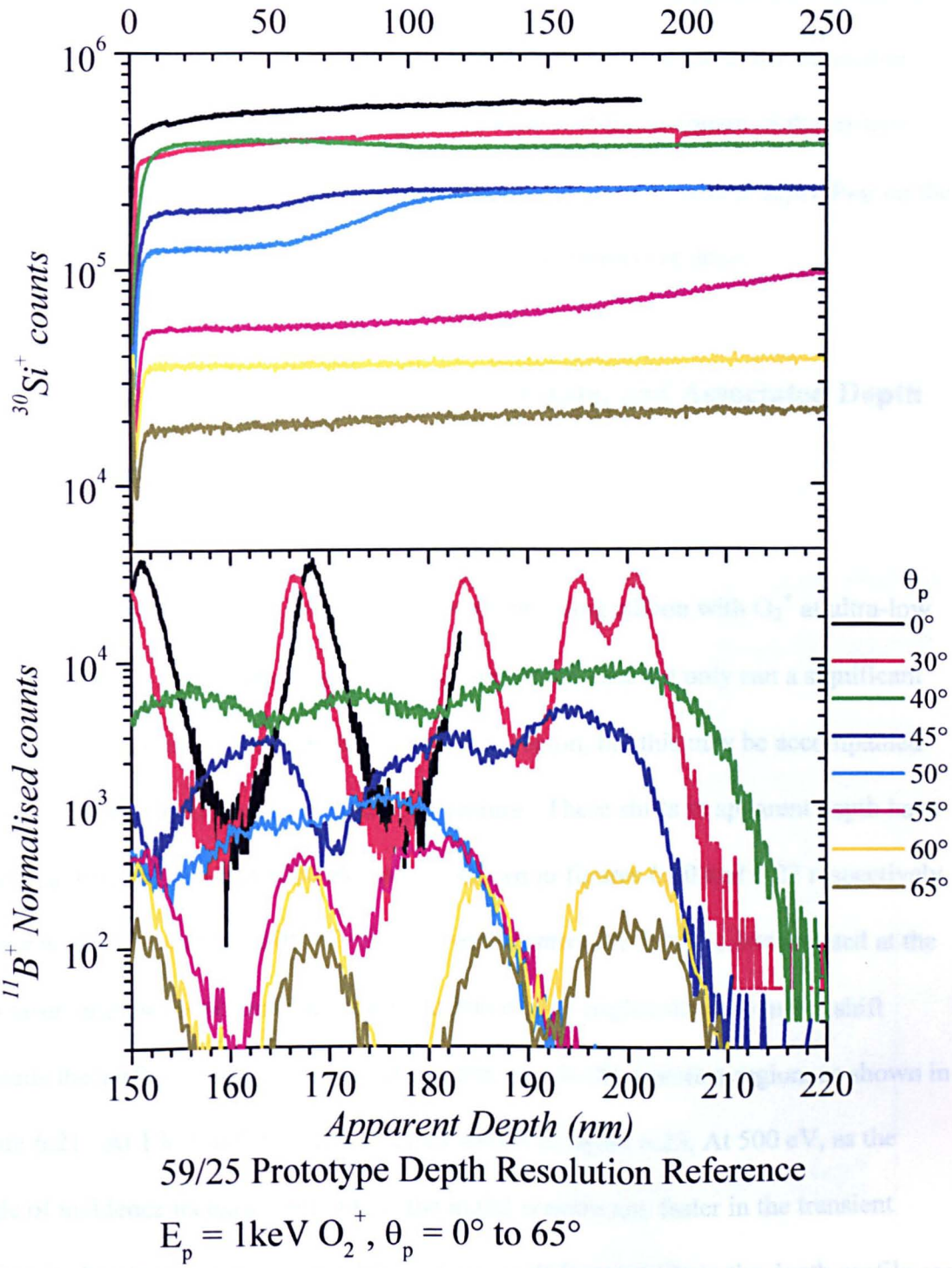

Figure 6.19: Various SIMS depth profiles obtained using 1 keV O_2^+ at various angles of incidence on sample 59.25, only the last 70 nm are shown for the $^{11}B^+$ signal. This is to show the significant loss of depth resolution over this depth range at oblique angles of incidence .

both the sputtering yield and the incorporation of oxygen are dependent on the local curvature. In many cases, it has been found that the resultant roughness of a sputtered surface evolves following scaling laws and that transitions between dynamic scaling regimes can occur (Smilgies D M et al., 1997). The root-mean-square of the surface roughness W and the ripple wavelength λ are proportional to t^{β}, with β depending on the angle of analysis, and where t is the analysis time, or cumulative dose.

6.3 Induced Variations in Erosion Rate, and Associated Depth Scale Errors

In section 6.2, it was indicated that when profiling silicon with O_2^+ at ultra-low beam energies (≤ 1 keV) at oblique angles of incidence, that not only can a significant loss of depth resolution occur in the near surface region, but this may be accompanied by large changes in the apparent depth of a feature. These shifts in apparent depth have been quantified at 500 and 1000 eV and are shown in figures 6.20 and 6.22 respectively. The only angle to exhibit shifts of <3 nm over the entire depth range investigated at the two beam energies is normal incidence. At 500 eV, all angles show an initial shift towards the surface, this is due to faster erosion rates in the transient region, as shown in figure 6.21. At 1 keV this is not the case as shown in figure 6.23. At 500 eV, as the angle of incidence increases not only is the initial erosion rate faster in the transient region, it also occurs over a larger depth. As a result larger shifts in the depth profile are observed in the first 50 nm of a profile, at oblique angles of incidence than at normal incidence, as shown in figure 6.20. At a depth of 25 nm all angles <60° have reached a steady erosion rate, although serious loss of depth resolution occurs at angles ≥55°.

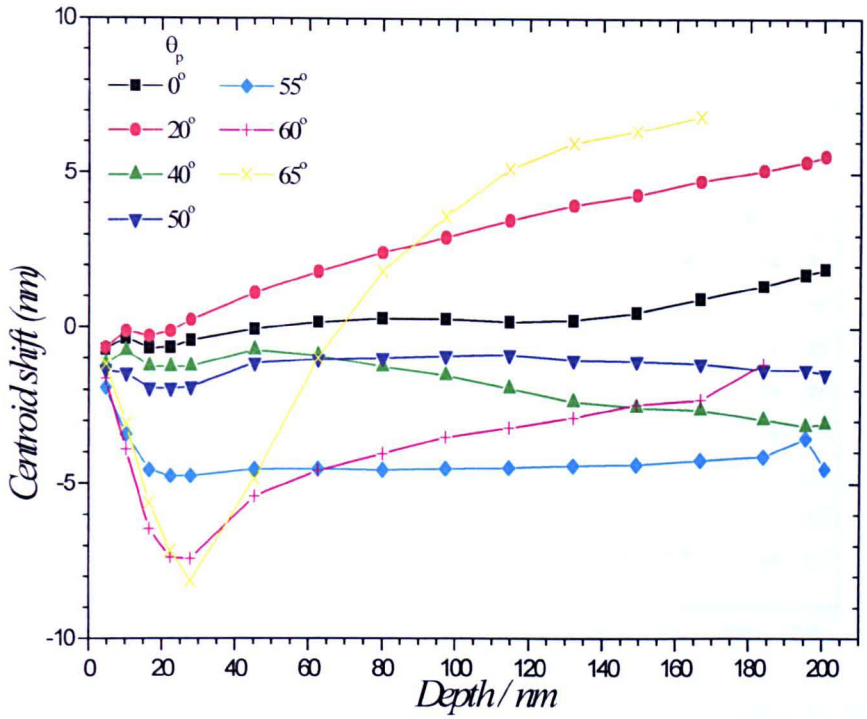

Figure 6.20: Observed centroid shifts for the 16 boron delta layers in sample 59.25, in the SIMS depth profiles obtained using 500 eV O_2^+ at various angles of incidence.

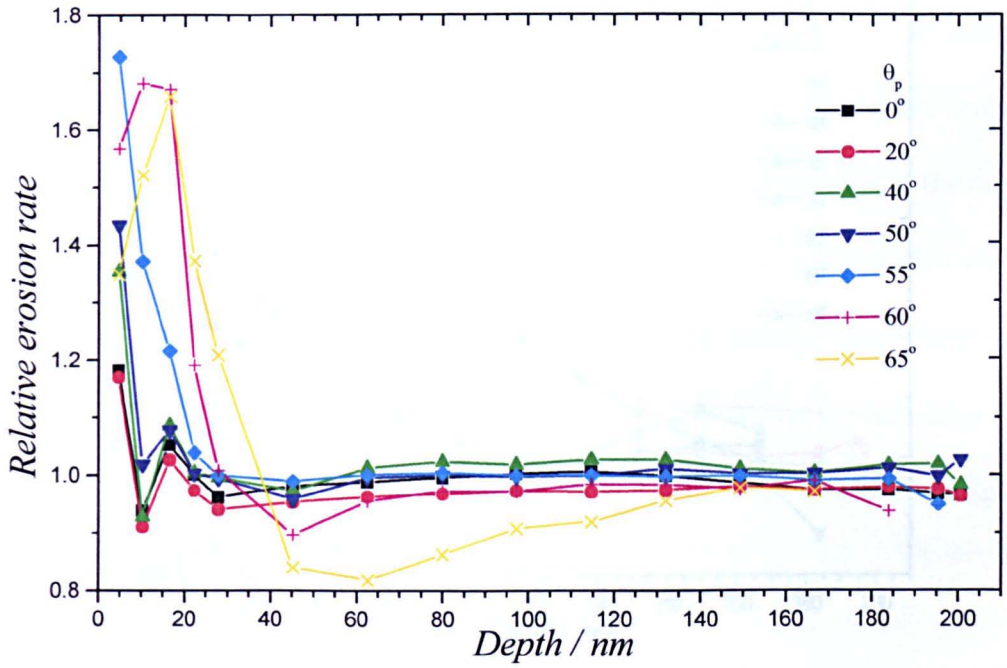

Figure 6.21: Observed variations in the relative erosion rates for sample 59.25 in the SIMS depth profiles, obtained using 500 eV O_2^+ at various angles of incidence.

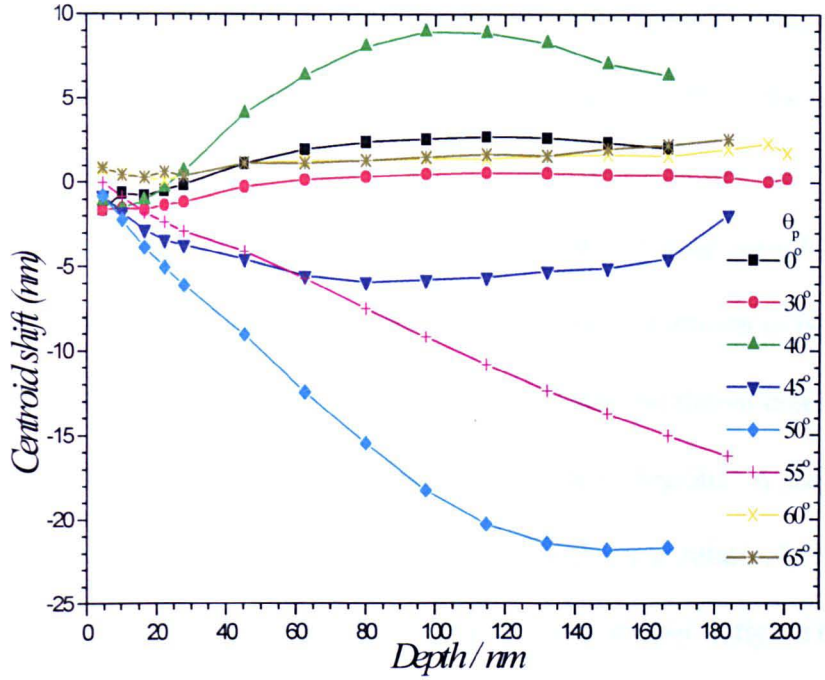

Figure 6.22: Observed centroid shifts for the 16 boron delta layers in sample 59.25, in the SIMS depth profiles obtained using 1 keV O_2^+ at various angles of incidence.

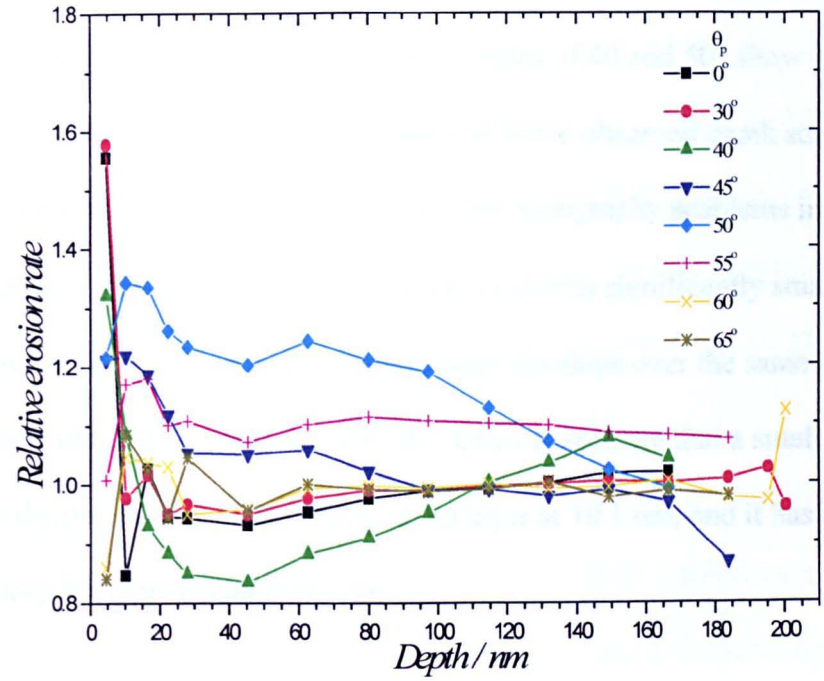

Figure 6.23: Observed variations in the relative erosion rates for sample 59.25 in the SIMS depth profiles, obtained using 1 keV O_2^+ at various angles of incidence.

At 65° dramatic changes in the erosion rate occur at depths between 20 and 60 nm, it decreases from a maximum - 170% of the average to 80% of the average, over this small range.

At a beam energy of 1 keV, a completely different and more complex pattern is observed in both the centroid shift and relative erosion rates, as shown in figures 6.22 and 6.23 respectively. The angles of 0, 30, 60 and 65° show an almost constant relative erosion rate over 200 nm (with the exception of the transient region). A similar pattern is also observed at 55° with the exception that the erosion rate is relatively fast and the observed shifts in the depth profile get continuely larger as shown in figure 6.22. The explanation for this is that surface topography starts to develop around a depth of 170 nm under these conditions, as shown in figure 6.19, and the total crater depth of this profile was 400 nm. If this profile obtained at 55° had been stopped at a depth of 200 nm, much smaller errors in the depth scale would have been observed and would have occured mainly in the surface region. The angles of 40 and 50° show completely different trends in the variation of erosion rate and hence observed depth scale errors, even though both conditions develop severe surface topography problems in the depth range 60 - 100 nm. The intermediate angle of 45° exhibits significantly smaller changes in the erosion rate, even though surface roughening develops over the same depth range.

The data obtained at 500 and 1000 eV, seems to indicate that a small error has occured with the positioning of the second delta layer at 10.1 nm, and it has been placed slightly too deep by approximately 0.3 nm.

All SIMS profiles will contain errors in the depth scale, due to either variations in the erosion rate, or problems in determining the true depth of the resultant crater. The results contained in this chapter for O_2^+, over a wide range of primary beam energies, angles of incidence and over a depth of 200 nm indicate that these errors can be minimised by profiling at normal incidence, using low (≤1 keV) beam energies. Under such conditions errors are reduced, so that the largest source of error is the actual determination of the crater depth, when using surface profilometry. Importantly, high depth resolution is also maintained under these conditions.

In the last 2-3 years there have been several papers published claiming (and counter-claiming) that a particular set of analytical conditions produce minimal (or large) depth scale errors (Wittmaack K and Corcoran S F, 1998; Mount G R et al, 1998). It is the authors opinion that any observed errors are dependent on a wide range of factors, including the actual angle of incidence (rather than the nominal angle of incidence); the beam energy; the actual sample composition (for instance the thickness of any surface oxide may affect the result); the vacuum conditions; the position of any feature and the depth of the SIMS profile. Jaing and Alkemade (1998b) have shown that if oxygen flooding is used, it is important that the surface is fully saturated as different variations in the erosion rate are observed at immediate oxygen pressures, and even larger ripples can develop on the sample surface.

The above profiles analysed at 500 eV and 1 keV, at angles of incidence 0-65° were also used to calculate the average sputter yields for these conditions, a summary of the data obtained, is shown in table 6.1. The data shows one of the main advantages of profiling with O_2^+ at oblique angles of incidence, significantly higher sputter yields. The sputter yield at 65° is 9 times faster at 500 eV and nearly 20 times faster at 1 keV,

than at normal incidence. Although at 65° the projected crater is approximately twice the size in the y-direction, than at normal incidence.

The sputter yield data in table 6.1, is plotted in figure 6.24 as a function of the angle of incidence, also included is data obtained using 10 keV O_2^+ (Wittmaack K, 1983). Figure 6.24 shows a similar trend in sputter yield behaviour as a function of the angle of incidence, at all three beam energies. The sputter yield value obtained at a energy of 1 keV and at 30°, appears to be smaller than expected, this is probably because the altered layer is still fully oxidised under these conditions and the equivalently data point at 500 eV is not available.

O_2^+ energy (keV)	Angle of incidence (°)	Crater depth (nm)	Crater size(μm)		Volume of crater (cm^3)	Analysis time (minutes)	Average I (nA)	Total O_2^+ dose	Average sputter yield
0.5	0	254.6	288	383	2.81E-8	299.53	97.72	1.096E16	0.128
0.5	20	322.8	287	402	3.72E-8	300.00	104.45	1.173E16	0.158
0.5	40	367.8	289	482	5.12E-8	200.00	115.89	0.868E16	0.295
0.5	50	317.6	282	561	5.02E-8	122.40	115.48	0.529E16	0.474
0.5	55	347.2	288	623	6.23E-8	133.33	106.48	0.532E16	0.585
0.5	60	308.0	283	698	6.08E-8	99.77	107.79	0.403E16	0.754
0.5	65	478.9	274	802	10.52E-8	133.33	96.16	0.480E16	1.094
1.0	0	183.2	285	373	1.95E-8	133.33	113.00	0.564E16	0.172
1.0	30	334.9	283	426	4.04E-8	148.52	135.74	0.755E16	0.267
1.0	40	273.3	275	474	3.56E-8	66.67	128.49	0.321E16	0.555
1.0	45	369.1	285	515	5.42E-8	66.67	121.89	0.304E16	0.889
1.0	50	207.1	287	564	3.35E-8	34.23	105.07	0.135E16	1.243
1.0	55	400.6	291	618	7.20E-8	50.00	97.61	0.183E16	1.968
1.0	60	251.2	282	698	4.94E-8	26.78	90.63	0.091E16	2.716
1.0	65	300.5	284	821	7.01E-8	33.33	89.81	0.112E16	3.121

Table 6.1: A summary of analytical conditions and the calculated average sputter yield.

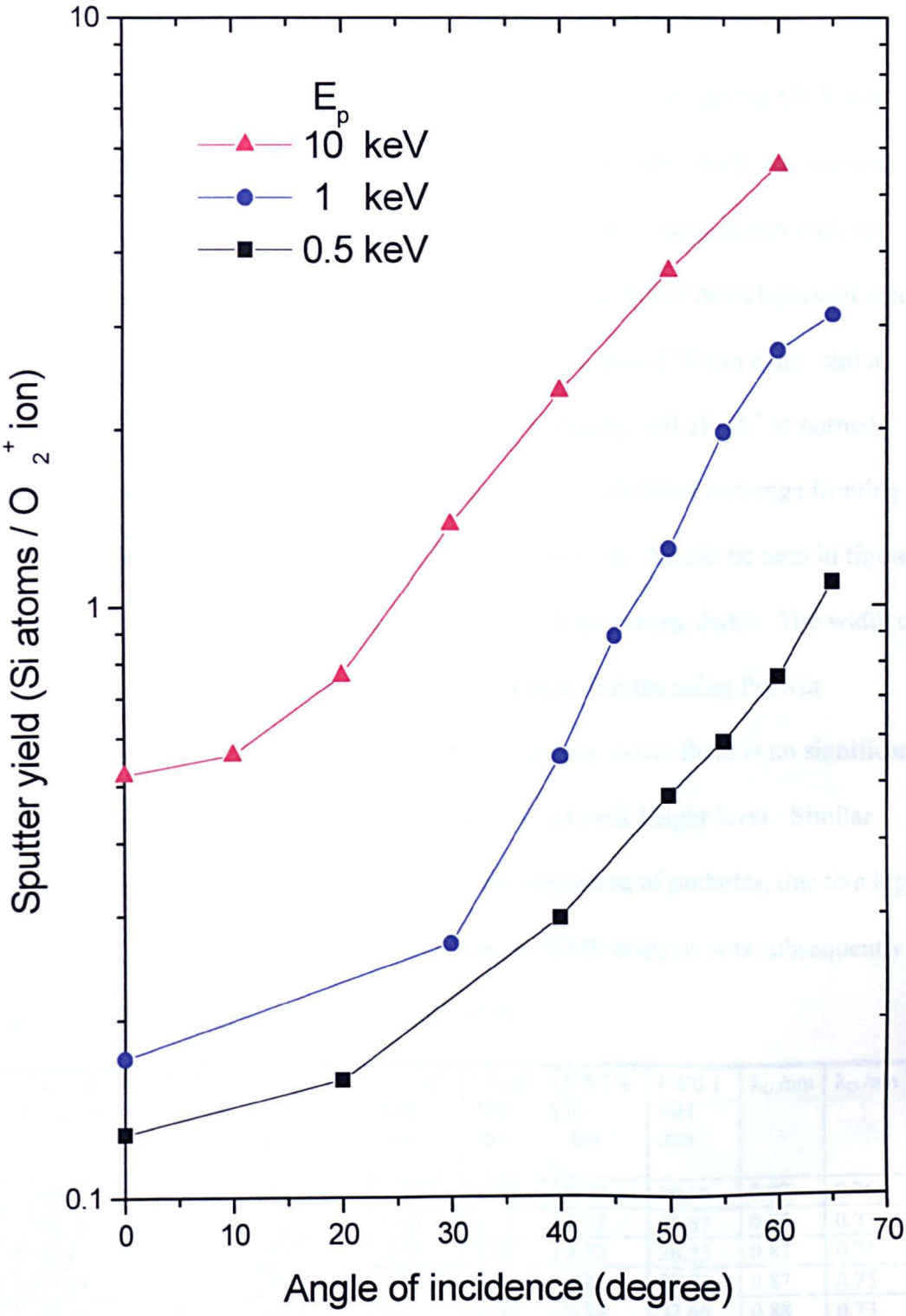

Figure 6.24: Average sputter yield for three beam energies as a function of angle of incidence. The 10 keV data was obtained from Wittmaack (1983).

6.4 Pinhole Formation

During my studies, I was asked to analyse a wafer grown by silicon MBE at a temperature of 470°C, because it possessed an abnormal blue hue, which was darkest around its edges. A number of similar structures had previously been grown with no colouration. The sample 55.15 nominally contained multiple boron delta layers all at a concentration of 2 x 10^{14} atoms cm^{-2}, with the top 4 layers spaced 50 nm apart, and a further 8 layers 100 nm apart. The sample was analysed using 500 eV O_2^+ at normal incidence on EVA3000. The resulting SIMS depth profile exhibited a strange fronting pattern, 3 orders of magnitude down from the peak maximum. As can be seen in figure 6.25, this unusual feature becomes more significant with increasing depth. The width of the individual delta layers was determined at several peak heights using Prowin software, and the results summarised in table 6.2. The data shows there is no significant loss of depth resolution with depth, except at the 0.1% of peak height level. Similar SIMS artefacts had previously been attributed to the formation of pinholes, due to a high concentration of lattice defects. The crater formed by SIMS analysis was subsequently investigated using the techniques of SEM and AFM.

Peak No.	Concentration /atoms cm^{-2}	Depth of peak max. /nm	Spacing /nm	FW50 %H /nm	FW10 %H /nm	FW1% H /nm	FW0.1 %H /nm	λ_U /nm	λ_D /nm
1	2.25E14	51	51	2.02	4.74	8.57	20.88	0.87	0.76
2	2.03E14	103	52	2.00	4.71	8.53	20.57	0.85	0.73
3	2.35E14	156	53	2.12	4.88	8.82	26.23	0.87	0.74
4	2.39E14	208	52	2.13	4.92	8.86	29.75	0.87	0.75
5	2.36E14	311	103	2.2	4.98	8.88	32.66	0.88	0.73
6	2.29E14	411	100	2.29	5.03	8.94	32.34	0.87	0.76
7	2.20E14	509	98	2.39	5.12	9.07	32.76	0.84	0.74
8	2.04E14	605	96	2.44	5.21	9.33	33.20	0.87	0.76
9	1.90E14	702	97	2.54	5.30	9.39	31.00	0.83	0.75
10	1.72E14	797	95	2.62	5.55	10.11	32.44	0.85	0.79

Table 6.2: A summary of SIMS data obtained on sample 55.15.

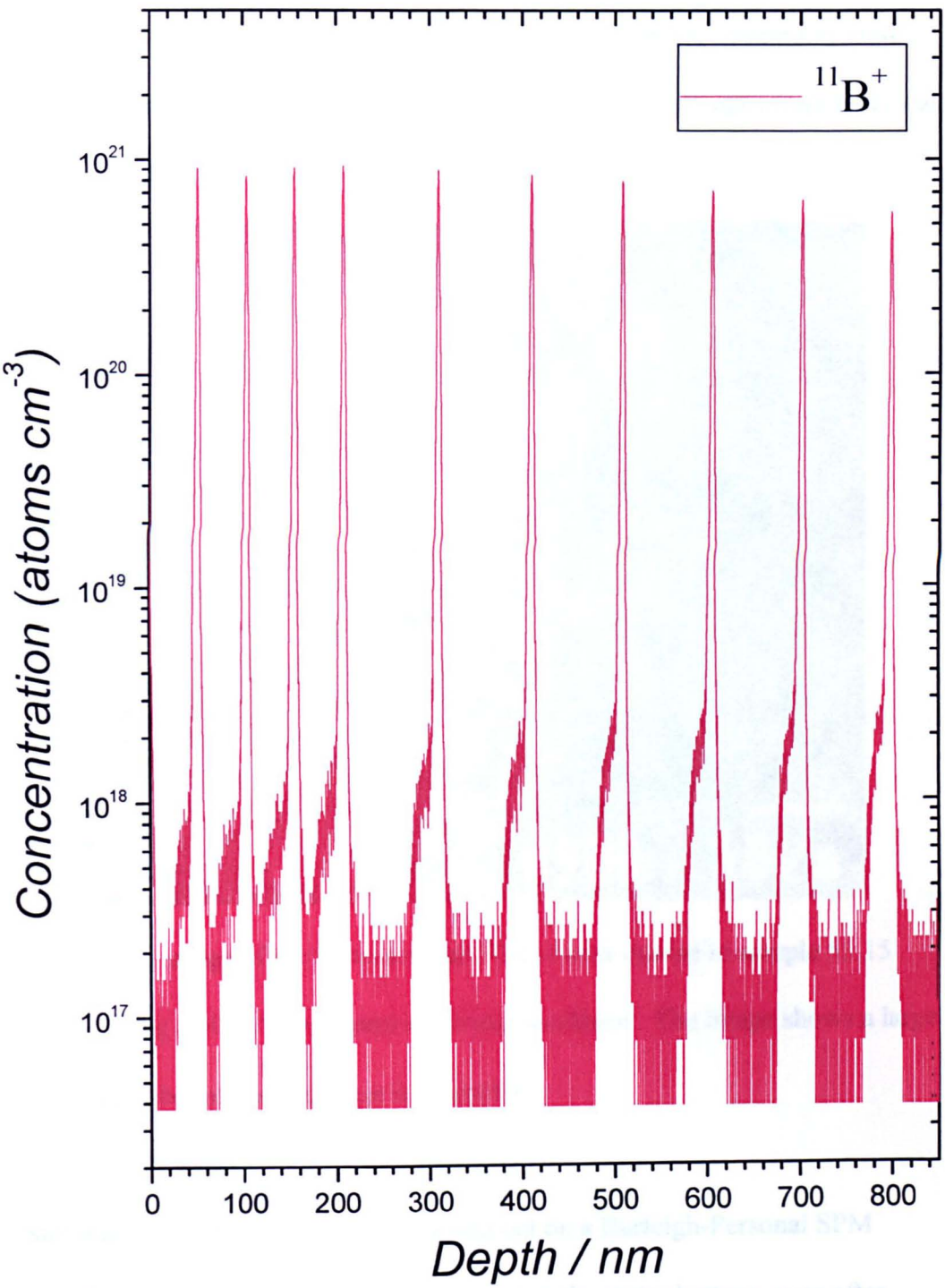

Figure 6.25: Calibrated SIMS profile of 10 of the boron delta layers in sample 55.15 showing a strange fronting pattern, 3 orders of magnitude down from the peak maximum. The profile was obtained using a 500 eV O_2^+ beam at normal incidence.

SEM analysis was carried out on an Jeol JSM-6100 using 10 keV electrons. While the developed photographs clearly showed the crater surface covered in small holes ≤ 2 μm in diameter, as shown in figure 6.26, the on-screen images were less clear. The pinholes also appeared to occur in bands.

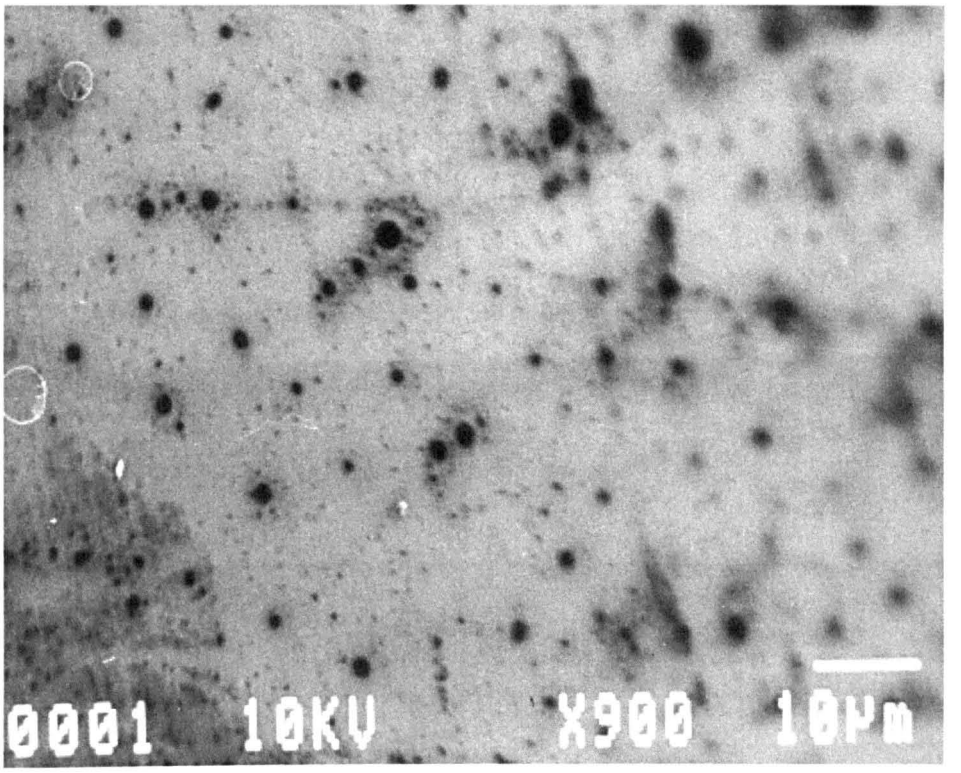

Figure 6.26: SEM image of the bottom of the SIMS crater eroded in sample 55.15 using a 500 eV O_2^+ beam at normal incidence. The image shows a large number of holes ≤ 2 μm in diameter.

Subsequently, AFM analysis was carried out on a Burleigh-Personal SPM instrument. Difficulties were encountered in locating the crater bottom, even after drawing round the crater with a marker pen. The images eventually obtained clearly showed pinholes, as can be seen in figure 6.27, which shows three pinholes in a 9 X 9 μm area near the crater edge. Cross sectional analysis of two such holes found them to be approximately 1 μm in diameter and 40 nm deep as shown in figure 6.28.

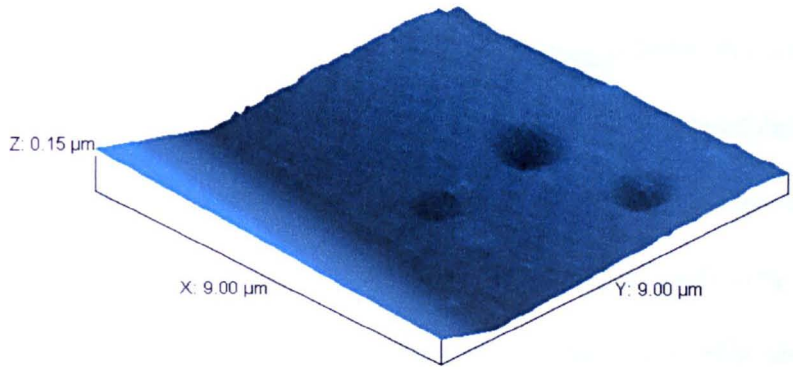

Figure 6.27: AFM image of the bottom of the SIMS crater eroded in sample 55.15 using a 500 eV O_2^+ beam at normal incidence. The image shows three pinholes in a 9 X 9 µm area near the crater edge.

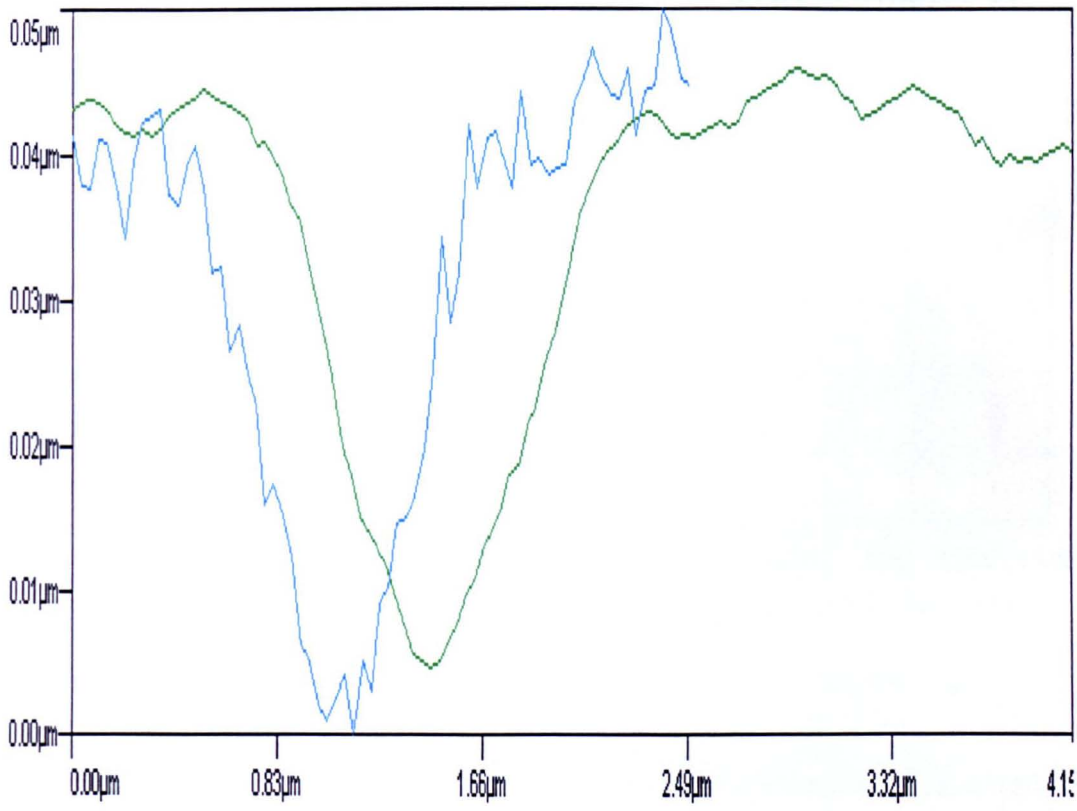

Figure 6.28: Cross sectional analysis of the AFM data of two such holes found them to be approximately 1 µm in diameter and 40 nm deep.

Subsequently, a similar sample 55.04 (which exhibited no obvious visual defects) was analysed using 1.0 keV O_2^+ on a Cameca IMS6F, by the Cameca sales department (angle of incidence unknown). The resulting profiles did not exhibit any unusual features, although there was a much more significant loss of depth resolution (FWHM) with depth. To investigate if this was sample related, or due to the analysis conditions used, an undipped piece of sample 55.15 was analysed using a 1.0 keV O_2^+ ion beam at 0, 45, 50 and 60° on the Atomika 4500. Only the profile obtained at normal incidence, showed the unusual feature. It is not clear whether this feature is not observed at oblique angles of incidence because it is obscured by the wider peaks, or that the pinholes do not develop because of ripple formation and their subsequent migration across the surface. Again, a significant loss of depth resolution (FWHM) with depth occurred for all profiles obtained at non-normal angles of incidence, as shown in figure 6.29.

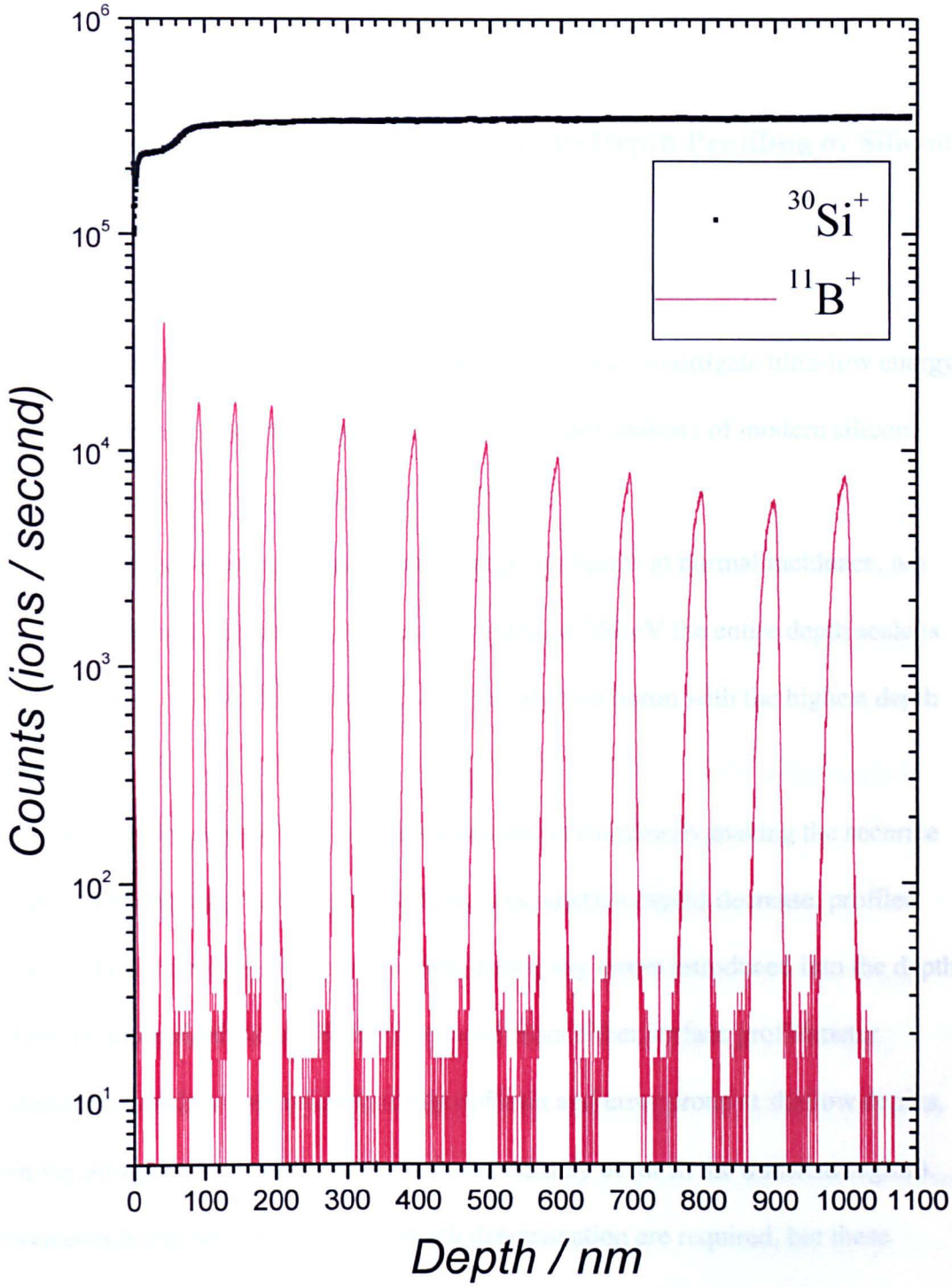

Figure 6.29: SIMS profile of all 12 of the boron delta layers in sample 55.15, obtained using a 1 keV O_2^+ beam at an angle of incidence of 45°. The profile shows no unusual features, but does exhibit a significant loss of depth resolution with depth.

7.0 Conclusions

7.1 Accurate Ultra-Low Energy SIMS Depth Profiling of Silicon Semiconductors

The aim of this research project has been to find and investigate ultra-low energy SIMS depth profiling conditions, suitable for the accurate analysis of modern silicon semiconductor devices.

This work has shown that ultra-low energy ion beams at normal incidence, not only produce the most accurate SIMS depth profiles, at 250 eV the entire depth scale is accurate to within 1.5 nm (2.5 nm at 500 eV), but also for boron with the highest depth resolution.

The shrinking size of semiconductor devices is continually making the accurate measurement of dopant profiles more difficult. As junction depths decrease, profiles only need to be sputtered to shallower depths, hence any errors introduced into the depth scale become more significant. Such errors arise from either surface profilometer measurements, which are significantly more difficult and error prone at shallow depths, or from variations in the erosion rate (which should only occur in the transient region). Improvements in the accuracy of crater depth determination are required, but these developments are down to the relevant instrumentation manufacturers. The apparent and true transient widths have been determined for a wide range of energies $230\ eV \leq Ep \leq 10\ keV$ for O_2^+ ion beams at normal incidence, and also at a number of angles of incidence at 500 eV. The apparent surface transient width reduces from over 10 nm to 0.5 nm as the primary beam energy decreases from 10 keV to 230 eV. The

true surface transient width is at least twice the size of the apparent surface transient width, reducing from over 23 nm to 1.0 nm over the same energy range.

At 500 eV, as the angle of incidence moves from normal to more oblique angles, the size of the apparent and true transient widths increased dramatically. However, at angles up to 40° the actual transient shift remains small < 0.5 nm. At angles of incidence > 40° the rapid increase in actual transient width is associated with the development of surface topography. At angles > 20° the size of the transient region can be different depending on which matrix species is monitored. However, the actual transient shift is the same.

The above values were determined using MBE grown material, different values may be obtained for implanted samples, especially those formed at ultra-low energies due to their high near-surface impurity concentration and accompanying variation in matrix composition. Only once studies on samples that combine multi-delta layered structures, with low energy implants (both with/without preamorphisation and with/without typical anneals) are completed, will typical values be available.

The variation of the erosion rate in the pre-equilibrium region is an important parameter, experiments to measure this using 500 eV O_2^+ at normal incidence have recently been completed, in a study combining the complementary techniques of MEIS and SIMS. The study found that the sputter yield changed by more than a factor of 10 in the transient region, starting at 0.37 increasing to 1.37 and rapidly decreasing to the steady state value of 0.12 (silicon atoms/ O_2^+ ion).

These studies have found that sub-keV normal incidence analysis with oxygen does not produce the extreme surface transients and spikes typical of higher beam energies. Below 750 eV all the matrix transients rise monotonically from a low level, suggesting that the surface spike is influenced by the energy deposition and/or

penetrating power of the primary beam and the top monolayer of the sample, and not solely related to the presence of native oxide.

Different surface oxide thicknesses were found to lead to differences in profile shape and more importantly in the equilibrium dose at sub-keV beam energies. This is because the transient dose is independent of oxidation at the surface (although the signal behaviour is not), provided that the true transient width is greater than the oxide thickness. The equilibrium dose was found to be relatively insensitive with regard to beam energy unlike the transition width. There is only a 4-5 fold decrease in equilibrium dose on decreasing the beam energy from 2.5 keV to 300 eV, but this corresponds to an approximate 30 fold decrease in the apparent transition depth, due to the dependence of sputter yield on energy.

Experiments to quantify the terminal shift, have shown that the observed energy dependent shift in the peak and centroid position of a delta layer, is also reliant on the feature to surface and feature to crater bottom distance. This is because two shift corrections are required to the depth scale, the transient shift and the terminal shift. The terminal shift for boron using normally incident oxygen ions is caused by two factors. The first is that when a profilometer measurement is made from the unmodified starting surface of a sample to the crater bottom. It differs from the depth of matrix eroded for two reasons:

(i) The matrix density (matrix atoms cm^{-3}) is modified by the presence of the implanted probe atoms. For example, for silicon fully saturated with oxygen from an O_2^+ beam, the stoichiometry is close to SiO_2, and the volumetric swelling of the matrix is around a factor of 2.2. If all the probe atoms were removed, and the silicon atoms were repacked at their original density, the crater would be deeper. This new depth gives the true position of the last ordinate in matrix channel, provided there is no roughening.

(Whether the matrix density is increased or decreased in general will depend on the details of the probe species/matrix reaction. For example, if the matrix and probe were an alkali metal and oxygen, the spacing between alkali metal atoms would be reduced compared to their metallic spacing - shrinkage as opposed to swelling.)

(ii) A profilometer stylus tip is typically 12 μm in diameter. This will ride over the crests of any roughening, resulting again in an underestimate of the true amount of matrix sputtered.

Secondly, a more subtle effect because it is impurity dependent: Suppose the primary beam induced mass transport is not solely due to random cascade mixing, but involves some preferential migration of the impurity into, or away from the altered layer (Dowsett M G *et al.*, 1992). A delta layer would be observed to be shallower or deeper respectively than its true depth, as would the dopant intensity from any broader distribution. For boron the migration is towards the altered layer. The magnitude of the terminal shift for boron is very similar to that determined for the full thickness of the altered layer, formed under identical analysis conditions (Dowsett M G *et al.*, 2000).

Utilising these two shifts a simple universal depth correction procedure has been described, applicable when profiling boron samples using O_2^+ at normal incidence.

The quantification issues of changing the beam energy within a single depth profile were investigated. It was found surprisingly that the only correction needed to the depth scale was the transient shift associated with the first energy used i.e. there is no depth correction required at the second energy (< 0.1 nm). Even though there is a second transient region (typically 0.8 - 1.0 nm) on switching the beam energy where there is a change in ion yield, provided that this does not obscure a feature it can be neglected from the final result. These surprising minimal extra effects on switching the

beam energy are thought to be due to the size of the altered layers being very similar within the analysis conditions studied.

The advantages of using dual beam energy profiling for the analysis of shallow implants are clearly demonstrated. It minimises the surface transient region, and both high depth resolution and high sensitivity are available in the desired parts of a profile, while significantly reducing the required analysis time.

The effect of varying the angle of incidence between 0 and 65° on depth resolution and sputter yield has been assessed for O_2^+ ion beam energies of 500 and 1000 eV. While faster erosion rates are possible at non-normal angles of incidence, no improvement in depth resolution was observed. In fact at angles of 30° and above, the reverse was found to be true, due to the formation of ripples at depths < 100 nm. Ripple formation was only previously observed at depths > 1 μm, when profiling silicon with oxygen ion beams at oblique angles of incidence, and energies of ≥ 2 keV.

An investigation which started of as looking at ways of obtaining the ultimate in depth resolution, when profiling with ultra-low energy O_2^+ ion beams, instead turned into a search for analytical conditions, which do not develop ripples within the top 200 nm of a profile. The development of surface topography *i.e.* ripples has two detrimental effects, it causes a variation in the sputter yield and a loss of depth resolution. Both of these effects have been quantified. A wide range of analysis conditions were investigated, at O_2^+ beam energies up to 1 keV, the only angles at which surface topography does not develop are those using near-normal incidence ($\theta_p \leq 30°$) ion bombardment. The best depth resolution was always observed at normal incidence. The change in sputter yield caused by ripple formation, induced errors larger than 20 nm in a depth of 200 nm, under one set of analysis conditions.

The limited data set obtained using the technique of oxygen flooding at oblique angles of incidence, demonstrated that while it suppresses ripple formation, it does not prevent it, and poorer depth resolution is observed under such conditions.

Attempts to quantify how the ion yield of boron varies in the transient region, were not successful. This was because the near-surface region of the uniformly doped sample always contained a higher concentration of boron, which was not completely removed by chemical treatment.

7.2 Further Work

The phenomenon that sub-keV normal incidence analysis with oxygen does not produce the extreme surface transients and spikes typical of higher beam energies will be further investigated. Several methods for doing this have been suggested, including using ^{18}O to bombard the surface of dipped and undipped silicon, the use of SNMS and the use of static SIMS.

The accuracy of the transient width and terminal shift values determined will be further investigate by further data processing, including the use of deconvulution techniques. The depthof craters will also be measured using an optical profilometer to compare the two set of values obtained.

As mentioned above a sample possessing a completely uniform boron concentration in the top 10 - 50 nm is required, so that a full depth and concentration quantification procedure can be developed for the analysis of boron containing samples, by ultra-low energy SIMS profiling.

Also as indicated in the previous section, special samples are required in order that the true transient width for typical ultra-shallow implants can be determined.

It is planned to investigate the terminal shift for germanium using O_2^+ at normal incidence. If our thoughts are correct the magnitude of the terminal shift for germanium is expected to be smaller than that determined for boron. This is because germanium tends to segregate away from the altered layer formed under these conditions.

It is also important that a range of angles of incidence are investigated at O_2^+ beam energies in the range 500 to 250 eV (the lowest energy currently used for routine depth profiling). This set of experiments should be done in conjunction with the commonly used technique of oxygen flooding.

The final stage would be to extend these studies to commonly used different implant species, different semiconductor materials (e.g. gallium arsenside) and also using different primary ion species (e.g. caesium, which must be profiled at oblique angles of incidence).

APPENDIX I

The Thickness of the Altered Layer at Normal Incidence.

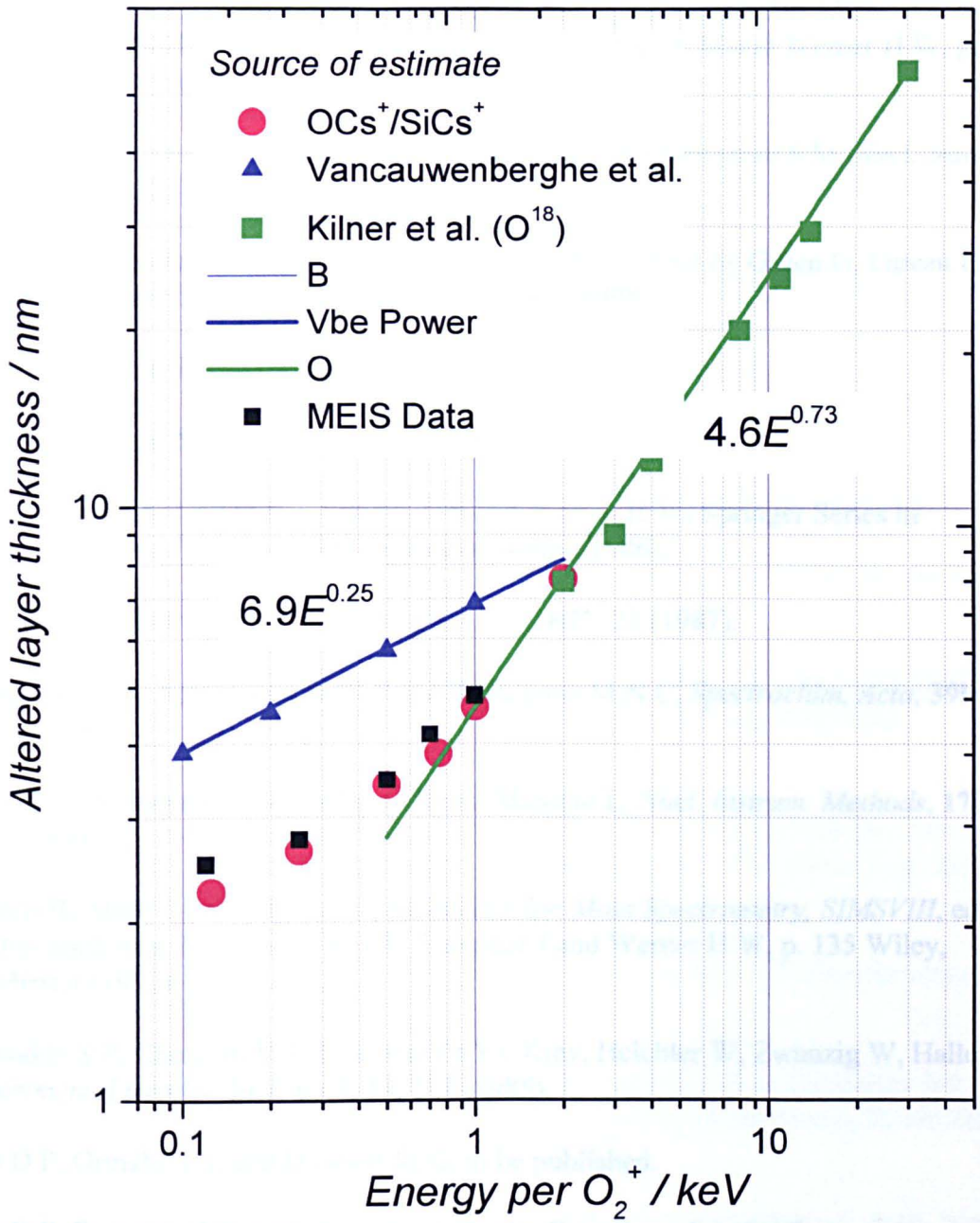

Figure I.1: Compilation of normal incidence altered layer thickness.
All data from Dowsett M G et al., (2000) .

References

Alton G D, *Rev. Sci. Inst.*, **59**, 1039 (1988).

Armour D G, Wadsworth M, Badheka R, van der Berg J A, Blackmore G, Courtney S, Whitehouse C R, Clark E A, Skyes D E and Collins R, *Secondary Ion Mass Spectrometry, SIMSVI*, edited by Benninghoven A, Huber A M and Werner H W, p. 399 Wiley, New York (1988).

Barlow R D, Dowsett M G, Fox H S, Kubiak R A A, and Newstead S M, *Nucl. Instrum. Meth. in Phys. Res.* **B72**, 327 (1992).

Bennett J, *Secondary Ion Mass Spectrometry, SIMSXI*, edited by Gillen G, Lareau R, Bennett J and Stevie F, p. 1011 Wiley, Chichester (1998).

Benninghoven A, *Z. Physik*, **230**, 403 (1970).

Benninghoven A, *Surf. Sci.*, **53**, 596 (1975).

Benninghoven A, Colton R J, Simons D S and Werner H W, Springer Series in Chemical Physics Vol. 44, p. 288, Springer, Berlin (1986).

Biersack J P, *Nucl. Instrum. Meth. in Phys. Res.* **B27**, 21 (1987).

Boudewijn P R, Ackerboom H W P and Kemperers M N C, *Spectrochim. Acta*, **39b**, 1567 (1984).

Buck T M, Stensgaard I, Wheatley G H and Marchut L, *Nucl. Instrum. Methods*, **170**, 519 (1980).

Canteri R, Moro L and Anderle M, *Secondary Ion Mass Spectrometry, SIMSVIII*, edited by Benninghoven A., Janssem K T F, Tumpner J and Werner H W, p. 135 Wiley, Chichester (1992).

Chenakin S P, Cherepin V T, Dyadkin Ya Ya, Kiev, Heichler W, Zwanzig W, Halle , *Experimental technik der Physik*, **33**, 277 (1985).

Chu D P, Ormsby T J, and Dowsett M G, to be published.

Chu D P, Dowsett M G, Ormsby T J and Cooke G A, *Proc. Int. Conf. on Characterisation and Metrology for ULSI Technology*, March 1998, AIP press, New York p771.

Clark E A, Dowsett M G, Fox H S and Newstead S M, *Secondary Ion Mass Spectrometry, SIMSVII*, edited by Benninghoven A, Evans C A, McKeegan K D, Storms H A and Werner H W, p. 627 Wiley, Chichester (1990).

Clegg J B, *Surf. Interfacl. Anal.*, **10**, 332 (1987).

Cooke G A, Dowsett M G, Ormsby T J, Chu D P and Pidduck A J, *USJ99 handbook*, March 1999, p41.

Cooke G A, Ormsby T J, Dowsett M G, Parry C, Murrell A and Collart E J H, *J.Vac. Sci. Technol.*, **B18,** 493 (2000).

Corcoran S F, in *Secondary Ion Mass Spectrometry, SIMS X* (Eds. A. Benninghoven, B. Hagenhoff and H.W. Werner), p. 107, Wiley, Chichester (1997).

Dowsett M G, private memo, unpublished.

Dowsett M G, *Secondary Ion Mass Spectrometry, SIMSX*, edited by Benninghoven A, Hagenhoff B and Werner H W, p. 355 Wiley, Chichester (1997).

Dowsett M G, *Secondary Ion Mass Spectrometry, SIMSXI*, edited by Gillen G, Lareau R, Bennett J and Stevie F, p. 259 Wiley, Chichester (1998).

Dowsett M G, Barlow R D, Fox H S, Kubiak R A A, and Collins R, *J.Vac. Sci. Technol.*, **B10,** 336 (1992).

Dowsett M G, Barlow R D, and Allen P N, *J.Vac. Sci. Technol.*, **B12,** 186 (1994).

Dowsett M G and Chu D P, The 11th Annual SIMS Workshop on Secondary Ion Mass Spectrometry, Austin, Texas, May 1998.

Dowsett M G and Clark E A, *Practical Surface Analysis, Volume 2 - Ion and Neutral Spectroscopy (second edition),* Chapter 5, Eds. Briggs D and Seah M P, Wiley, Chicester (1992).

Dowsett M G, Cooke G A, Elliner D I, Ormsby T J and Murrell A, *Secondary Ion Mass Spectrometry, SIMSXI*, edited by Gillen G, Lareau R, Bennett J and Stevie F, p. 285 Wiley, Chichester (1998a).

Dowsett M G, Elliner D I, Patel S B and Cooke G A, *Secondary Ion Mass Spectrometry, SIMSXII*, to be published (2000).

Dowsett M G, Jeynes C, Clark E A, Webb R and Newstead S M, in *Secondary Ion Mass Spectrometry, SIMS VII* (Eds. Benninghoven A, Evans C A, McKeegan K D, Stroms H A and Werner H W), p. 615, Wiley, Chichester (1990).

Dowsett M G, Ormsby T J, Cooke G A and Chu D P, *J.Vac. Sci. Technol.*, **B16,** 302 (1998b).

Dowsett M G, Ormsby T J, Elliner D I and Cooke G A, *Secondary Ion Mass Spectrometry, SIMSXI*, edited by Gillen G, Lareau R, Bennett J and Stevie F, p. 371 Wiley, Chichester (1998c).

Dowsett M G, Parker E H C, King R M and Mole P J, *J. Appl. Phys.* **54,** 6340 (1983).

Dowsett M G, Smith N S, Bridgeland R,Richards D, Lovejoy A C and Pedrick P, in *Secondary Ion Mass Spectrometry, SIMS X* (Eds. Benninghoven A, Evans C A, McKeegan K D, Stroms H A and Werner H W), p. 367, Wiley, Chichester (1997).

Drummond I W, *PhD. Thesis*, St. John's College Cambridge (1968).

Drummond I W, *Vacuum*, **34**, 51 (1984).

Fox H S, Dowsett M G, Barlow R D, Sykes D E, Chew A, Kilner J A, Bhan M K and Hill C, in *Secondary Ion Mass Spectrometry, SIMS VIII*, edited by Benninghoven A., Janssem K T F, Tumpner J and Werner H W, p.131, Wiley, Chicester (1991).

Gill S S and Wilson J H, *Thin Solid Films*, **55**, 435 (1978).

Gibbons R, *Low Energy Erosion Rates in Si and SiO_2*, unpublished.

Gräf D, Grundner M, Schultz R, and Mühlhoff L, J. Appl. Phys. **68**, 5155 (1990).

Herzog R F K and Viehböck F, *Phys. Rev.*, **76**, 855 (1949).

Hillion F, Daigne B, Girard F, Slodzian G and Schuhmacher M, *Secondary Ion Mass Spectrometry, SIMS IX*, edited by Benninghoven A., Nihei Y, Shimizu R and Werner H W, p. 254, Wiley, Chichester (1994).

Horn T C M, Haochang P, van den Hoek P J and Kleyn A W, *Surf. Sci.*, **201**, 573 (1988).

Hulpke E and Mann K, *Surf. Sci.*, **133**, 171 (1983).

Iltgen K, Bendael C, Niehuis E and Benninghoven A, in *Secondary Ion Mass Spectrometry, SIMS X* (eds. Benninghoven A, Hagenhoff B and Werner H W, p. 375, Wiley, Chichester (1997).

Iltgen K, Benninghoven A and Niehuis E, Secondary Ion Mass Spectrometry SIMS XI, eds. G.Gillen , Lareau R, Bennett J and Stevie F, p. 367 Wiley, Chichester (1998).

Jede R, Ganschow O and Kaiser U, *Practical Surface Analysis, Volume 2 - Ion and Neutral Spectroscopy (second edition)*, Chapter 2, Eds. Briggs D and Seah M P, Wiley, Chicester (1992).

Jiang Z X and Alkemade P F A, *Surf. Interface Anal.*, **25**, 817 (1997).

Jiang Z X and Alkemade P F A, *Appl. Phys. Lett.*, **73**, 315 (1998a).

Jiang Z X and Alkemade P F A, *J. Vac. Sci. Technol.*, **B16**, 1971 (1998b).

Jiang Z X and Alkemade P F A, *Secondary Ion Mass Spectrometry, SIMSXI*, edited by Gillen G, Lareau R, Bennett J and Stevie F, p. 375 Wiley, Chichester (1998c).

Jiang Z X and Alkemade P F A, *Surf. Interface Anal.*, **27**, 125 (1999).

Kilner J A, Chater R J, Hemment P L F, Peart R F, Maydell-ondrusz E A, Taylor M R and Arrowsmith R P, *Nucl. Instrum. Methods*, **B7/8**, 293 (1985).

Liebl H, *J.Appl. Phys.*, **38**, 5277 (1967).

Liebl H, *Int. J. Mass Spectrom.*, **6**, 401 (1971).

Liebl H J and Herzog R F K, *J.Appl. Phys.*, **34**, 2893 (1963).

Littmark U and Hofer W O, *Nucl. Instrum. Meth.*, **168**, 329 (1980).

Maul J L and Patel S B, in *Secondary Ion Mass Spectrometry, SIMS XI*, (Eds. Gillen G, Lareau R, Bennett J and Stevie F) p. 707, Wiley, Chichester (1997).

Meuris M, DeBisschop P, Leclair J F and Vandervorst W, *Surf. Interface Anal.*, **14**, 739 (1989).

Mount G R, Smith S P, Hitzman C J, Chia V K F and Magee C W, *Proceedings of 1998 International Conference on Characterization and Metrology for ULSI Technology*, March 1998, NIST, Gaithersburg, MD, AIP Press, New York p757 (1998).

Morgan A E and Maillot P, *Appl. Phys. Letters*, **50**, 959 (1987).

Ormsby T J, Chu D P, Dowsett M G, Cooke G A and Patel S B, *Applied Surf. Sci.*, **144**, 292 (1999).

Poelsema B, Verhey L K and Boers A L, *Surf. Sci.*, **64**, 537 (1977).

Prewett P D and Jefferies D K, *Proceedings LIEB-2, Inst. Phys. Conf. Ser.*, **54**, 316 (1980).

Schueler B W and Reich D F, *USJ99 handbook*, March 1999, p120.

Schuhmacher M, Rasser B, Desse F, *J.Vac. Sci. Technol.*, **B18,** 529 (2000).

Schulze D, Finster J, Hensel E, Skorupa W and Kreissig U, *Phy. Stat. Sol. (a)*, **76**, K21 (1983).

Sigmund P, *Physical Review*, **184**, 383 (1969).

Sigmund P, *Appl. Phys.*, **A30**, 43 (1983).

Sigmund P, *J. Vac. Sci. Technol.*, **A7**, 585 (1989).

Sigmund P and GrasMarti A, *Nucl. Instrum. Meth.*, **182-183**, 25 (1981).

Smeenk R G, Tromp R M, Kersten H H, Boerboom A J H and Saris F W, *Nucl. Instrum. Methods*, **195**, 58 (1982).

Smilgies D M, Eng P J, Landemark E and Nielsen M, *Surf. Sci.*, **377**, 1038 (1997)

Smith D P, *J. Appl. Phys.*, **38**, 340 (1967).

Smith N S, *PhD. Thesis,* Physics Department, University of Warwick (1996).

Smith N S, Dowsett M G, McGregor B, and Phillips P, *Secondary Ion Mass Spectrometry, SIMSX*, edited by A. Benninghoven, B. Hagenhoff and H. W. Werner, p. 363 Wiley, Chichester (1997).

Stensgaard I, Feldman L C and Silverman P J, *Surf. Sci.*, **77**, 513 (1978).

Stevie F A, Kahora P M, Simons D S and Chi P, *J.Vac.Sci.Technol.*, **A6,** 76 (1988).

Sze S M, *Semiconductor Devices - Physics and Technology*, p. 344, Wiley, New York (1985).

Tielsch B J and Fulghum J E, *Surf. Interface Anal.*, **21**, 621 (1994).

Thomson J J, *Phil. Mag.*, **20**, 252 (1910).

Tromp R M, Practical Surface Analysis (Ed. II) vol.2, edited by Briggs D and Seah M P, p.577 Wiley, Chichester (1992).

Turkenburg W C, Smeenk R G and Saris F W, *Surf. Sci.*, **74**, 181 (1978).

Turkevich A L *et al.*, *in Surveyor Project Final Report, Part II. Scientific Results, NASA Tech. Rep. 32-1265*, pp. 303-387 (1968).

Ukraintsev V A, List R S, Mi-Chang Chang, Edwards H, Machala C F, Martin R S, Zavyalov V, McMurray J S, Williams C C, De wolf P, Vandervorst W, Venables D, Neogi S S, Ottaviani D L, Kopanski J J, Marchiando J F, Rennex B G, Nxumalo J N, Li Y and Thomson D J, *Characterization and Metrology for ULSI Technology*, edited by Seiler D G, Diebold A C, Bullis W M, Shaffner T J, McDonald R, Walters E J, p.741 AIP conference proceedings 449, American Institute of Physics, New York 1998.

Vajo J J, Doty R E, Cirlin E H, *J. Vac. Sci. Technol.*, **A14**, 2709 (1996).

van der Veen J F, *Surf. Sci. Reports*, **5**, 199 (1985).

Vandervorst W and Remmeire J, in *Proceedings of the Fifth International Conference on Secondary Ion Mass Spectrometry, SIMS V*, edited by Beninghoven A, Colton R J, Simons D S and Werner H W, p. 288 Springer Verlag (1986).

Vandervorst W and Shepherd F R, *Appl. Surf. Sci.*, **21,** 230 (1985).

Vandervorst W and Shepherd F R, *J.Vac. Sci. Technol.*, **A5,** 313 (1987).

Vandervorst W, Shepherd F R, Newman J, Phillips B F and Remmerie J, *J.Vac. Sci. Technol.*, **A3,** 1359 (1985).

Vandervorst W, Shepherd F R, Swanson M L, Plattner H H, Westcoft O H, and Mitchell J V, *Nucl. Instrum. Methods* **B15**, 201 (1986).

von Ardenne M, in *Tabellen der Electronenphysik, Ionphysik und Übermikroskopie*, Deutscher Verlag der Wissenschaften, Berlin (1963).

von Criegen R, Weitzel I, Zieninger H and Lange-Gieseler R, *Surf. Interface Anal.*, **15,** 415 (1990).

Werner H W, *Vacuum*, **24**, 493 (1974).

Wittmaack K, *Surface Sci.* **68**, 118 (1977).

Wittmaack K, *Nucl. Inst. and Meths.*, **168**, 343 (1980).

Wittmaack K, *Surf. Sci.*, **112**, 168 (1981).

Wittmaack K, *Nucl. Instrum. Methods* **218**, 307 (1983).

Wittmaack K, *J. Vac. Sci. Technol.*, **A8**, 2246 (1990).

Wittmaack K, *Practical Surface Analysis, Volume 2 - Ion and Neutral Spectroscopy (second edition),* Chapter 3, Eds. Briggs D and Seah M P, Wiley, Chicester (1992).

Wittmaack K, *Philos. Trans. R. Soc. London A*, **354**, 2731 (1996a).

Wittmaack K, *Surf. Interface Anal.*, **24**, 389 (1996b).

Wittmaack K and Corcoran S F, *J.Vac. Sci. Technol.*, **B16,** 272 (1998).

Wittmaack K and Wach W, *Nucl. Instr. and Methods*, **191**, 327 (1981).

Yu M L, *Phys. Rev. Lett.* **47**, 1325 (1981).

Zalm P C, *Rep. Prog. Phys.* **58**, 1321 (1995).